AD-A068 333 BATTELLE COLUMBUS LABS OHIO F/G 11/6
INVESTIGATION OF REJUVENATION OF FATIGUE DAMAGE IN IN-718.(U)
AUG 78 A H CLAUER, B N LEIS, G HOOVER F33615-76-C-5100
UNCLASSIFIED AFML-TR-78-90 NL

1 OF 2
AD A068333

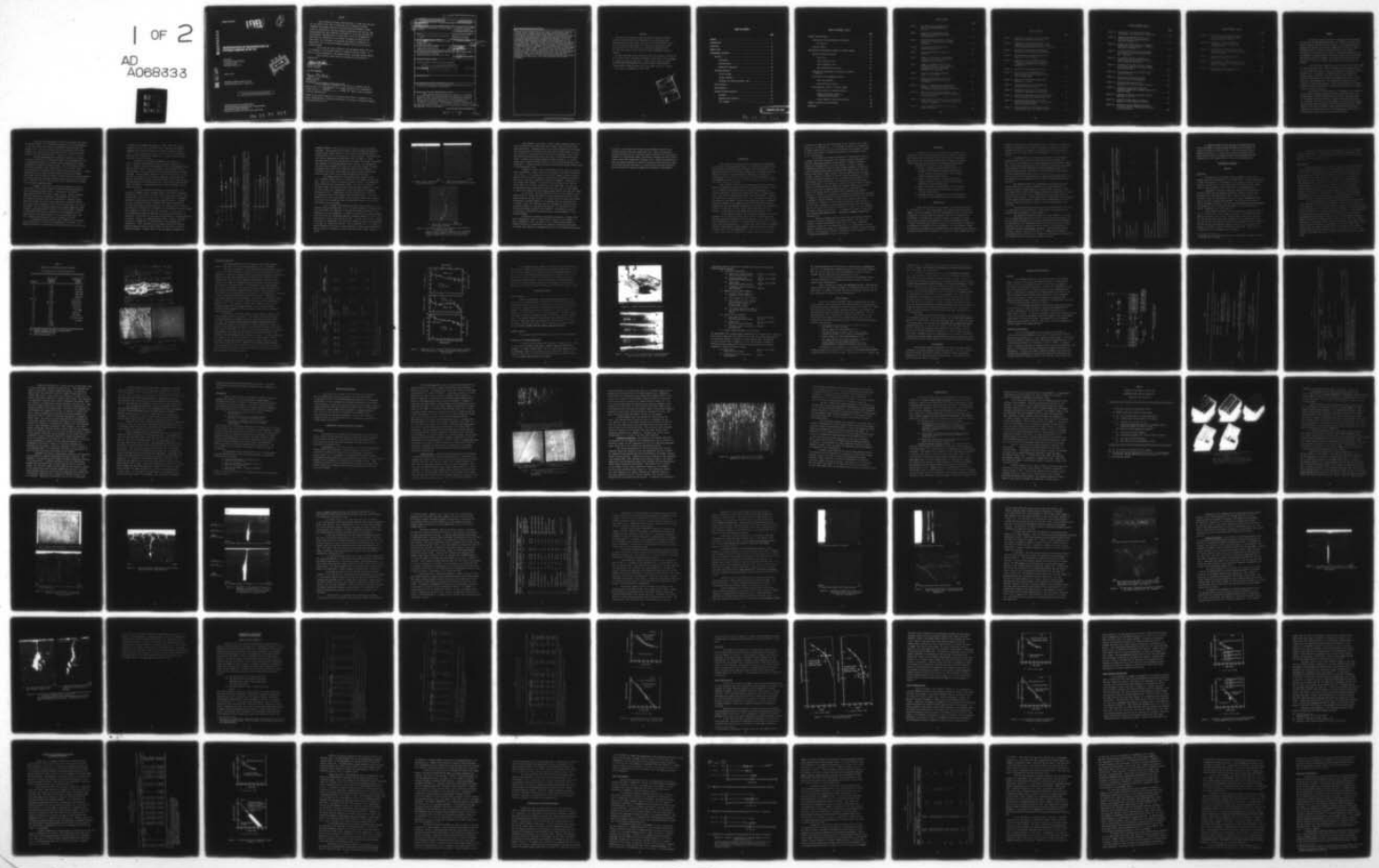

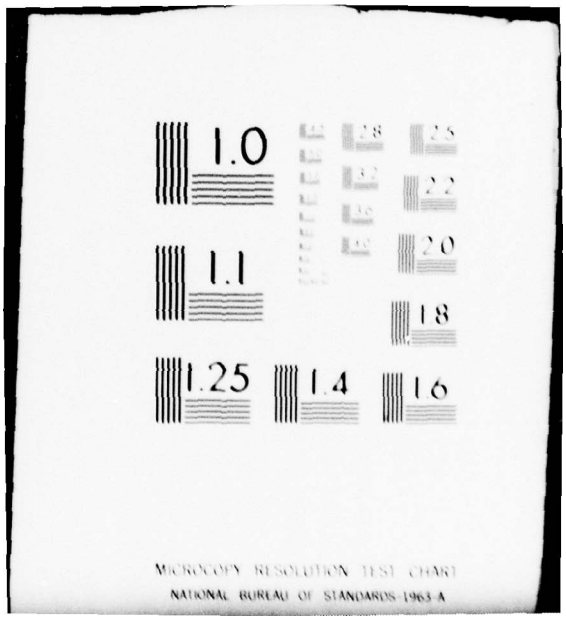
1.0
1.1
1.25
1.4
1.6
2.0
2.2
2.5
MICROCOPY RESOLUTION TEST CHART
NATIONAL BUREAU OF STANDARDS-1963-A

AFML-TR-78-90

LEVEL

AD A068333

DDC FILE COPY

INVESTIGATION OF REJUVENATION OF FATIGUE DAMAGE IN IN-718

BATTELLE
COLUMBUS LABORATORIES
505 KING AVENUE
COLUMBUS, OHIO 43201

AUGUST 1976

TECHNICAL REPORT AFML-TR-78-90
Final Report January 1976 -- January 1978

AIR FORCE MATERIALS LABORATORY
AIR FORCE WRIGHT AERONAUTICAL LABORATORIES
AIR FORCE SYSTEMS COMMAND
WRIGHT-PATTERSON AIR FORCE BASE, OHIO 45433

NOTICE

When Government drawings, specifications, or other data are used for any purpose other than in connection with a definitely related Government procurement operation, the United States Government thereby incurs no responsibility nor any obligation whatsoever; and the fact that the government may have formulated, furnished, or in any way supplied the said drawings, specifications, or other data, is not to be regarded by implication or otherwise as in any manner licensing the holder or any other person or corporation, or conveying any rights or permission to manufacture, use, or sell any patented invention that may in any way be related thereto.

This report has been reviewed by the Information Office (OI) and is releasable to the National Technical Information Service (NTIS). At NTIS, it will be available to the general public, including foreign nations.

This technical report has been reviewed and is approved for publication.

Attwell M. Adair

ATTWELL M. ADAIR
Project Engineer

FOR THE COMMANDER

Norman M. Geyer

NORMAN M. GEYER
Acting Chief
Processing & High Temperature Materials Branch

"If your address has changed, if you wish to be removed from our mailing list, or if the addressee is no longer employed by your organization please notify AFML/LLM, W-PAFB, OH 45433 to help us maintain a current mailing list".

Copies of this report should not be returned unless return is required by security considerations, contractual obligations, or notice on a specific document.

AIR FORCE/56780/16 April 1979 — 320

(9) Final rept. 1 Jan 76-31 Jan 78,

SECURITY CLASSIFICATION OF THIS PAGE (When Data Entered)

(19) REPORT DOCUMENTATION PAGE

READ INSTRUCTIONS BEFORE COMPLETING FORM

(18) 1. REPORT NUMBER: AFML-TR-78-90

2. GOVT ACCESSION NO.

3. RECIPIENT'S CATALOG NUMBER

(6) 4. TITLE (and Subtitle): Investigation of Rejuvenation of Fatigue Damage in IN-718.

5. TYPE OF REPORT & PERIOD COVERED: Final Report for the period 1-1-1976 to 1-31-1978

6. PERFORMING ORG. REPORT NUMBER

7. AUTHOR(s): A. H. Clauer, B. N. Leis, D. A. Seifert and G. Hoover

(15) 8. CONTRACT OR GRANT NUMBER(s): F33615-76-C-5100

9. PERFORMING ORGANIZATION NAME AND ADDRESS: Battelle Memorial Institute ✓ Columbus Division, 505 King Avenue, Columbus, Ohio 43201

10. PROGRAM ELEMENT, PROJECT, TASK AREA & WORK UNIT NUMBERS

(12) 115p

11. CONTROLLING OFFICE NAME AND ADDRESS: Aeronautical Systems Division, Wright-Patterson Air Force Base, Ohio 45433

(11) 12. REPORT DATE: Aug[redacted]78

13. NUMBER OF PAGES: 104

14. MONITORING AGENCY NAME & ADDRESS(if different from Controlling Office): Air Force Materials Laboratory, Wright-Patterson Air Force Base, Ohio 45433

15. SECURITY CLASS. (of this report): Unclassified

15a. DECLASSIFICATION/DOWNGRADING SCHEDULE

16. DISTRIBUTION STATEMENT (of this Report)

Approved for public release, distribution unlimited.

(10) 17. DISTRIBUTION STATEMENT: Allan H./Clauer, Brian N./Leis, G./Hoover David A./Seifert

18. SUPPLEMENTARY NOTES

19. KEY WORDS (Continue on reverse side if necessary and identify by block number)

Hot Isostatic processing, HIP, Fatigue Damage, Fatigue Rejuvenation, Coating, IN-718, Inconel 718, Physical Vapor Deposition.

20. ABSTRACT (Continue on reverse side if necessary and identify by block number)

This research program investigated the feasibility of rejuvenating the elevated temperature, low cycle fatigue (LCF) properties of a nickel base superalloy, IN-718. The starting material was bar extruded from vacuum-cast billets. The microstructure of the bar was quite heterogeneous, and was not representative of a typical wrought product. The study addressed the rejuvenation of both pre-crack initiation damage, and surface-connected cracks (post-crack initiation damage). The investigation included an evaluation of

DD FORM 1 JAN 73 1473 EDITION OF 1 NOV 65 IS OBSOLETE

SECURITY CLASSIFICATION OF THIS PAGE (When Data Entered)

407080

different surface finishing and coating procedures on simulated crack specimens to assess the most reliable approach for bridging surface-connected cracks. It was found that a combination of shot peening, physical vapor deposition of an IN-718 coating, and a final ceramic coating was able to bridge cracks and provide crack closure and bonding during HIP. Fatigue predamaged bars were given the rejuvenation processing along with undamaged control specimens, and the post-rejuvenation fatigue properties were compared with baseline properties. The results showed that the baseline properties were quite dependent on the rejuvenation process. Direct comparison of fatigue life of the HIP control specimens and predamaged specimens after rejuvenation show no increase in total fatigue life. If the possible effect of predamage on the rejuvenated fatigue life is taken into account, it is noted that there is no rejuvenation of pre-crack initiation damage, but there is a positive effect of rejuvenation on post-crack initiation life. Fatigue cracks closed and bonded during HIP were found with their position marked by particles present in the previously existing crack. Thus, the feasibility of closing and bonding surface-connected fatigue cracks in IN-718 has been demonstrated. However, not all cracks were closed and bonded after this procedure, indicating crack closure and/or crack cleaning procedures require further development.

FOREWORD

This report was prepared by Battelle Memorial Institute, Columbus Division, Columbus, Ohio under USAF Contract No. F33615-76-C-5100. This program was funded in part by the use of Director's Funds from the Air Force Materials Laboratory. The contract was administered under the direction of Air Force Materials Laboratory, Wright-Patterson Air Force Base, Ohio, with Mr. Attwell M. Adair (AFML/LLM) as Project Engineer.

The work described in this report was carried out between 1 January 1976 and 31 January 1978. Principal researchers on the project were Dr. Allan H. Clauer, Dr. Brian N. Leis, Mr. G. Hoover, and Mr. David A. Seifert and were under the direction of Mr. Hugh D. Hanes, Program Manager. Contributions by AFML were made by Mr. A.M. Adair and Dr. H.A. Lipsitt.

This report was submitted on 5 May 1978.

TABLE OF CONTENTS

TABLE OF CONTENTS (Con't)

LIST OF TABLES

LIST OF FIGURES

LIST OF FIGURES (Con't)

LIST OF FIGURES (Con't)

SUMMARY

Hot isostatic processing (HIP) is undergoing rapid development as a materials processing method because of its ability to readily close internal porosity and bond interior surfaces. HIP accomplishes this by exerting high pressure at an elevated temperature to encourage creep and diffusion closure of voids and diffusion bonding of the interfaces. Although much of the early use of HIP was for diffusion bonding, its use has expanded to densifying powder metallurgy preforms, and closing shrinkage and gas porosity in castings. More recently, the concept has been extended to void and crack damage originating from creep and low cycle fatigue.

A serious form of damage that occurs in aircraft gas turbine disks is surface-connected cracks. Such cracks may be either preexisting, but of a size below the detection level, or initiated from fatigue in service. In either case, the lifetime of components subject to predominantly fatigue damage is limited by the cyclic growth of these cracks. For disks the replacement cost is large and the design life is only a small fraction of the possible life. If a procedure for healing all preexisting or fatigue induced surface cracks could be devised, the allowable lifetime of disks could probably be extended substantially with attendant savings in cost and materials.

The objective of this program was to demonstrate the feasibility of using surface treatments and hot isostatic processing (HIP) to heal fatigue damage in the gas turbine disk alloy IN-718. The program was to (1) investigate coating procedures to bridge surface-connected cracks, (2) investigate two levels of fatigue damage, pre-crack initiation damage and post-crack initiation damage, (3) assess the response of the fatigue damage to the surface treatments and HIP (rejuvenation processing) by comparison of fatigue lives, and (4) metallographically characterize the fatigue damage before and after rejuvenation processing.

The material investigated was IN-718 bar extruded from vacuum arc melted billets. The extruded bar retained much of the inhomogeneity of the cast material and cannot be considered as representative of a wrought alloy. After the standard solution treatment and aging (STA) sequence, the microstructure consisted of bands of Ni_3Nb and carbides parallel to the extrusion direction. Laves phases were also present.

Four HIP experiments were conducted to determine the effect of the HIP conditions on the material properties and microstructure, and to investigate the effect of different surface treatment and coating procedures on bonding of simulated cracks. The HIP conditions selected were those developed to heal casting defects in cast IN-718, since it was known these conditions would close and bond casting porosity. Tensile specimens were near minimum AMS specifications after HIP and aging. The fatigue life increased only about 9 percent after HIP and aging compared to the STA condition, although substantial grain growth did occur during HIP. Therefore, this HIP cycle was used for the rejuvenation processing of the fatigue damaged specimens.

A number of simulated crack specimens consisting of three or four layers of IN-718 sheet welded on three sides were given different surface treatment-coating sequences. Coatings used were physical vapor deposited (PVD) IN-718 and a ceramic coating. Surface treatments were shot peening and wire brushing. Metallographic sectioning of the simulation specimens after HIP indicated that a sequence of glass bead shot peening, PVD coating, shot peening and a second PVD coating, for a total coating thickness of about 75 μm, enabled cracks to be closed and bonded. The specimens experiencing actual fatigue damage were given a ceramic coating before HIP in addition to the PVD coatings. Cleaning of the fatigue cracks before rejuvenation was not attempted since the cracks had only very short exposures to air at temperature and a suitable cleaning process appeared to be very difficult to develop.

Fatigue tests were performed at 538 C (1000 F) in air and argon under strain control at a total strain amplitude of 0.8 percent. The baseline properties of the extruded and STA material were a total life, N_f,

of 6,620 cycles (standard deviation of $\pm$ 1,887 cycles) and a crack initiation life, N_i, of 4,487 $\pm$ 819 cycles. After HIP and aging of undamaged, bare fatigue specimens, the fatigue properties were N_f = 7,197 $\pm$ 1,585 cycles and N_i = 5,412 $\pm$ 1,124 cycles. This comparison shows that HIP increased the fatigue life by 9 percent and the crack initiation life by 20 percent.

Specimens were fatigue pre-damaged 2,100 cycles to a Level 1 condition representing pre-crack initiation damage and to a Level 2 condition representing pre-damage in the crack propagation stage, wherein visible surface cracks are present. These specimens, along with undamaged control specimens were given the rejuvenation processing treatment. This treatment consisted of an initial vapor blast to clean the surface followed by two consecutive sequences of glass bead shot peening, vapor blast, and PVD coating with IN-718. The ceramic coating was then added and the specimens were HIP. After HIP the specimens were lightly polished in a longitudinal direction before subsequent fatigue testing to failure.

After the rejuvenation processing (coating plus HIP), the previously undamaged control specimens showed a significantly increased fatigue life. The fracture life was 12,367 $\pm$ 1,956 cycles and the crack initiation life was 9,976 $\pm$ 424 cycles. The fatigue lives of undamaged specimens in the different conditions are shown in Figure 1. Because the total rejuvenation process, including the coating, substantially increased the baseline fatigue properties, the coating plus HIP condition was selected as the baseline for comparison of rejuvenation of fatigue damage. This comparison is shown for total life in Figure 2. Total life of the pre-damaged specimens includes both the cycles before and after rejuvenation. On the basis of these data no rejuvenation of fatigue properties is evident. However, two comments should be made. Firstly, specimens having Level 2 damage had the visible surface cracks mapped before rejuvenation. After rejuvenation two specimens failed well away from previously mapped cracks and their average life was about the same as baseline specimens. Secondly, many of the pre-damaged specimens had a

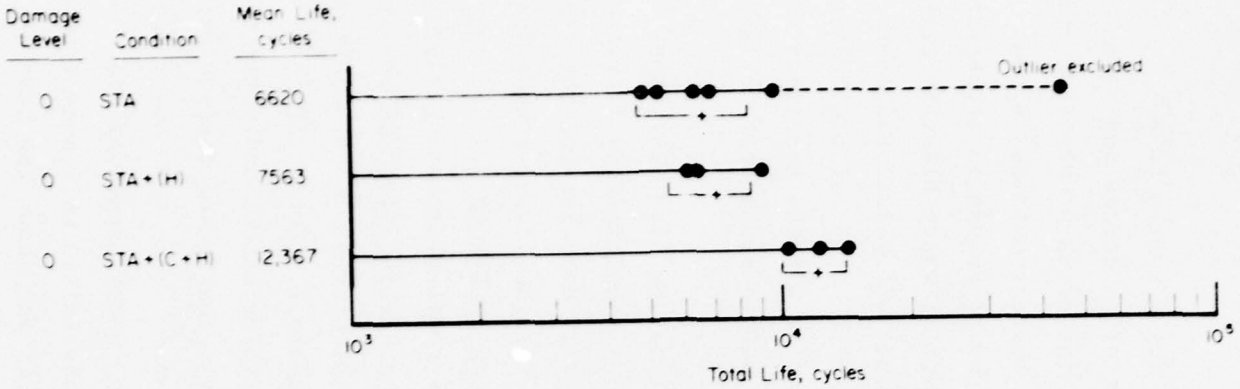

Figure 1. Comparison of Fatigue Lives of Undamaged Specimens in Different Conditions as Follows: STA = Extruded, Solution Treated and Aged, H = HIP, and C = PVD and Ceramic Coated. Tests were run at 538 C (1000 F) at a Total Strain Amplitude of 0.8 Percent. The + is the Mean of the Fatigue Lives and the Bracket with it Spans the Standard Deviation.

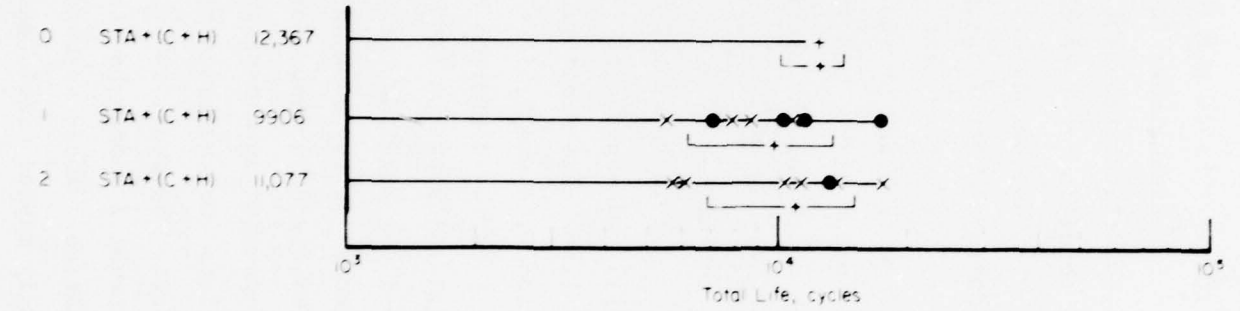

Figure 2. Comparison of Total Fatigue Lives of Predamaged and Rejuvenated Specimens to That of the Rejuvenation Processed Control Specimens. 0 = Undamaged Specimens, 1 = Pre-Crack Initiation Damaged Specimens, 2 = Post-Crack Initiation Damaged Specimens. The + is the Mean of the Fatigue Lives and the Bracket with it Spans the Standard Deviation.

somewhat different crack initiation site appearance from the undamaged specimens. The initiation site in many of the pre-damaged specimens was a semi-circular region about 0.5 to 1 mm long at the specimen surface, extending about 0.25 to 0.5 mm into the fracture surface. Specimens having this fracture appearance are indicated by an X in Figure 2. These specimens tend to have the shortest lives and lower the average "rejuvenated" life compared to the average baseline life. However, the average life excluding these specimens still does not increase the average life after rejuvenation above that of the baseline coated plus HIP condition. It is possible that these "flaws" were fine surface cracks not previously observed, which failed to bond during rejuvenation processing.

The biggest obstacle to interpreting these fatigue results is the enhanced fatigue life after coating plus HIP compared to after HIP only. There are at least two possible reasons for this. HIP homogenizes the microstructure and causes grain growth. The first of these would increase fatigue life while the second would decrease fatigue life. These two effects might have compensated for each other when bare undamaged specimens were HIP. Alternatively, the PVD coating on the coated plus HIP specimens was much finer grained than the bulk material. This fine-grained surface layer could inhibit crack initiation significantly compared to the bare HIP specimens and cause the observed increase in life in the rejuvenated control specimens.

If it is assumed that the material before and after HIP does have different fatigue properties and accumulates fatigue damage at different rates, then the baseline for comparison of rejuvenation should be modified to be consistent with this assumption. In Figure 2 the baselines are drawn assuming that the STA and the rejuvenated materials accumulate damage at a cyclic rate proportional to their crack initiation lives. In this case the Level 1 damage still shows no rejuvenation, but the Level 2 damage does show some rejuvenation of fatigue life (Figure 26, page 88). This is probably due to the healing or partial healing of the Level 2 cracks during HIP, thereby requiring additional time to reopen or reinitiate new cracks during post-HIP fatigue testing to failure.

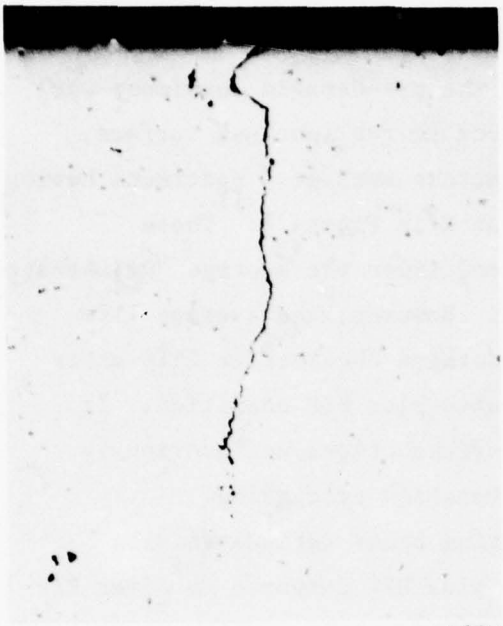

100X

(a) Typical fatigue crack before rejuvenation processing

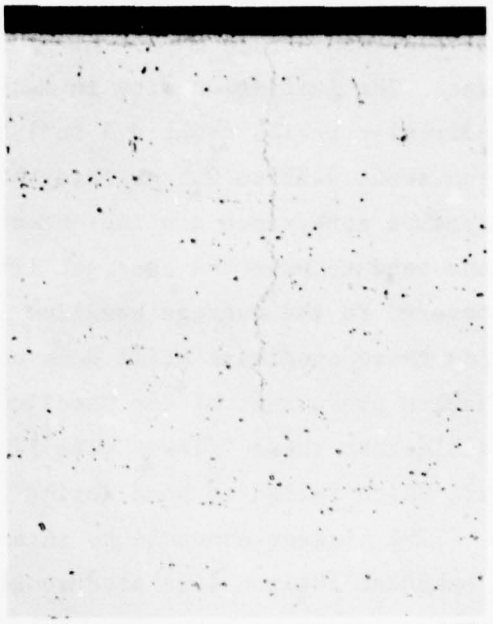

100X

(b) Typical fatigue crack after rejuvenation processing, as-polished

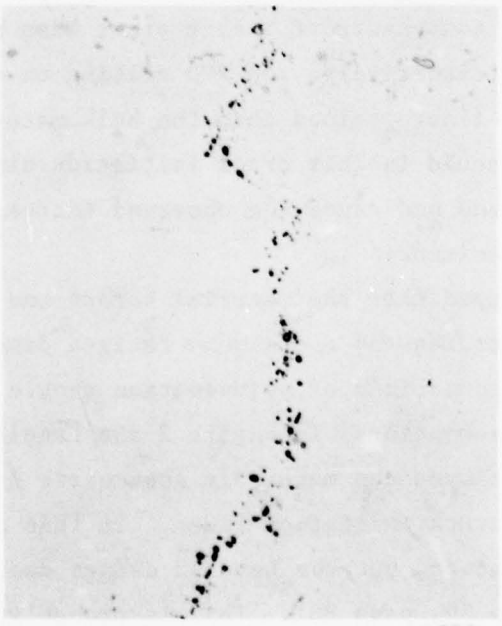

1000X

(c) Same fatigue crack after rejuvenation processing, as-polished

Figure 3. Comparison of Fatigue Crack Appearance Before and After Rejuvenation Processing.
Figures (b) and (c) Show the Appearance of a Crack Which Has Been Closed and Bonded by HIP but Whose Location Is Marked by Second Phase Particles and Possibly Voids.

Metallographic sectioning of fatigue damaged specimens before and after rejuvenation processing showed that fatigue cracks were closed and bonded during HIP. Specimens having crack locations mapped after pre-damage were sectioned after rejuvenation processing and fatigue testing to failure. The locations of the previously existing cracks were marked by small second phase particles and possibly voids, indicating a closed and nearly bonded crack. A typical crack before bonding is shown in Figure 3a. A typical bonded crack is shown in Figures 3b and c in the as-polished and the etched conditions. It should be noted that these cracks did not reopen during fatigue testing subsequent to HIP.

Unbonded or poorly bonded cracks known to be the site for fracture after rejuvenation in some of the Level 2 specimens could result from either of two effects. It is possible that the PVD and ceramic coatings contained defects over the crack and failed to bridge the crack adequately during HIP. This can be corrected by improved PVD coating techniques. Alternatively, if the coatings were adequate, it is possible that cleaning of the oxide out of the cracks is a critical step even for thin oxide films. In this case, the adequately healed cracks may be those with less than a critical amount of oxide, while those which are not healed might contain more than this amount.

In conclusion, the most significant result of this program was the demonstration of closure and bonding of fatigue cracks which did not reopen during subsequent fatigue testing. In cracked parts, this alone should enable rejuvenation to extend fatigue life if nothing else, e.g. microstructure, is changed. Thus, HIP conditions should be developed to limit bulk microstructural changes, e.g. minimize grain growth. The reliability of crack closure and bonding observed in this program is unacceptable but should be increased by improved PVD coating procedures and development of crack cleaning methods.

A definitive conclusion concerning the extension of fatigue life by HIP rejuvenation cannot be drawn from the results of this program. A direct comparison of the total fatigue life of rejuvenated specimens to a baseline condition is complicated by the apparent substantial improvement of fatigue life imparted to undamaged materials by the rejuvenation processing.

In effect, the extruded and STA material pre-damaged before HIP was a different material from that tested after HIP. Since the fatigue and rejuvenation processes are conceivably modified between these two material conditions to some unknown degree, appropriate allowances for these effects cannot be made when comparing the fatigue lives. Further investigations in this area should establish the complete rejuvenation process and its effect on the final baseline properties of a material which has been stabilized before entering the fatigue pre-damage and rejuvenation investigation.

INTRODUCTION

Hot isostatic processing (HIP) is undergoing rapid development as a materials processing method because of its ability to rapidly close internal porosity and bond interior surfaces. HIP accomplishes this by exerting high pressure at an elevated temperature to encourage creep and diffusion closure of voids and diffusion bonding of the interfaces. Although much of the early use of HIP was for diffusion bonding, its use has expanded to densifying powder metallurgy preforms, and closing shrinkage and gas porosity in castings.

More recently, the concept has been extended to void and crack damage originating from creep and low cycle fatigue (LCF) strain. In the case of internal voids and intergranular cracking representative of elevated temperature creep and LCF damage, HIP alone can readily remove these. After HIP the creep properties are largely restored[1-3] and the LCF properties are partially restored[3], i.e., these properties have been rejuvenated to some degree. However, when dealing with surface cracking, the most prominent form of damage produced by LCF, HIP must be used in conjunction with crack bridging techniques and this makes the procedure more complex. In this case, the preliminary results indicate that it is feasible to remove surface crack damage and lengthen fatigue life[4].

Strain induced cavitation and cracking are important in hot path components in aircraft gas turbines, such as blades or buckets, and an important form of this damage is surface-connected cracks. These may be either preexisting cracks of a size below the detection level, or fatigue cracks initiated during service. In either case, the lifetime of components subject to predominantly fatigue damage is limited by the cyclic growth of these cracks. One such component is a disk. The replacement cost of a disk is large, and the consequences of a disk failure are so dangerous

to aircraft and human life that the design life of a disk is only a small fraction of its possible life. If a procedure for healing all preexisting or fatigue induced surface cracks could be devised, the allowable lifetime of disks could probably be extended substantially with attendant savings in cost and materials.

As revealed by the previous studies[1-4] the healing of surface-connected cracks and restoration of the original fatigue properties is a much more challenging problem than the removal of internal cavitation, because the problems appear to be more difficult to solve. Firstly, to enhance the ability to bond the crack surfaces together, an effective surface cleaning technique must be devised which ideally would reach into narrow, deep cracks to remove surface films and compounds such as oxides. Secondly, a means of blocking off the crack from the atmosphere is required so that the external pressure will act to squeeze the crack closed. For this purpose a sound coating able to bridge and seal all surface cracks must be developed. If the coating is to remain on the part when it reenters service, its presence must not impair the original properties of the part; if the coating is to be removed before the part is placed back in service, the coating must be removable without impairing the original properties. Thirdly, if the material's properties are significantly decreased by changes in its microstructure incurred during the HIP cycle, the alloy must be amenable to reheat-treatment to restore the original microstructure or properties. Fourthly, if alloy depleted zones form in the vicinity of the crack due to oxidation or other compound formation, these deficiencies must be corrected or their effect accounted for. Fifthly, a final finishing procedure to restore the original surface dimensions, finish, or properties, e.g., hardness and chemistry, must be developed to prepare the part for subsequent use.

While the problems and risks associated with healing of surface-connected cracks and rejuvenation of fatigue properties are large, the potential economic and materials benefits are also large. Successful rejuvenation would not only enable used disks to be rejuvenated one or more times to increase their useful life substantially compared to that with present practice, but could also conceivably increase the initial design life of disks by removing nondetectable cracks before service.

OBJECTIVES

The principal goal of this program was to demonstrate the feasibility of HIP and refinishing procedures to remove or neutralize defects which limit the fatigue life of aircraft gas turbine disks. These defects are both fabrication and service induced, and include surface-connected cracks and pre-crack initiation fatigue damage.

The specific objectives of this program were to

- Develop a coating(s) procedure which would (1) be mechanically and chemically compatible with IN-718, (2) not degrade fatigue properties, and (3) bridge surface-connected fatigue cracks
- Induce controlled amounts of fatigue damage into fatigue specimens, both pre-crack initiation damage and surface cracking damage types
- Assess the response of the different types of fatigue damage to the rejuvenation processes by comparison of total fatigue lives
- Metallographically characterize the fatigue damage and the effect of the rejuvenation process on this damage.

PROGRAM PLAN

To meet the objectives of the program, four important areas had to be addressed, (i) coating development, (ii) inducing controlled fatigue damage, (iii) HIP parameters, and (iv) metallographic studies. Because the rejuvenation of surface-connected fatigue cracks was to be studied, the development of an appropriate coating procedure was necessary to bridge these cracks and render them amenable to closure and bonding during HIP. To ensure the highest likelihood of success, the coating should be chemically and mechanically compatible with the substrate. For these reasons a number of simulated crack samples were prepared and HIP to ascertain the most promising bridging technique before applying it to the actual fatigue damaged specimens.

Cleaning of cracks was not investigated in detail. Cleaning of oxide-filled cracks is a complex problem. Since the fatigue test duration for cracked specimens was short, the formation of oxide films in the cracks would be minimal, and it was expected that cleaning might not be critical for crack healing.

To simulate the type of damage representative of that expected in turbine disks after service, it was decided to subject smooth test bars to low cycle fatigue at an elevated temperature to two levels of damage. One of these levels represents the crack initiation stage with no detectable surface damage; the other represents the crack propagation stage, with surface-connected cracks. The point of crack initiation was to be defined in terms of back extrapolation of the asymmetric load drop, a percentage decrease in load, or visual observation of cracks under maximum tensile load. The fatigue tests were conducted at 538 C (1000 F) in either argon or air atmosphere.

HIP parameters were to be determined by performing several preliminary HIP cycles to provide information on both microstructural and mechanical property changes caused by the selected HIP conditions. There was concern that too high a HIP temperature would cause undesirable coarsening of the grain size, while too low a temperature would not cause the crack surface to bond together. The starting point for determining the HIP parameters was the conditions established by General Electric/AEG-Evendale for IN-718 castings, since casting porosity could be closed and bonded under these conditions.

Optical metallography and replica electron metallography were used to characterize the microstructures, fatigue damage, and response of the simulated crack specimens to coating and HIP.

The planned test matrix is shown at the top of Table 1. It allows for (i) establishing baseline tensile and cyclic stress-strain behavior as well as fatigue resistance of the original extruded plus solution treated and aged material, (ii) determining the effect of HIP alone on the baseline properties, and (iii) comparing the effect of HIP on the rejuvenation of coated and uncoated fatigue damaged specimens. The test matrix actually followed is shown at the bottom of Table 1. It emphasizes statistical characterization of particular test parameters at the expense of establishing the influence of HIP on the baseline fatigue resistance.

TABLE 1

TEST MATRIX FOR REJUVENATION OF LOW CYCLE FATIGUE

PROPERTIES OF IN-718

Condition	Room Temperature Tensile	538 C (1000 F) Tensile	538 C (1000 F) Cyclic Deformation	Fatigue at 538 C (1000 F) Undamaged	Fatigue at 538 C (1000 F) Level 1[a]	Fatigue at 538 C (1000 F) Level 2[b]
Planned Test Matrix						
Extruded and STA[c]		X	X	X		
HIP (Preliminary)				X		
HIP (Final)				X	X	
Coat and HIP (Final)				X	X	X
Actual Test Matrix						
Extruded and STA[c]		X	X	X		
HIP (Preliminary)[d]	X	X (649 C (1200 F))		X		
HIP (Final)						
Coat and HIP (Final)				X	X	X

(a) Level 1 is pre-crack initiation damage.

(b) Level 2 includes surface connected crack damage.

(c) STA: solution treated and aged.

(d) The HIP conditions were the same as for the final HIP experiment.

It should be noted that the results of rejuvenation of the control and damaged specimens include the effects of the complete rejuvenation process, not just HIP alone. This was necessary because a separate evaluation of all the process variables would have been too costly, and the result of ultimate interest in the evaluation of HIP rejuvenation is the cumulative effect of all the processing steps.

EXPERIMENTAL PROCEDURE

Material

Processing

The material was received* as eleven nominal 2.5 cm (1 inch) diameter bars each approximately 120 cm (4 feet) long. The bars were extruded at AFML from nominally 7.2 cm diameter by 17.8 cm long (2.8 inch by 7 inch) vacuum arc melted billets. The as-cast billets were first upset at 1038 C (1900 F), then extruded at 1093 C (2000 F) at a 10:1 extrusion ratio.

Radiographic and visual inspection indicated the extruded bars to be mostly sound, with radiographic indications of defects usually being associated with observable surface flaws. Based on this inspection, sections of sound bar approximately 26 cm (10.3 inches) long were cut from nine of the bars as program test material. These sections were labeled firstly by number, referring to the extruded bar from which they were obtained, and secondly by letter, indicating the sequence the section appeared in the bar, beginning with A at the nose end.

After initial sectioning, the bar segments were solution treated in air for 1 hour at 954 C (1750 F) and oil quenched. The segments were then aged for 8 hours at 718 C (1325 F), furnace cooled to 607 C (1125 F) over a 2 hour period, aged at this lower temperature for a further 8 hours, and air cooled. Each bar segment was again visually examined, and the nose and tail sections and any other obviously defective portions of the bars were then excised. Sufficient 13 and 26 cm sections of sound heat treated bar were obtained for up to 62 mechanical test specimens.

---

* This material was obtained from the Air Force Materials Laboratory, Wright-Patterson Air Force Base.

An analysis of material taken from extruded bar No. 4 is presented in Table 2 along with the composition limits published by Huntington Alloys for Inconel Alloy 718. All alloy additions and trace elements in the program material are within the limits shown.

Microstructure

The microstructure of the solution treated and aged (STA) materials is quite heterogeneous (Figure 4). It is fine grained (ASTM grain size of 7 to 8, 22 to 30 μm diameter) and has a somewhat laminar appearance created by the extrusion of large primary carbides and alloy-rich interdendritic regions in the cast billet parallel to the bar length. The stringers of small dark particles in the upper half of Figure 4a are representative of some regions having large particles, possibly both inclusions and massive primary carbides, which are broken up and strung out during extrusion. Associated with these regions are voids (Figure 4a). These may be due to fallout of particles during metallographic preparation, indicating weak interparticle interfaces, or they may be voids remaining after extrusion. Considering the 10 to 1 extrusion ratio, it is more likely that the holes result from loss of particles during metallographic preparation.

The acicular phase in the (horizontal) precipitate-containing bands in the lower half of Figure 4a is orthorhombic δ-Ni_3Nb which precipitated in the segregated alloy-rich regions during cooling from the extrusion temperature and/or during the 954 C (1750 F) solution treatment. In these same regions a finer precipitate, the coherent body-centered tetragonal γ''-Ni_3Nb phase[6-8], has precipitated during aging (Figure 4b). Between the alloy-rich bands containing the acicular phase, there is a very fine precipitate (Figure 4c), probably a mixture of γ''-Ni_3Nb and some γ'-Ni_3 (Al,Ti). The size of these precipitates is presumably smaller because of the lower alloy content in these regions and their precipitation during aging at the lower temperatures. The equiaxed particles appearing predominantly in the regions of the coarse, acicular Ni_3Nb are blocky carbides, probably MC and $M_{23}C_6$ type.[6-9] Also, pockets of Laves phase are often present in the bands containing the acicular Ni_3Nb.

TABLE 2

COMPARISON OF SPECIMEN MATERIAL CHEMISTRY

WITH COMPOSITION LIMITS FOR INCONEL-718

Element	Bar No. 4[a] Chemistry, percent	Composition[b] Limits, percent
Si	0.02	0.35 max
Mn	0.03	0.35 max
P	0.005	0.015 max
S	0.010	0.015 max
C	0.05	0.08 max
Nb + Ta	4.97	4.75-5.50
Ni	Bal (53.7)	50.00-55.00
Cr	17.90	17.00-21.00
Mo	2.99	2.80-3.30
Cu	0.02	0.30 max
Ti	1.10	0.65-1.15
Al	0.59	0.20-0.80
Fe	17.99	Bal (11.3-23.5)
Co	0.54	1.00 max
O	0.0013	-
N	0.100	-

(a) Chemical analysis prepared by Bowser-Morner Testing Laboratories, Inc.

(b) Taken from Reference (5).

3J330 250X

(a) Overall microstructure showing stringers of inclusions and columns of acicular Ni_3Nb precipitate

5000X

(b) Region in a column of acicular Ni_3Nb

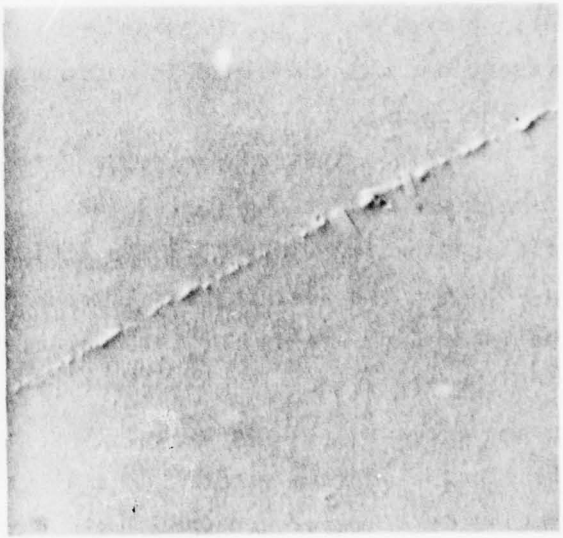

15000X

(c) Region between columns of acicular Ni_3Nb

Figure 4. Microstructure of Solution Treated and Aged Inconel-718 Extruded Bar. Micrographs (b) and (c) Are Replica Electron Micrographs.

Mechanical Properties

The average hardness of the STA material was 422 DPH (Vickers) using a 10-kg load. This is roughly equivalent to 43 R_C or 398 BHN.

The tensile properties of the extruded and STA material were measured at 538 C (1000 F) on Specimens 4B-1 and 5B-2 before fatigue testing at this temperature. These tests showed serrated stress-strain response at strains well beyond yield, with each serration being accompanied by an audible "ping". Examination of the tension test samples showed evidence of surface cracks, visible to the naked eye, oriented normal to the tensile axis but aligned in rows parallel to the tensile axis. The formation of each crack evidently gave rise to a serration in the stress-strain curve based on a correlation of the pinging with serration formation during testing. The stringing out of these cracks in rows suggested they were related to the drawing out of inclusions or alloy segregated regions during the extrusion process. There were significant differences noted in modulus, yield stress, and ultimate strength between the tensile test specimens taken from two different extruded bars - Numbers 4 and 5. This implies a possibly large amount of scatter in the fatigue resistance of the baseline material in that certain of these properties, when combined in various parametric forms, serve as measures of fatigue resistance.[8]

The results of the 538 C tension tests on samples from Bars 4 and 5 are presented at the top of Table 3. The average true fracture stress of these specimens was 1318 MPa (191.2 ksi), and the true fracture strain was 0.206. The average tensile properties compare reasonably well with published data trends for this material in its STA condition[9] (Figure 5). Both the yield and ultimate strengths of the experimental material are lower than the mean of the data, but they still lie in the scatterband. In contrast, the elongation lies within the scatterband, but is above the trend. The modulus is likewise somewhat above the mean (4 percent). (In these comparisons use is made of the fact that at and above 538 C (1000 F) there is little difference between sheet properties and those of other hot worked product forms such as extruded bar.[9]) Insofar as the ultimate tensile strength can be considered as a direct measure of fatigue resistance, one might expect that the fatigue resistance of this material might be below the mean trend of data published in the open literature.

TABLE 3

ROOM AND ELEVATED TEMPERATURE TENSILE

PROPERTIES OF INCONEL 718 IN DIFFERENT CONDITIONS

Specimen Number	0.2% Yield Stress ksi	0.2% Yield Stress MPa	Ultimate Strength ksi	Ultimate Strength MPa	Elongation, % in 2 in.	Reduction in Area, percent	Young's Modulus 10^6 psi	Young's Modulus 10^3 MPa	Hardness
				Extruded, Solution Treated And Aged 538 C (1000 F)					
4B-1	125.9	868	150.9	1040	21.8[b]	18.1	25.8	178	--
5B-2	128.9	889	161.1	1111	28.1[b]	19.1	25.1	173	--
				HIP And Aged 20 C (68 F)					
1	147.2	1015	186.4	1285	20.5	27.0	28.5	196	BHN 380
2	145.9	1006	185.2	1277	22.5	24.1	28.7	198	
AMS 5662B[a]	150.0	1034	185.0	1276	12	15	--	--	BHN 331
				649 C (1200 F)					
7A	124.4	858	151.8	1046	14.5	17.6	23.15	150	--
11A	123.3	850	149.5	1031	16.0	19.2	23.13	159	--
AMS 5662B[a]	125.0	862	145.0	1000	12	15	--	--	--

(a) AMS specification for wrought solution-treated and aged material.

(b) In 1.22 cm (0.5 in) gage length.

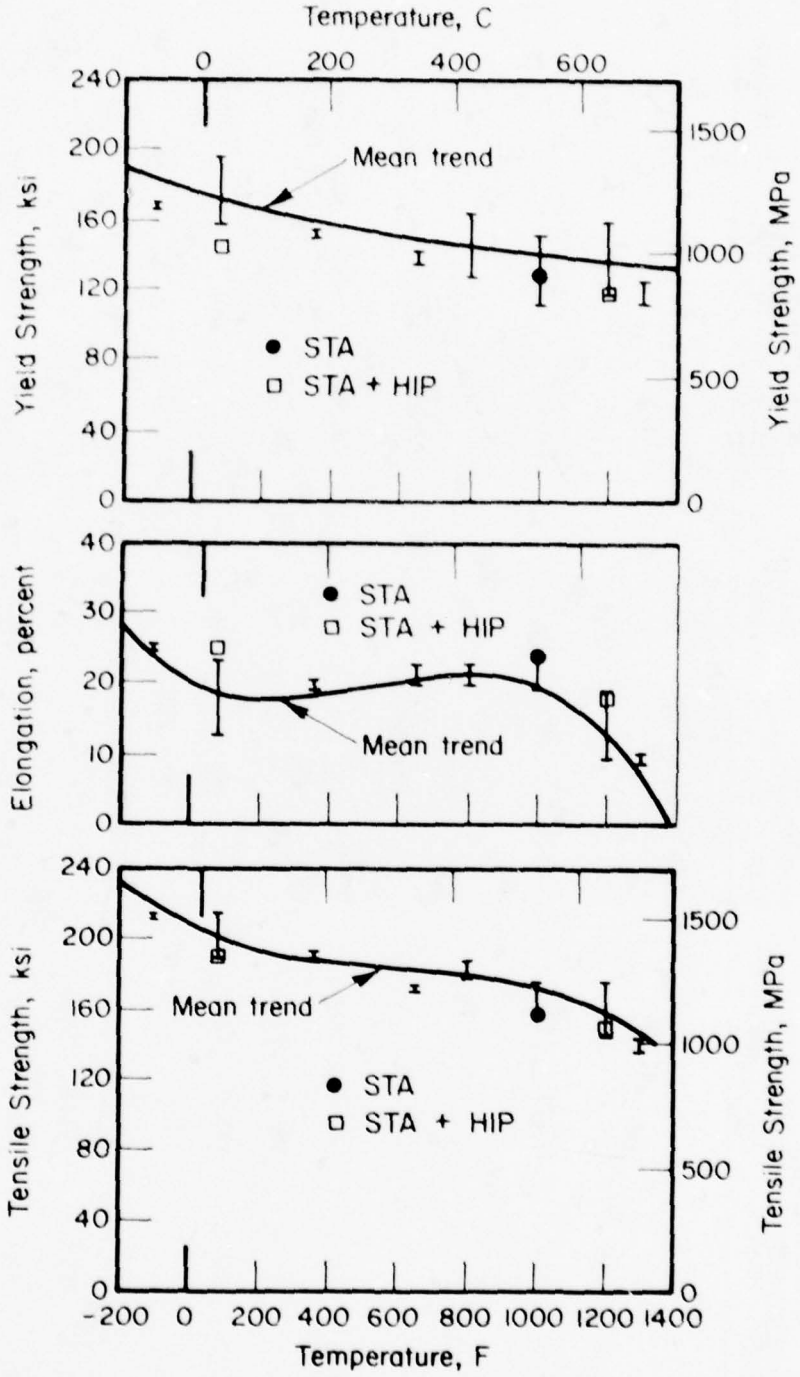

Figure 5. Comparison of 538 C (1000 F) Tensile Properties of Extruded and STA Material to Handbook Properties of Wrought STA IN-718[4,11]

The baseline material condition for this study is the extruded and STA condition. However, it should be noted that the present material in this state is not representative of wrought, solution treated and aged material. It is clear from the microstructure and the tensile properties that the cast microstructure exerts a substantial influence on properties, even after extrusion and heat treatment. This should be kept in mind when comparing the effects of HIP on the microstructure and properties of this material. The effects of HIP on the tensile properties is discussed in a later section.

Coating Procedures

IN-718 Coating

Magnetron sputtering, a physical vapor deposition process, was selected as the coating process for applying the metallic alloy coating, since complex alloys such as IN-718 can be easily applied by this technique. In addition, coatings deposited by sputtering typically have excellent adherence. The sputtering process was conducted in a vacuum chamber at a vacuum of 1×10^{-3} to about 5×10^{-2} torr of argon gas. The source material or cathode was held at a negative voltage of from 500 to several thousand volts. The negative voltage on the cathode causes energetic electrons to ionize the argon gas: these ions bombard the cathode and physically eject, or sputter, atoms off the surface of the cathode which are then deposited with high kinetic energy onto the adjacent substrate material.

Ceramic Coating

The ceramic coating was applied by General Electric/AEG-Evendale.

Procedure for Coating Fatigue Bars

A fixture for both heating and rotating six fatigue bars at a time in a horizontal orientation was built. Figure 6 shows the chain drive assembly, and Figure 7 shows three of the six fatigue bars and four of the seven 600-watt quartz heating lamps in the fixture before coating. In operation, the source is a 6 mm (0.25 inch) thick plate of IN-718 located 7.6 cm (3 inches) above the axis of the bars.

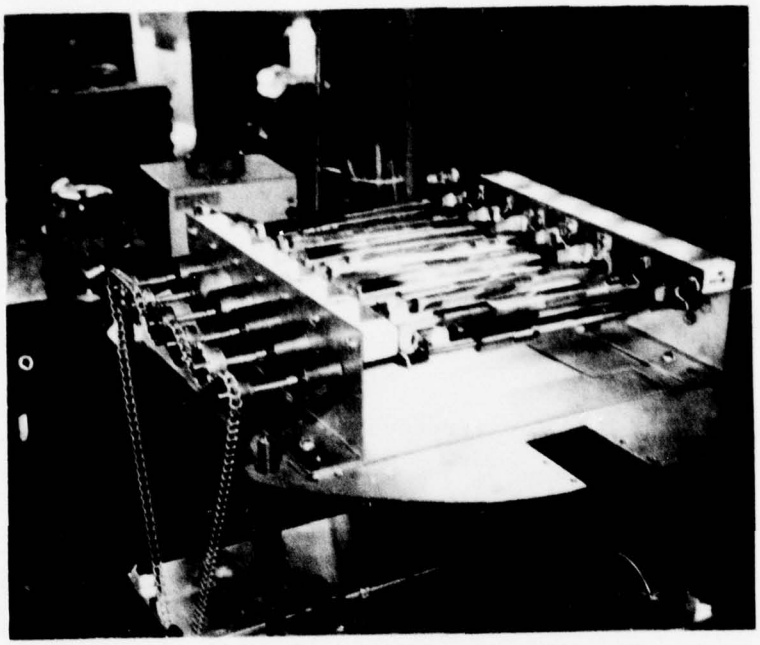

3879VD

Figure 6. Fatigue Bar Rotating/Heating Fixture.

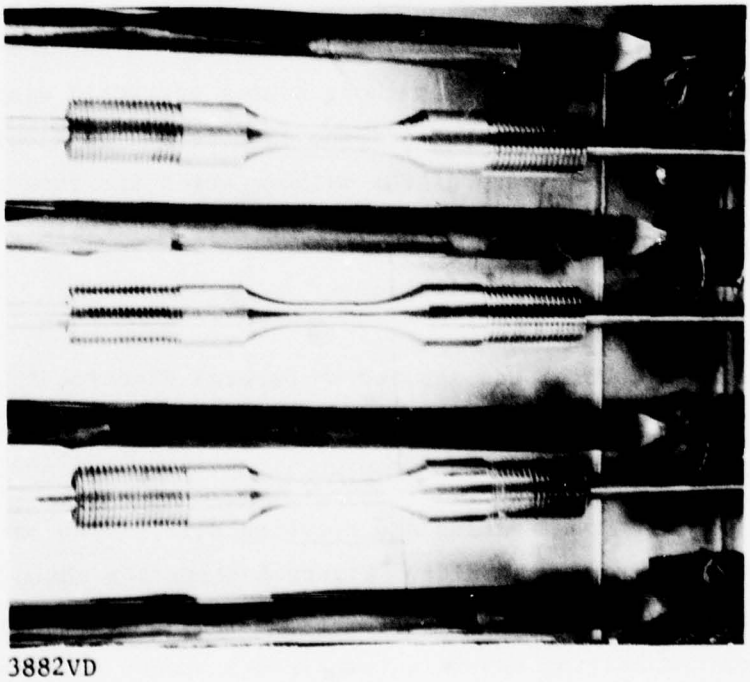

3882VD

Figure 7. Three of up to Six Fatigue Bars in Position Between Four of Seven 600-Watt Quartz Heating Lamps

The process sequence selected for cleaning and coating the fatigue bars before HIP was as follows:

(1) Fatigue bar preparation

(a)	Vapor blast (liquid honing) Nozzle-to-specimen distance	120 sec at 0.31 MPa 5 cm
(b)	Glass bead shot peen Nozzle-to-specimen distance	300 sec at 0.31 MPa 5 cm
(c)	Vapor blast Nozzle-to-specimen distance	120 sec at 0.31 MPa 5 cm
(d)	Ultrasonic clean in electronic grade methanol	300 sec

(2) Magnetron sputtering parameters

(a) Evacuate coating chamber to a pressure of 1.33×10^{-3} Pa

(b) Heat specimens to 700 C (1292 F)

(c) Coat 4 hours at 620 V, 4.8 amp, and an argon gas pressure of 0.4 Pa to give 38 μm (0.0015 inch) coating

(d) Cool coated specimens to 100 C or less before removal from coating system

(3) Second surface treatment

(a)	Glass bead shot peen Nozzle-to-specimen distance	30 sec at 0.31 MPa 12.7 cm
(b)	Vapor blast Nozzle-to-specimen distance	30 sec at 0.31 MPa 12.7 cm
(c)	Ultrasonic clean in electronic-grade methanol	300 sec

(4) Second coating procedure as in (2) above

The approximate total coating target thickness was 75 μm (0.003 inch). However, first layer coating time for samples 9B, 7D2, 7D1, 8C1, and 8C2 was reduced to three hours because of arcing of a quartz heating lamp. In addition, the first coating layer on samples 5D1, 5C2, and 3B2 spalled during the second glass bead peening (as in 3a above) and were given the following treatment to remove the spalled coating:

(1)	Vapor Blast Nozzle-to-work distance	600 sec at 0.31 MPa 5 cm
(2)	Ultrasonic clean in electronic-grade methanol	300 sec

The cleaned specimens were then recoated as described above, beginning at Step (2). All samples had a bright matte metallic finish except Specimens 8C2, 9B, 7C1, 8C1, and 7D2, which were darkened as a result of being removed from the system while the temperature was >100 C.

After the IN-718 coatings were applied, the predamaged fatigue bars were overcoated on the reduced section with a ceramic applied by General Electric/AEG-Evendale.

After cleaning and coating, the specimens were HIP. After HIP the specimen surfaces were lightly polished in a longitudinal direction with fine emery paper to a nominal 32 μm RMS finish before subsequent fatigue testing. The coating was not removed by this polishing step.

HIP Procedures

A total of four HIP experiments were performed during the course of the program. The procedures and the conditions used, as detailed below, were those previously established for HIP of Inconel-718 castings.[12] These HIP conditions provided a logical starting point since it was known that casting porosity was closed and bonded under these conditions. The first experiments were used to ascertain the effects of the HIP cycle on the microstructure and properties of the extruded material, and to process simulated crack specimens investigating crack closure and bonding procedures. The HIP conditions were:

- Simultaneously heat and pressurize to 1163 C (2125 F) and 103 MPa (15 ksi) pressure
- Hold at 1163 ± 10 C and 103 MPa for 2 hr
- Cool under pressure to 1066 C (1950 F) at a minimum pressure of 83 MPa (12 ksi) within a 40-minute period
- Hold at 1066 ± 15 C and 83 MPa minimum for 1 hr
- Cool under pressure as rapidly as possible, achieving 760 C (1400 F) or below within 90 minutes further static cooling or simultaneous cooling and depressurization to ambient temperature and pressure.

Following HIP, all mechanical test specimens and certain of the bonding specimens were subjected to the standard 18 hour dual aging treatment at ambient pressure in argon as follows: age at 718 C (1325 F), 8 hours, then

furnace cool at 55 C (100 F) per hour to 608 C (1125 F), and age at 608 C (1125F), 8 hours. After aging, the specimens were removed from the furnace and cooled rapidly in flowing argon.

The first HIP experiment was in fact accomplished by including two of the round bar bonding couples in a HIP cycle performed in Battelle's large autoclave system to densify a number of large castings. This cycle differs from the remaining experiments in that, due to technical difficulties, 12 hours were required to attain the 1163 C, 103 MPa, HIP conditions. A substantial portion of this time was at temperatures above 954 C (1750 F).

The second HIP experiment was accomplished in a normal fashion in the 25.4-cm (10 inch)-diameter autoclave, requiring only 4 hours to attain the specified 1163 C and 103 MPa. The six specimens of the first series of simulated crack specimens, a third round bar bonding couple, two tensile specimen blanks (Nos. 8A and 4E), and three fatigue specimens (Nos. 3D-1, 3D-2, and 4B-2) were processed. In order to preserve their axial straightness, the fatigue specimens were suspended along their longitudinal centerlines during HIP identical to the method described previously.[4] The tensile blanks, fatigue specimens, and rod diffusion couple were subsequently aged as described above.

The third and fourth HIP experiments were also performed in the 25.4-cm-diameter autoclave in a normal fashion, only 3 hours being required to attain 1163 C and 103 MPa. In the third HIP experiment, the twelve specimens of the second series of simulated crack specimens and two additional tensile specimen blanks (Nos. 7A and 11A) were treated. The fourth HIP experiment served to process the undamaged and predamaged fatigue specimens used for the principal fatigue rejuvenation investigation. These fatigue specimens were, again, suspended along their longitudinal axes to preserve straightness. A previously fractured fatigue specimen showing secondary cracking was coated and HIP along with the fatigue specimens for post-HIP metallographic examination.

Metallography

Optical metallographic examination was carried out using standard techniques for specimen preparation and glyceregia etch. The replica electron microscopy studies used acetate replicas, followed by carbon coating and dissolution of the acetate to form the final replica. The etchant for the replica microscopy was also glyceregia.

Fatigue Testing Procedures

Specimen

All specimens used in this investigation were of the geometry shown in Figure 8. Note that this geometry provides a reduced section 1.905 cm (0.75 inch) in length and 0.952 cm (0.375 inch) in diameter. This rather stocky geometry was chosen to provide (i) a reasonable section for crack propagation, (ii) a large surface free from extensometer knife edges to permit surface replication for damage studies if necessary, and (iii) a reasonably high buckling load for testing in a low to moderate capacity test system. A total of 50 specimens were fabricated, the machining being performed at Met-Cut, Cincinnati, following their low-stress cylindrical grind procedure detailed in Table 4.

All 50 specimens were machined from sound extruded and STA blanks taken from the full length extrusions. Specimens were numbered from 1, for each combination of bar and blank, designated respectively by a number and by a letter. Of these 50 specimens, 2 were used in tension testing, 2 were used as setup and procedure verification samples, and 2 were damaged during setup on the initial loading. The disposition of the remaining samples was as indicated in Table 5. Note that 2 of the 50 specimens, 2C2 and 2D2, remain in the virgin STA state.

Apparatus and Procedure

Each of the experiments in this program was performed in a servo-controlled electrohydraulic test system in strain control with all specimens being subjected to a fully reversed forcing function. The environment was prepurified laboratory argon (99.998 percent minimum purity), the testing being performed at a temperature of (538 C) 1000 F, as detailed below. Although the majority of testing was done in an inert atmosphere, some portion of the baseline data were developed in an ambient laboratory air environment. A check of the oxide's character revealed little difference between these atmospheres, nor was there any detectable difference in the fatigue resistance, probably because of the relatively short testing time.

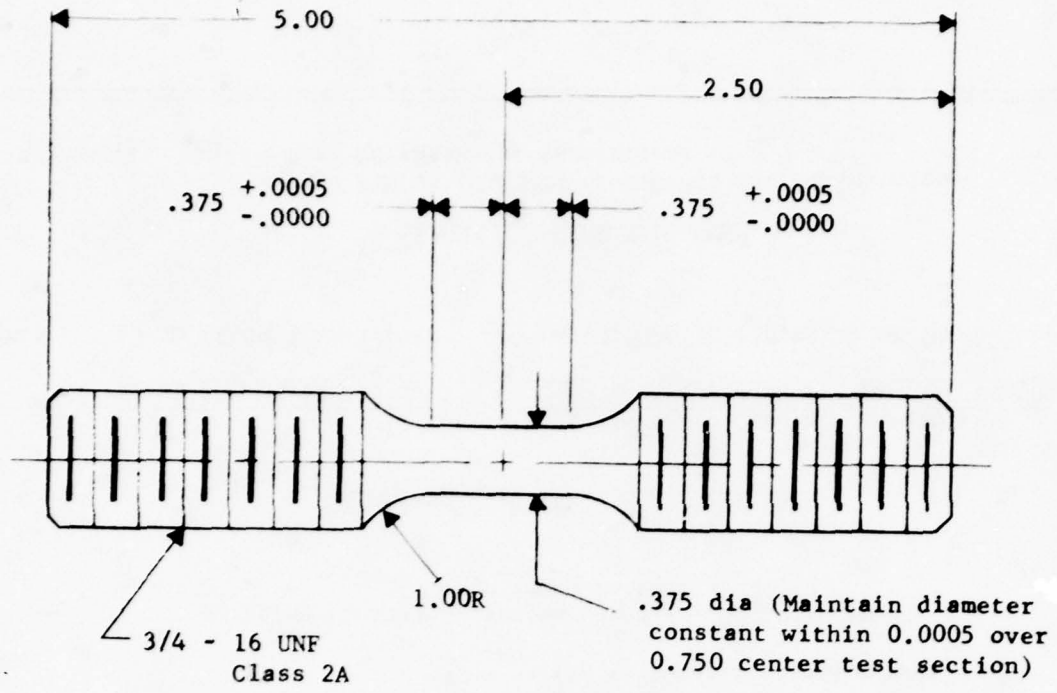

Figure 8. Geometry of The Fatigue Specimen With Dimensions in Inches

TABLE 4

CYLINDRICAL GRIND PROCEDURES FOR SPECIMEN MANUFACTURE

Work Surface:	243 to 790 cm/min (8 to 26 ft/min)
Table Speed:	17.8 cm/min (7 in./min)
Wheel Speed:	Traverse Grinding - 843/990 m/min (2800/3250 ft/min) maximum, 30.5 to 35.6 cm (12 to 14 in.) diameter wheel.
Grinding Fluid:	Stuart Thredkut No. 99, diluted 1:1 with Sohio Factoil 39

Traverse Grinding - Depth per Pass

Roughing	Finishing Last 250 µm (0.010 in.) on Radius		
	First 200 µm (0.008 in.)	Next 20 µm (0.0008 in.)	Last 30 µm (0.0012 in.)
25 µm (0.001 in.)/pass	13 µm (0.0005 in.)/pass	10 µm (0.0004 in.)/pass	5 µm (0.0002 in.)/pass spark out

Plunge Grinding - In Feed

0.5 to 2.0 µm (0.00002 to 0.00008 in.)/revolution
+ 5 to 20 spark-out revolutions

TABLE 5

FATIGUE REJUVENATION PROGRAM TEST MATRIX[a]

Material Condition		Baseline	Incremental Damage	Fatigue Damaged Level 1	Fatigue Damaged Level 2
Solution treated + age (STA)	(b)	3B-1, 3C-1, 3E-2 4D-1, 4D-2, 5B-1		--	--
	(c)	2B-1, 2C-1, 3C-2, 4C-1, 4C-2, 7C-1 11B-2	5C-1, 5D-2, 8D-1, 8D-2	--	--
	(d)		11B-1, 11C-1, 11C-2, 12C-1	--	--
HIP + Age[c]		3D-1, 3D-2, 4B-2			
Coated + HIP + Age[c,e]		2B-2, 3B-2, 12C-2		5C-2, 5D-1, 7C-2, 7D-1 7D-2, 8B-2, 8C-1, 8C-2 9B	7B-1, 7B-2, 8B-1 11D-1, 12B-1 12B-2

(a) Matrix supplemented by 2 tension tests - specimens 4B-1 and 5B-2. Specimens 2D-1 and 3E-1 were used to verify the uniformity of the temperature and strain fields in the gage section (See text).
(b) Tested at total strain ranges from 0.5 to 2.0 percent.
(c) Tested at a nominally identical total strain range of 0.80 percent.
(d) Tested at a nominally identical total strain range of 1.30 percent.
(e) Coated: A permanent 75 μm (0.003 inch) thick PVD coating of nominal IN-718.

Strain was controlled over a 1.905 cm (0.750 in) gage length using a clip-on extensometer calibrated to ASTM Class B_1. The extensometer was typical of that used in elevated temperature testing. Two high-purity alumina probes with knife-edge points were lightly clamped against the specimen gage section. These probes were connected to a bracket with two parallel beams joined together by a flexible elastic hinge. The transformer of a magnetically shielded linear variable differential transformer (LVDT) was attached to one beam and the core was attached to the other beam. Thus, the output signal obtained from the LVDT was directly proportional to the average deformation over the gage length. The mass of the extensometer was counterbalanced and supported at the center of gravity to minimize probe force. While no specimens failed because of knife-edge notching, one specimen did fail as a result of knife-edge slippage into a propagating fatigue crack. Two strain cycles which employed several combinations of strain range, waveform, and frequency were imposed on set-up specimens to establish the character of the deformation response of the IN-718 material at 538 C, under systematic variations in these variables. The results showed no observable difference between constant strain rate and sinusoidal results for frequencies from 0.1 to 1 Hz over the range of strain of interest in this program. Therefore, for the remainder of the testing, strain was programmed to follow a sinusoidal waveform at frequencies ranging from 0.1 to 1 Hz, depending on the amplitude of the control strain. The ability of the extensometer to operate over this range of frequencies was independently verified as a function of the strain amplitude prior to beginning the test program. Strain was controlled to within 1 percent of the programmed signal. The extensometer calibration was performed at the outset and verified several times during the test program.

Specimens were heated by high-frequency induction, and temperature was controlled by a standard proportional-type power controller. The geometery of the heating coil was designed to minimize temperature gradients in the test section. A specimen instrumented with five Chromel-Alumel thermocouples spot-welded along the gage length was used to verify this design. With the final design, the peak temperature was within $\pm$ 1 percent of the desired value, and the overall gradient was less than 2.5 percent. During fatigue testing the control/feed-back temperature was obtained from a thermocouple looped about and in contact with the gage section of the test specimen. Temperature was controlled to $\pm$ 2.8 C (5 F) during test.

Load was monitored in all tests using a commercially available load cell mounted in series with the specimen. Calibration of the load cell was performed prior to, and verified once during, the test program. The load cell was observed to be accurate and linear within 0.1 percent of the operating range used in the present program. A peak load detector was incorporated in the control loop for use in determining crack initiation based on load drop from the saturation (stable cyclic) load (stress) level.

All specimens were gripped in a fixture arrangement similar to that detailed in Reference (13). It is noteworthy that such an arrangement features a liquid-solid Wood's metal grip which serves to minimize specimen mounting stresses. Prior to commencing the test program, the alignment was adjusted to minimize bending strains, the adopted standard being bending strains less than 1 percent of the imposed axial strain.

Monotonic and cyclic deformation response was recorded continuously during the first ten cycles and at logarithmic intervals thereafter on an X-Y recorder, while both load and strain along with temperature were continuously recorded on a time-based strip chart recorder.

Before commencing with the experimental program, the closed loop system was tuned to establish the optimum system gain. Concurrently, the load cell and extensometer were calibrated along with the related recording devices. After this preliminary phase, the test phase began. The procedure used for each test follows: after mounting the specimens in the upper grip, the load train was closed in load control and the liquid-solid grip frozen. (All grips were watercooled during testing.) Maintaining the system at zero load, the extensometer was mounted and zero suppressed and all recording devices activated and zero suppressed. Subsequently, the induction heating system was activated, and the load train was allowed to equilibrate for 1 hour after the testing temperature was reached. The system was then switched to strain control and allowed to stabilize before beginning the strain cycling. During this stabilization period, the environmental chamber was sealed and purged at a flow rate of 3 cfm for 2 hours. During testing, the chamber was held at a positive back pressure equal to 1 inch of water. In tests where the system had to be periodically shut down and restarted (such as for predamage), care was taken to unload and

thereafter reload without inducing spurious mean stresses. All tests were terminated either upon reaching a prescribed level of damage or at failure.

Test Program

Table 5 details the final test program to generate results for assessing the feasibility of HIP rejuvenation of fatigue damage in extruded and STA IN-718. This matrix was patterned after that set forth as the Actual Test Matrix in Table 1. Tests were initially performed to establish the strain amplitude for the ensuing feasibility assessment. That strain amplitude had to concurrently satisfy three requirements:

(1) Be sufficiently inelastic so as to reduce fatigue scatter

(2) Be sufficiently small so as to induce fatigue fracture at levels greater than 10^3 cycles

(3) Give rise to a reasonable fraction of life spent in propagating a fatigue crack from observable surface damage.

From the results of 13 tests which encompassed strain ranges from 2.12 percent to 0.52 percent, that strain level was determined to be 0.80 percent. Results of the 13 tests are presented later in Tables 8, 9 and 10. The data reported in Table 8 represent experiments designed to show the progress of fatigue damage with increasing cycles. Two strain amplitudes presumed to bound the above three requirements were selected. These data were essential to establish the crack initiation life and subsequent crack propagation behavior necessary to define the predamage levels described below. The data in Tables 9 and 10 establish the baseline to assess the extent of rejuvenation.

To differentiate between the different levels of fatigue damage given the specimens prior to the rejuvenation treatments, the following designations are introduced:

- Level Zero pre-damage: specimens given no previous fatigue cycling
- Level One pre-damage: specimens cycled just short of crack initiation
- Level Two pre-damage: specimens containing known cracks.

Results of tests that pertain to the rejuvenation process are presented later in Tables 10 and 11.

RESULTS AND DISCUSSION

The results are presented in four sections which approximate the four general task areas in the program: (i) the determination of the effect of HIP on the microstructure and properties of the extruded and STA bar, (ii) the coating and refinishing investigation to ascertain the best method to prepare the surface and bridge surface cracks, (iii) the fatigue characterization and rejuvenation studies, and (iv) metallographic examination of fatigue damage and the response of damaged specimens to HIP. The first two aspects are considered in the context of the rejuvenation process parameter development. The last two topics are examined in terms of the application of the chosen process parameters to fatigue damage rejuvenation.

Rejuvenation Process-Parameter Development

HIP Studies

The objective of this phase of the program was to ascertain the effect of HIP on the microstructure and the tensile and fatigue properties of the extruded and STA bar. The specimens to be discussed here were HIP in the first through third HIP experiments described earlier in the Experimental Procedures section.

Microstructure. The first specimens to be HIP for microstructural examination were also designed to provide evidence of the effect of the selected HIP conditions on closure of holes and bonding of surfaces. Bonding couples of 2.5 cm segments of extruded and STA rod were prepared by grinding one end surface flat on each segment and drilling a 6 mm (0.25 inch) diameter conical indentation in one surface to represent a cavity. After cleaning the surfaces, two such segments were gas tungsten arc (GTA) welded together around the circumference of the mating surfaces while inside an argon filled chamber.

For the preliminary HIP cycles, it was decided to duplicate the conditions used to HIP IN-718 castings, followed by the duplex age as described previously. The microstructure before HIP, that of the extruded and STA material, is shown in Figure 4. After HIP the bands of acicular precipitate are absent, but the rows of equiaxed carbides remain, as shown in Figure 9a. The bond line at the mating surface between the two halves of the bonding couple runs across the micrograph. Stringers of fine, dark particles similar to those referred to as inclusions are still present in the upper half of the couple (Figure 9a) after HIP, but these areas are not common. In the first HIP experiment, which took 12 hours to attain the HIP conditions, the grain sizes of the specimens (from Bars 4 and 7) were ASTM 1 to 0 (250 to 350 μm). In the succeeding HIP experiment, which took only 4 hours to reach the HIP conditions and was representative of the others, the average grain size of a specimen from Bar 8 was ASTM 3 to 4 (90 to 120 μm) with a finer grain size, ASTM 5 to 6 (40 to 60 μm) in the bands of fine carbide. Therefore, the larger grain size in the first HIP experiment was attributed to the longer time at temperature. The microstructure from the second HIP cycle was then taken to be representative of the microstructure after HIP for the succeeding HIP experiments. The acicular Ni_3Nb, the γ''-Ni_3Nb platelets, and the Laves phases have been dissolved by the HIP treatment, resulting in an overall homogenization of the microstructure. The fine coherent γ''-Ni_3Nb plate-like precipitate in the matrix, shown in Figure 9b, is more evident after HIP than before, presumably because more Nb is available for the coherent precipitate formation after the large Ni_3Nb platelets and Laves phases were dissolved during HIP.

Bonding Studies. Four GTA welded bonding couples were prepared as described in the previous section on microstructure. These were then examined for closure of the conical drilled hole and bonding of the mating surfaces after HIP. The first two couples were included together in a HIP cycle, one wrapped in stainless steel foil and one unwrapped. This first HIP cycle was held quite long at higher temperatures due to control problems. The surface of the wrapped specimen came out shiny and clean after HIP, but the unwrapped specimen had a black chromium oxide coating. The surface-affected layer in this specimen was examined on a taper section giving a 10X apparent magnification. The affected layer extended 27 μm

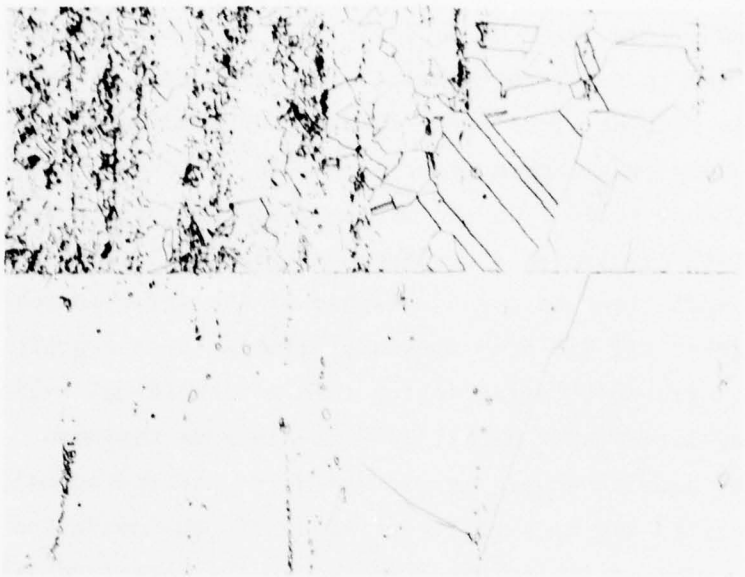

35327 250X

(a) Overall microstructure, stringers of carbides and inclusions remain after HIP. The bond line between two different parts of the bond-couple specimen runs horizontally across the micrograph

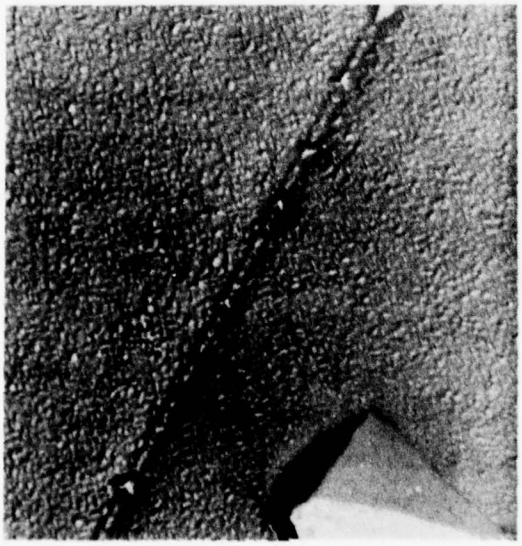

EH7254 15000X

(b) Fine γ"-Ni_3Nb platelets and large carbide particles

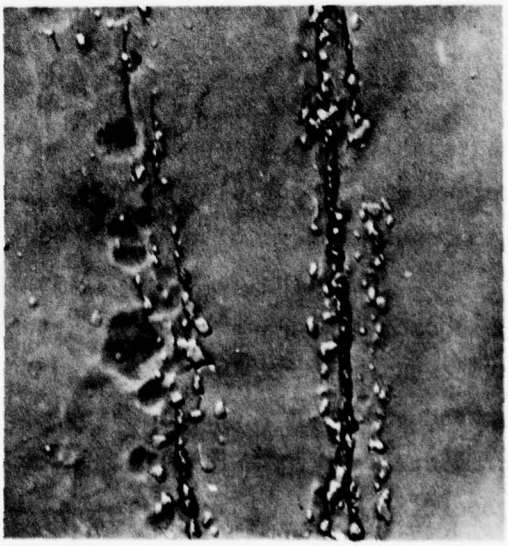

EH7255 5000X

(c) Stringers of fine particles, possibly carbide

Figure 9. Microstructure of IN-718 Extruded and STA Bar After HIP and Aging. Micrographs (b) and (c) Are Replica Electron Micrographs.

deep and included a 2 μm thick oxide layer, a 7 μm thick region of intergranular attack and an 18 μm thick carbide depleted zone. Subsequent sectioning of the couples after aging showed that bonding between the two halves of the couples was intermittent, possibly because of the presence of some oxide film or residue on the mating surfaces (Figure 9a). Very little grain growth across the interfaces was observed, although the HIP conditions were sufficient to cause collapse of the large conical voids. The interfaces after HIP did etch unevenly, similar to the grain boundaries. Significant grain growth occurred during this prolonged HIP cycle, with grain sizes being larger than ASTM 1 (250 μm) in some regions.

Another bonding couple was included in a second normal HIP cycle. This specimen had no significant areas of nonbonding and only a few spherical voids or inclusions remained in the interface (Figure 10). There was also significantly more grain growth across the bond interface than was found in the earlier specimens. This is particularly noticeable toward the periphery of the specimen (but well inside the weld beads originally joining the two components). The grain size of this couple averaged ASTM 3.5 ($\sim$ 0.10 mm) in the HIP + aged condition.

Mechanical Properties. The hardness of the material after HIP was relatively low, averaging 245 DPH (approximately 21 R_C or 233 BHN), but increased to about 415 DPH (approximately 42 R_C or 392 BHN) upon subsequent aging, nearly that of the extruded and STA baseline material.

The tensile properties of the IN-718 extrusions after HIP and subsequent aging were measured at both room temperature and 649 C (1200 F) for comparison with published AMS 5662B specifications for wrought, solution treated and aged material. Duplicate tests were conducted at each temperature using standard ASTM ".505" specimens and, as shown in Table 5, the tensile properties of the HIP material compare very favorably with the specification values despite significant grain growth. This behavior is in contrast to the response at 538 C which showed these properties to be somewhat less than those published trends (Figure 5). More importantly, however, the stress response of all tensile specimens was completely smooth at both room temperature and 649 C with no evidence of the serrations experienced with the extruded and STA material. In addition, the differences

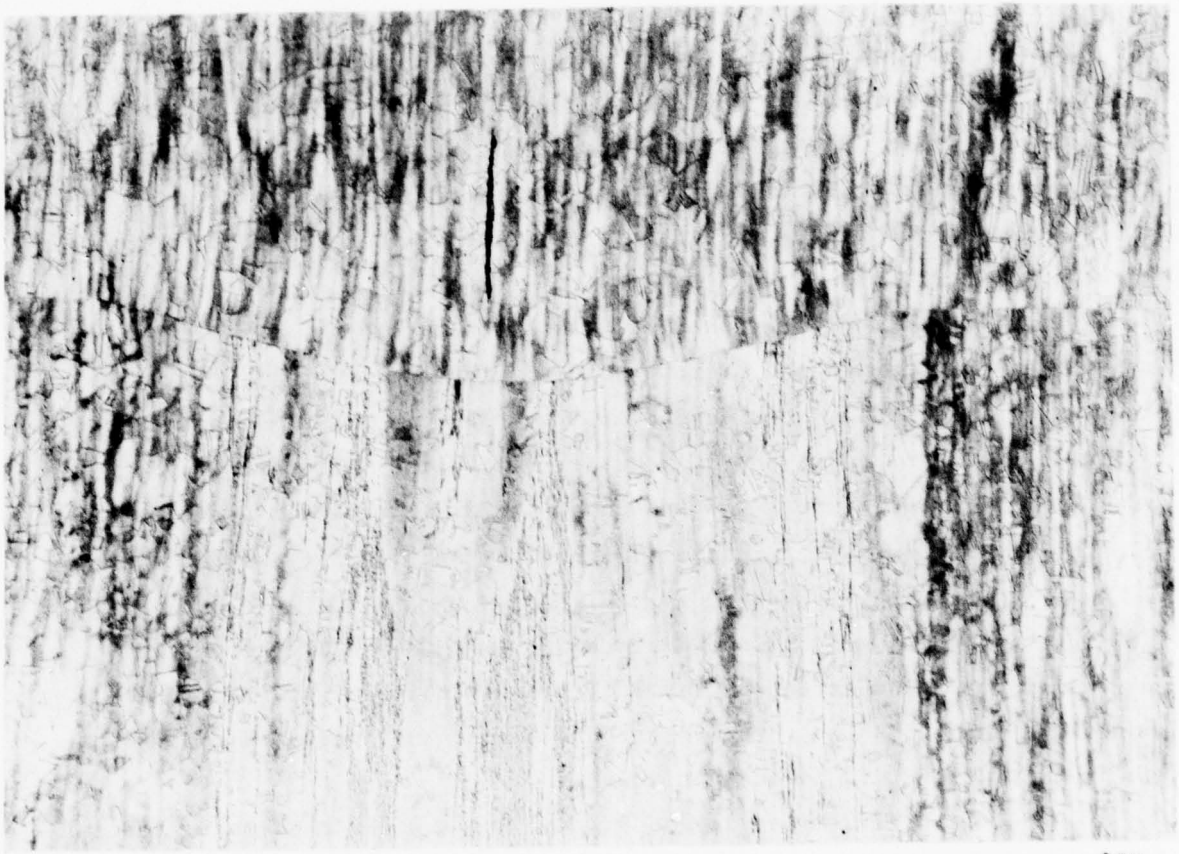

33278 20X

Figure 10. Longitudinal Section of IN-718 Bonding Specimen No. 8A-8E after HIP and Aging.

in the strength and modulus values for the individual test specimens at each temperature are small. Since each specimen was machined from a different extruded rod, these results strongly indicate that HIP followed by the appropriate aging treatment causes significant homogenization of the extruded material in support of the metallographic results, and has a normalizing effect on mechanical properties.

The 538 C (1000 F) LCF fatigue properties of two extruded and STA test bars after HIP and aging showed approximately 15 percent higher cyclic life than the baseline material. This relatively small change in fatigue properties is attributed to counteracting effects of coarser grain size decreasing fatigue life and homogenization of the microstructure increasing fatigue life. These properties are discussed at length in the fatigue section.

This second HIP experiment was satisfactory in several ways. It materially homogenized the microstructure without causing an unacceptable increase in grain size much beyond ASTM 4. This is the maximum acceptable grain size designated in the military specification AMS 5662B. In addition, the room temperature and 649 C (1200 F) tensile properties were close to or exceeded the minimum specified by AMS 5662B (Table 3). It is seen later that the fatigue properties of the control specimens HIP in this cycle were not too different from the baseline properties. In addition, it was expected that lower temperatures might not produce bonding of cracks. Thus, the higher HIP temperature was used throughout the remainder of this investigation.

It should be mentioned here that grain sizes measured later in the program on sections taken from the fatigue bars showed a much larger increase in grain size after HIP than the metallographic specimen referred to above, which was to provide the background for the microstructural changes occurring during HIP. The grain sizes in the fatigue bars were ASTM 1 and larger, in the range 200 to 400 μm. The effects of these larger grain sizes are discussed later along with the fatigue results.

Coating Studies

The purpose of this phase of the program was to investigate the feasibility of bridging surface-connected fatigue cracks with a coating applied by a physical vapor deposition (PVD) process (sputtering), so that a subsequent HIP operation could effectively heal them. The approach was to apply IN-718 superalloy onto IN-718 simulated crack coupons, and later onto fatigue bar specimens. Both single and multiple coatings were tried. The effort included examination of different treatments of the surface before, between, and after applying the coating(s). The coating composition, thickness, density, and adherence were the parameters studied.

The coating program was carried out in three stages:

(1) Determination of the suitability of magnetron sputtering for depositing IN-718 coatings of acceptable alloy composition and the limitations of crack bridging capability of magnetron sputtering using simulated crack specimens

(2) Development of mechanical surface treatments to bridge cracks wider than those which could be bridged by sputtering alone

(3) Development of fixtures and procedures from (1) and (2) above for coating actual fatigue bars.

Coating and Surface Treatment Studies. An initial series of simulated crack specimens was developed to investigate different methods of bridging cracks, both coating alone and in combination with other surface treatments. Each specimen in this series of twelve specimens was fabricated by stacking five layers of 3 mm (0.125 inch) thick sheet of IN-718 to form four cracks of different widths between neighboring sheets. After degreasing, three of the four "open" surfaces on each stack of coupons were welded by gas tungsten arc (GTA) welding in an argon-filled chamber. The remaining open face then presented four simulated cracks having nominal widths of (i) a "tight" crack of a few micrometers, (ii) 25 μm (0.001 inch), (iii) 150 μm (0.006 inch), (iv) 250 μm (0.010 inch). Although the narrow cracks were of most interest to this program, the wider cracks were included so that information could be obtained to determine the maximum crack

opening for which a particular method might be applicable. If a substantial crack opening could be bridged, this would increase the confidence level of the method's application to narrower cracks.

With these twelve specimens, the six treatment sequences listed in Table 6 were evaluated. Duplicate specimens were prepared for each condition. The rationale for the conditions selected are as follows. The basic condition is to apply a PVD or ceramic coating only, over smooth, untreated surfaces with the original range of crack widths. There is also the possibility that shot peening cracks will close the cracks somewhat, depending on their original width, and enable the subsequent PVD or ceramic coating to bridge a wider starting crack than would be possible without shot peening. The shot peen followed by an anneal to recrystallize the cold worked peened layer was intended to determine whether peening alone could seal narrow cracks sufficient for HIP closure, as observed in another material by General Electric/AEG, Evendale. Finally, an attempt to look into a simple pickling procedure as a surface and crack cleaning option was included in the series. To avoid the possibility of not bonding because of a defective coating rather than by the characteristics of the cleaned surfaces, the cracks in the pickled specimens were closed by a plate of IN-718 electron-beam welded over the top of the specimen.

After welding, but before further coating or treatment, the open surface of each specimen was ground through No. 600 grit paper to even the surface. The specimens were then pickled 5 minutes in a solution of 8 parts H_2O, 2.5 parts HNO_3 and 0.5 part HF to remove any oxide, followed by a water rinse. To further clean the cracks, the specimens were leached 1 minute in a solution of 1/3 HNO_3 and 2/3 HCl. After this, they were water rinsed, ultrasonically cleaned in 200-proof alcohol, then air dried at 100 C.

The PVD coatings of 75 to 250 μm (0.003 to 0.010 inch) thick were deposited at 10 to 25 μm/hr (0.0004 inch/hr). Substrate temperatures ranged from 200 to 500 C. Both the shot peening and the ceramic coating, Solaramic 5210, were carried out by General Electric/AEG, Evendale. Steel shot was used for shot peening. The specimens appeared as shown in Figure 11 after surface treatment but before HIP. Before surface

TABLE 6

SUMMARY OF THE SURFACE COATINGS AND

TREATMENTS GIVEN THE FIRST SERIES OF

SIMULATED CRACK SPECIMENS

• PVD coated with 250 μm coating of IN-718
• Ceramic coated with Solaramic 5210 coating
• (i) Shot peened surface to 0.015A intensity[a] (ii) Ceramic coated with Solaramic 5210 coating
• (i) Oxidized 6 hr at 816 C in air (ii) Cleaned with HNO_3-HF solution[b], ultrasonic rinse in water and alcohol, air dried at 100 C (iii) Plate of IN-718 welded over surface[c]
• (i) Shot peen to 0.015A intensity (ii) Recrystallize anneal 1 hr. at 954 to 982 C in vacuum
• (i) Shot peen to 0.015A intensity (ii) PVD coated with 250 μm coating of IN-718

(a) "A" is a scale of intensity for shot peening.

(b) The pickling solution consisted of 8 parts H_2O, 2.5 parts HNO_3 and 0.5 part HF. The specimen was pickled 10 minutes at 32 C (90 F).

(c) Electron beam welded.

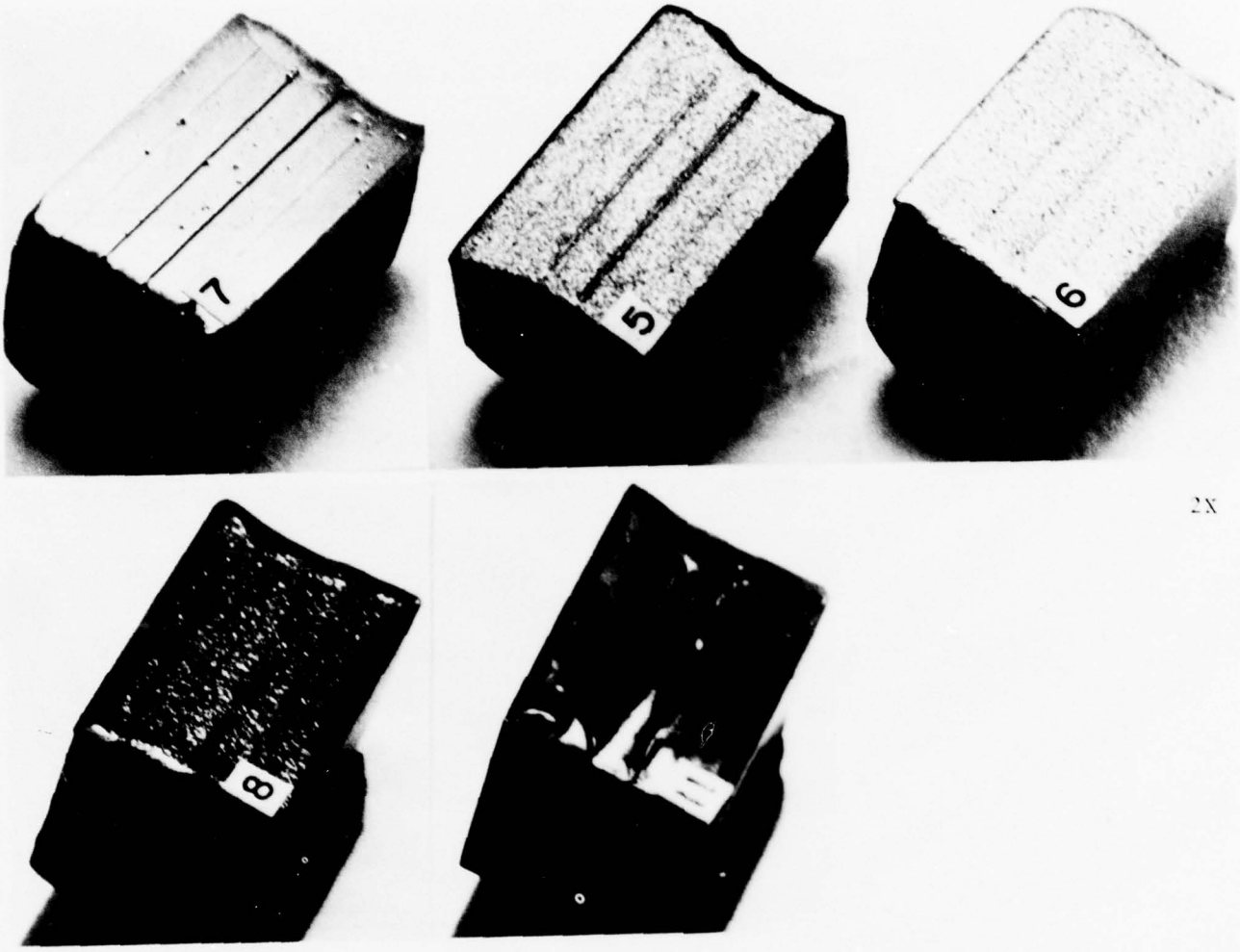

Figure 11. First Series of Simulated Crack Specimens After Surface Treatment and Coating, Before HIP.
No. 7 Is PVD Coated with IN-718 Only, No. 5 Is Shot Peened and Annealed, No. 6 Is Shot Peened and PVD Coated, No. 8 Is Shot Peened and Ceramic Coated, No. 11 Is Ceramic Coated Only.

treatment, the specimens looked similar to Specimen 7 (Figure 11).

Six specimens, one for each condition, were HIP at 1163 C (2125 F) and 103 MPa for 2 hours followed by a 1 hour 1066 C (1950 F) in-situ pressure anneal. After HIP, the specimens were examined visually, helium pressure leak tested, and sectioned for metallographic examination without subsequent aging.

Only the cracks in the shot peened and ceramic coated specimen, No. 8, were found to be completely closed and bonded, Figure 12. The unpeened ceramic coated specimen, No. 11, showed some evidence of partial bonding in the narrower cracks but also showed intrusion of the ceramic coating into the cracks during HIP. The wider cracks were not bridged (Specimen 11, Figure 11), indicating that cracks in the range of 50 to 150 μm wide and wider cannot be bridged by the ceramic coating alone. After HIP, the coated surfaces of both ceramic coated specimens had a thin, 20 μm wide, surface interaction zone resulting from an interaction between the coating and IN-718 substrate during HIP (Figure 13).

It should be noted that very little ceramic coating remained on the surface of the specimens after HIP. There were strong indications that rather than spalling off during cooling, the coating had become sufficiently liquid at the HIP temperature to run off the surface during HIP. Thus, this ceramic coating is able to effectively bridge narrow cracks, especially if the opening is narrowed by prior shot peening. The intrusion of the coating into the cracks can be prevented by shot peening or a PVD coating to bridge the cracks before coating with the ceramic.

Neither of the magnetron PVD coated specimens (Nos. 7 and 6) showed evidence of crack healing. Metallographic examination showed that the PVD coating did not adhere to the peened specimen, No. 6, probably due to insufficient cleaning of the peened surface prior to coating. In the unpeened specimen, the coating adherence was good, and the two narrower cracks (25 and 30 μm wide) appeared to be bridged even though they did not heal. Post-HIP sectioning of this specimen showed that these narrow cracks were propagated nearly all the way through the coating because of the surface-normal-oriented growth tendency of the coating. Typical bridged and unbridged regions over the two narrow cracks are shown in Figure 14. Thus, even the

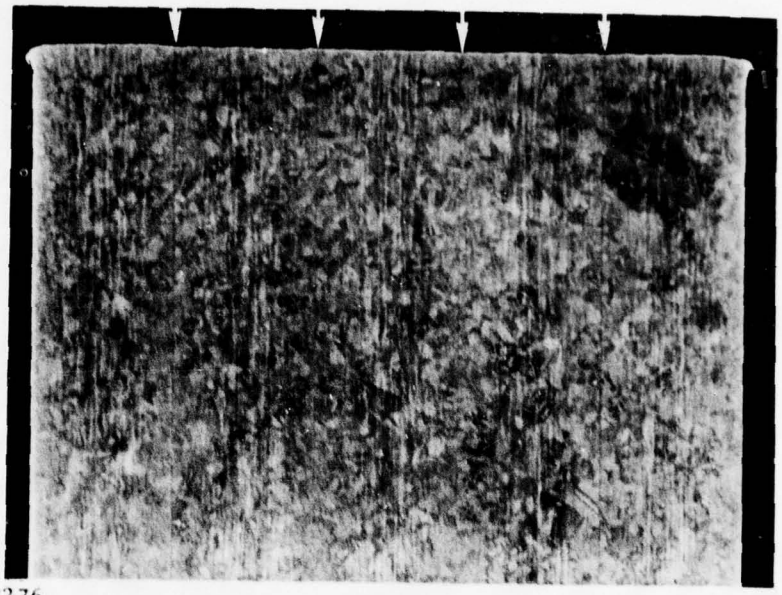

3J276 7X

(a) Cross section of the specimen with the arrows showing the locations of the four cracks

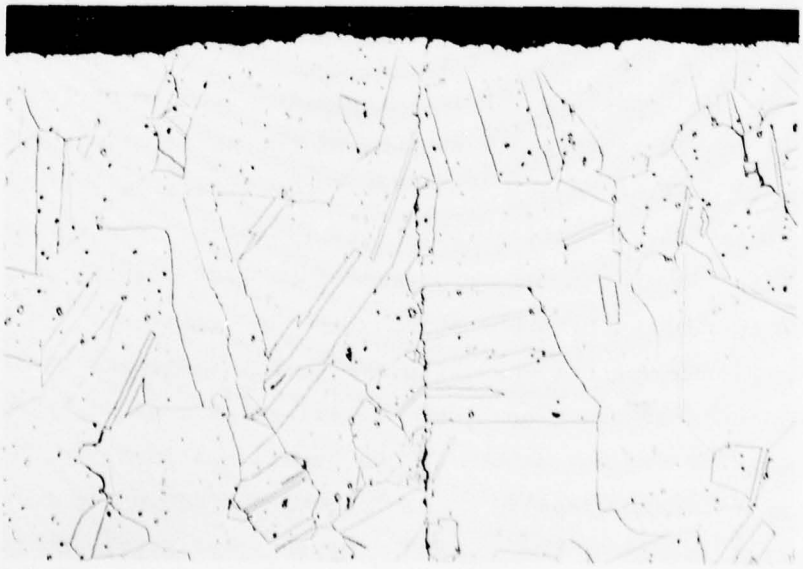

3J267 100X

(b) Typical bond line of the cracks, showing the migration of the bond surface

Figure 12. Simulated Crack Specimen No. 8, Shot Peened and Ceramic Coated then HIP, Showing Crack Closure and Bonding

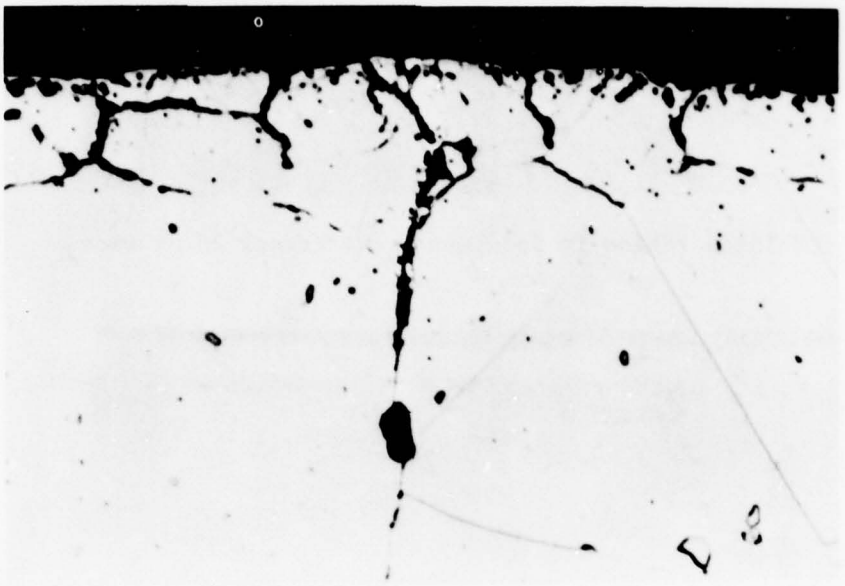

3J268 1000X

Figure 13. Surface Interaction Zone between Ceramic Coating and Inconel-718 Formed During HIP.

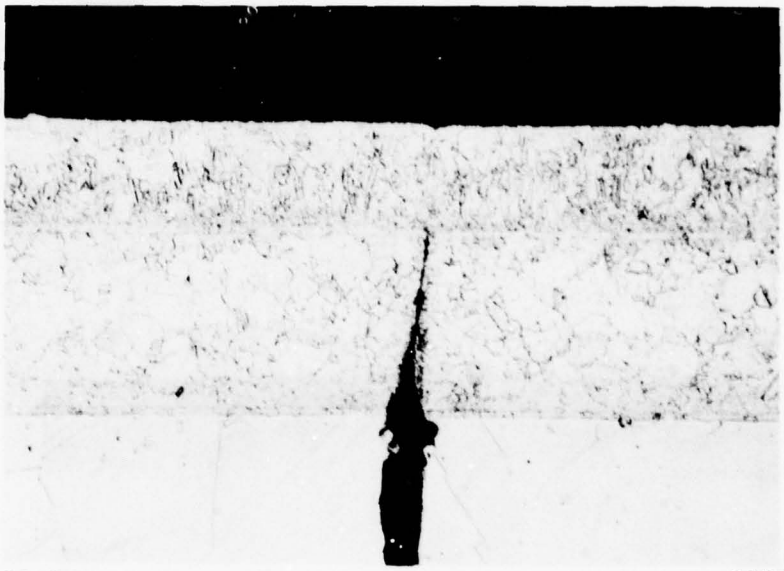

3813VD 213X

(a) Bridged region in Specimen 1 over crack 25 μm wide

3812VD 213X

(b) Unbridged region in Specimen 1 over crack 38 μm wide

Figure 14. Appearance of PVD Coating Over Cracks in Specimen 7, Unpeened Surface, After HIP. The Layering of the Coating Was Caused By an Interruption in Sputtering Power.

narrow, seemingly bridged cracks in the PVD coated specimens did not close and bond because coating defects somewhere along the crack prevented the coating from isolating the crack.

From these results, it is clear that great care is required to get clean surfaces for good PVD coating adherence after surface treatments such as shot peening. Also, although cracks of 25 to 40 μm can be bridged by a 250 μm thick PVD coating of IN-718, ways must be found to ensure that coating defects are eliminated. Possible approaches are multiple coatings and interim mechanical surface treatments such as shot peening.

Of the cracks which were only shot peened and annealed prior to HIP, one of the narrow cracks appears to have partially bonded. The other narrow crack, which was not bonded, exhibited a helium-detectable leak in the weld area adjacent to one end of that crack when checked after HIP. It is possible that the leaky weld prevented crack closure and bonding in this case. The edges of all the cracks were heavily worked by the peening. The edges of the wider cracks were peened well into the crack and exhibited considerable cracking after HIP.

It is interesting that none of the cracks in the shot peened and PVD coated specimen (No. 6) closed, while the narrow crack in the shot peened and annealed specimen (No. 5) did close and bond. Both specimens were shot peened under identical conditions and the narrower cracks were completely peened closed. This would indicate that the recrystallization anneal of the peened layer might help to "heal" together the peened edges of the crack.

No bonding was detected in the oxidized and pickled specimen because of a gas leak defect in the side GTA welds joining the plates together. It is not known, however, whether this leak was generated during welding, oxidation and pickling, or HIP. In this type of specimen a leak in any one of the welds is open to all the cracks because the individual cracks are not sealed, as in the other specimens. Thus no conclusions regarding the bonding of oxidized and pickled surfaces could be drawn from this specimen, but a duplicate specimen was included in the next series of simulated crack specimens.

A second series of simulated crack specimens was designed to expand on the surface treatment/coating sequences, based on the results

of the first series. Twelve 2.5 by 2.5 by 1.9 cm (1 by 1 by 0.75 inch) specimens were fabricated from three coupons of 0.6 cm (0.25 inch) thick IN-718 plate stacked and welded together on three sides. Each coupon had two simulated cracks, one with essentially no width dimension and one having a width of either 20 to 25 μm (0.0008-0.001 in.) or 50 to 100 μm (0.002-0.004 in.).

The twelve conditions selected are shown in Table 7 along with two duplicate conditions from the first series. The rationale for selection of these conditions was as follows. It was concluded from the first series of experiments that an initial surface treatment to mechanically close the cracks considerably enhances the probability that subsequent coating will seal the crack opening. Two types of mechanical surface treatment were selected, glass-bead shot peening and wire brush. Glass bead peening was chosen over steel shot to decrease the intensity of peening on the surface compared to the severe peening given the first series specimens (Figure 11), which significantly altered the surface finish. The glass shot peening used nominally 500 μm diameter bends under 0.30 MPa (44 psi) air pressure at a standoff distance of 7.6 cm (3 inches) or 0.33 MPa (48 psi) pressure at 3.8 cm (1.5 inches) for 1 minute. After coating, a milder peen was used, 0.14 MPa (20 psi) air pressure at 7.6 cm (3 inches) for 10 seconds. The wire brush was a still milder form of treatment to minimize the disturbance to the surface while still partially closing the narrow cracks. Wire brushing has one disadvantage in that it tends to open one edge of a crack while it is closing the other.

It was decided that a coating was required to ensure sealing of cracks even though mechanical closure can be achieved by methods such as shot peening. The lighter peening selected for this series would not be expected to close cracks nearly as effectively as the severe steel shot peen given the first series. In addition, a permanent PVD coating has some advantages which make it desirable to include it in the rejuvenation sequence. For example, it replaces material lost by oxidation or erosion. It also adds material which could be subsequently removed in part, either to provide the desired surface finish to final dimensions or to remove surface reaction layers developed during processing, or both.

TABLE 7

SUMMARY OF MECHANICAL AND COATING TREATMENTS APPLIED TO SECOND SERIES OF REJUVENATION PROCESS DEVELOPMENT SIMULATED CRACK SPECIMENS

Specimen	Treatment[a]	Crack[b] Widths, μm Wide	Narrow	Bridging[c]	HIP	Closure and Bonding[c]	Remarks[d]
1-2	Peen/coat/peen/coat	25	2.5	yes, yes	yes	no, yes	Large crack closed to 3 μm (0.00015 inch) wide: coating broken next to large crack
1-6	Peen/coat	2.5	2.5	yes, yes	yes	yes, no	
2-5	Peen/coat/peen/sand/coat	37	2.5	yes, yes	yes	no, yes	Large crack leaked before HIP
2-1	Peen/coat/SH/peen/coat	62	2.5	yes, yes	yes	no, no	Large crack leaked before HIP
2-6	Peen/coat/SH/peen/coat	100	2.5	yes, yes	no	no, no	Both cracks leaked before HIP
1-1	WB/coat/WB/coat	12	2.5	no, no	no	no, no	Both cracks leaked before HIP
1-4	WB/coat/SH/WB/coat	50	2.5	yes, no	yes	no, no	Small crack leaked before HIP
1-3	VB/coat	2.5	2.5	yes, yes	yes	no, no	One crack leaked before HIP
1-5	Coat/SH/peen/coat	25	2.5	yes, yes	yes	no, no	One crack had offset crack in coating after HIP
2-3	Coat/peen/coat	100	2.5	no, yes	yes	no, no	
2-4	Peen/VB/coat/peen/VB/coat	6	2.5	yes, yes	yes	no, no	
2-2	45 deg tilt coat/peen/coat	53	2.5	no, yes	no	no, no	Cracks visible in coated surface
2[e]	Oxidized/acid clean			Weld Plate	yes	yes	
14[e]	Peen/anneal			yes, yes	yes	no, no	

(a) Peen = glass bead shot peen; coat = 75 to 100 μm thick sputtered IN718 coating; sand = 240 grit dry sand to uniform surface; SH = solution heat treat anneal 1010 C (1850 F), 1 hr, He quench; WB = wire brush; VB = vapor liquid grit honing.

(b) Each specimen contains either a wide and a narrow crack or two narrow cracks.

(c) Notations refer, respectively, to the cracks widths listed in the column to the left.

(d) The specimens were leak tested with pressurized He before HIP.

(e) First generation coupons having 5 laminations - 4 cracks.

Vapor blast liquid grit honing was included because it has been found to provide a good clean surface which enhances the adherence of PVD coatings. It will be used to remove the light oxide coating on the fatigue tested bars before coating, but it would help in closing only the very tight cracks. Sanding was tried because it could simulate a process required to smooth a peened and coated surface.

The PVD coatings had an undesirable tendency to reproduce the substrate surface contour in the coating, resulting in the cracks being extended into the coating for some distance. To avoid this, different sequences of multiple coatings separated by a mechanical surface treatment were investigated. The purpose of the intermediate mechanical treatment was to homogenize the character of the surface of the previous coating so that the subsequent coating would not extend either the cracks or closure faults present in the underlying coating.

To determine whether some angle of coating would be more favorable to crack closure then the usual normal direction, one experiment was tried wherein the specimen was first tilted at 45° to the direction of sputtering. This was then followed by peening and normal coating.

The as-deposited coatings were quite hard, having a hardness of DPH 579 (R_C 52). (Compared to bulk hardness of R_C 21 in HIP material and R_C 42 in STA material). This hardness is probably due to both the fine grain size and aging of the coating at the coating temperature. In this case, solution treating and quenching could possibly increase the grain size and inhibit precipitation hardening so as to decrease the hardness of the coating. This would help to keep the coating from cracking and spalling off during subsequent shot peening of the coating. In addition, this anneal could serve as a recrystallization anneal for the underlying shot peened surface layer as done in the first series of experiments.

Before each coating cycle the specimens were cleaned in the pickling solution described earlier, for 1 minute at 78 C (180 F). After this treatment the specimens were ultrasonically cleaned in water and electronic-grade methyl ethyl ketone, and dried. The methyl ethyl ketone leaves no residue during evaporation after flushing the cracks clean. The specimens were then coated with 100 μm (0.004 inch) thick coatings.

Inspection of the coated specimens showed that the narrow cracks less than 25 μm (0.001 inch) in width were bridged without shot peening to close the cracks. The results with the larger cracks were inconsistent, but in general cracks less than 50 μm wide that had been peened bridged satisfactorily. Larger cracks, and those that were wire brushed, did not bridge. When shot peened after coating, some of the larger cracks showed cracking of the coating next to the crack in the substrate. The coating was evidently too thin and brittle to deform and flow into the substrate crack during peening as desired.

In addition to the second series of 12 specimens, 2 specimens containing four cracks each were included from the first series. These are shown at the bottom of Table 7. One of these is the second specimen to be oxidized then pickled and cleaned to investigate the bonding behavior of oxidized surfaces.

The overall results of the experiments with regard to crack bridging, closure and tightness of crack are summarized in Table 7. Possible leaks through the coating or weld for each crack were looked for in a simple test by pressurizing the specimens in helium at 2.1 MPa (300 psi) to drive gas through any leak into the crack, then transferring the specimen to a methanol bath to detect bubbles of helium gas escaping from the crack. This method will work for a reasonable range of defect sizes, but will not work for either very small or very large defects. None of the cracks in which leaks were detected before HIP closed during HIP. Two of the 12 specimens were not included in the HIP experiment because leaks were detected in both cracks.

After HIP, all of the specimens were sectioned and examined by optical microscopy. Three cracks had definitely closed and bonded. All three were narrow, 2.5 μm wide, and had been peened before coating. Two of these had been given a double sequence of peening and coating.

Typical appearances of the crack-coating intersection and the crack interface along the bond line after HIP are shown in Figures 15 and 16. Figure 15 is representative of Specimen 2-5 also. Figure 15a shows a case where the coating adhered well during HIP and Figure 16a shows a case where the coating did not adhere well. Both adhering and nonadhering coatings

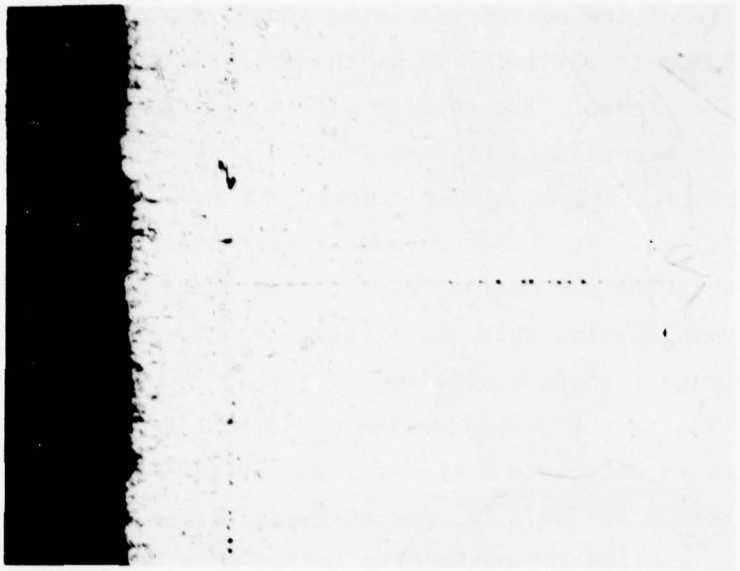

3865VD 213X

(a) Crack and surface of specimen

3866VD 213X

(b) Bond line farther below coated surface

Figure 15. Bridging and Healing of Crack (2.5 μm Width before HIP); Coating Sequence: Peen/Coat, Specimen 1-6.

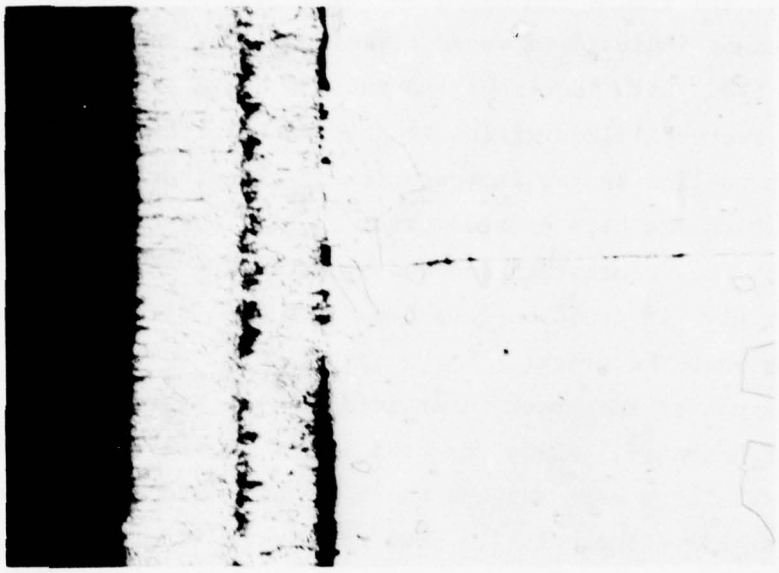

3863VD 213X

(a) Crack and surface of specimen

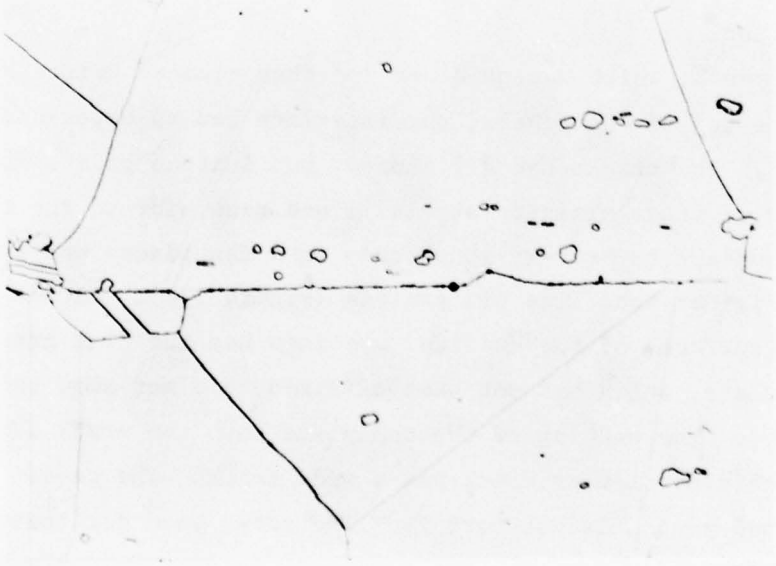

3J565 500X

(b) Bond line farther below coated surface

Figure 16. Bridged and Healed Crack (2.5 μm Width Before HIP); Coating Sequence: Peen/Coat/Peen/Coat, Specimen 1-2.

were also associated with cracks which did not close and bond. The sporadic adherence might indicate improved cleaning of the surface is necessary before PVD. Both Specimens 1-2 and 2-5 had a small cluster of what appeared to be recrystallized grains at the crack-surface intersection (Figure 16a). The bond line at the intersection in both instances shows a slight deviation which may have existed prior to HIP. The recrystallization may thus be caused by the deformation induced by squeezing this region together. Alternatively, it could be caused by localized deformation induced by peening the edges into the crack.

The bond lines of the crack interfaces for the most part etched similarly to a grain boundary. Also, the bond line voids being spherical indicated bonding had occurred. There were regions where grain growth across the bond line did occur during HIP (Figure 16b). However, in many regions the bond did contain a significant amount of porosity or "dirt" (Figures 15 and 16); this bond line porsity or dirt is expected to weaken the bond and is thus undesirable. Improved cleaning techniques for cracks are clearly required to remedy this situation.

In Specimen 2, which was oxidized and then cleaned before having a lid welded over the top of the cracks, the interface had an appearance as shown in Figure 17. The cracks had all closed, but instead of a simple bond line, a layer of finer grained material lined each side of the bonded crack. The bond appears to be very good; only in a few places was the position of the original bond line discernible (Figure 17a). Although both the top and crack surfaces of the oxidized specimen had the fine grained layer, the cover plate, which had not been oxidized, did not show this effect (Figure 17b). The wedging of the top plate into the crack (Figure 14b) happened because this particular crack was a wide crack. The cause for the fine grained region is not certain. The sheet used for these specimens was cold rolled and aged. One rationale is that subsurface internal oxidation or nitride or carbide formation occurred during oxidation and these particles inhibited grain growth in this layer during HIP. Any compositional changes in this reaction zone, e.g. enrichment of nickel, may have aided the diffusion bonding process. This observation is interesting in that it suggests that some oxidation of the surfaces to be bonded, e.g. crack surfaces, may be beneficial in producing surfaces which bond well during HIP.

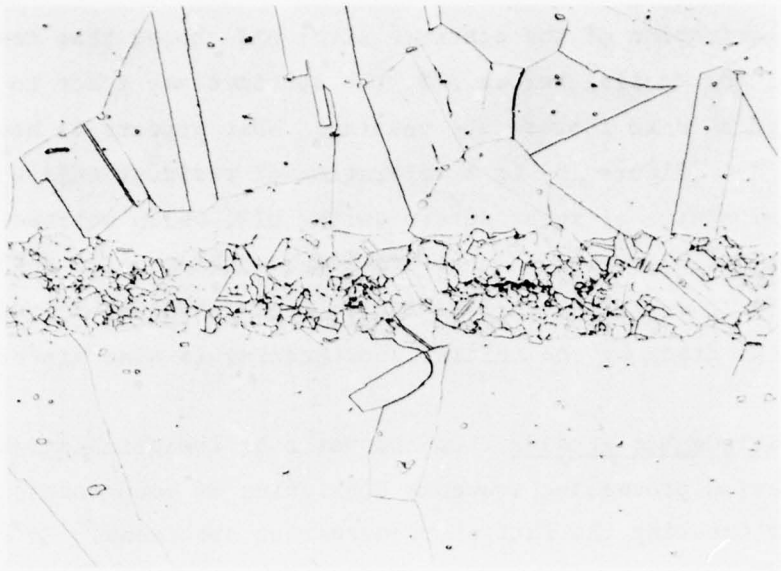

35560 250X

(a) Bond line away from specimen surface

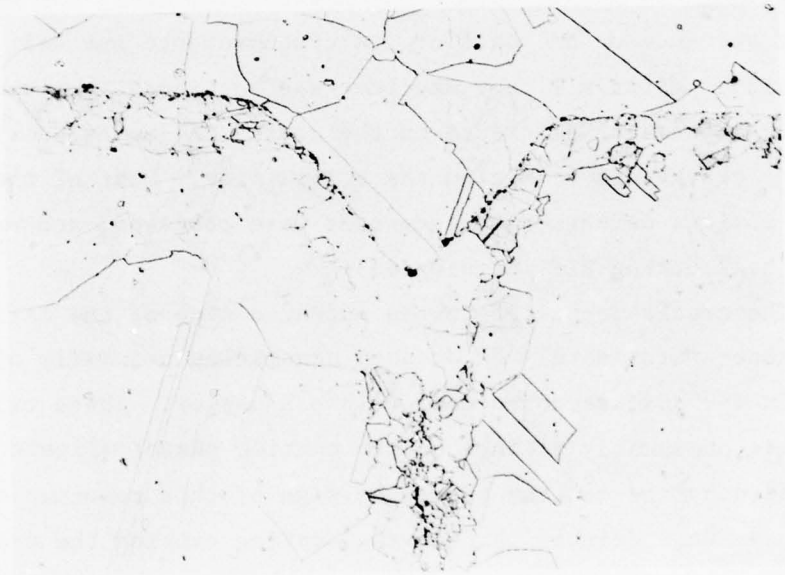

35561 250X

(b) Crack intersection with surface. Top part is the cover plate of the specimen. Vertical fine grained region marks the original crack location

Figure 17. Microstructure of Bond Line and Surface of Oxidized and Cleaned Specimen after HIP. Specimen 2

Examination of the coatings after HIP showed that despite apparent integrity of the coating before HIP, the specimen may react to HIP as shown in Figure 18 to rupture the coating. What appears to have happened in Specimen 2-4 (Figure 18) is a relaxation of residual weld stresses or some other source of shear stress during HIP, which shifted the opposite sides of the crack sufficiently to break the coating above the crack. The shift is only 10 μm at the surface as measured in the micrograph. The partial closing of the crack by the initial shot peening is also visible in Figure 18.

Fatigue Bar Studies. On the basis of these investigations, a pre-HIP rejuvenation processing sequence consisting of peen/coat/peen/coat was selected for treating the fatigue rejuvenation specimens. To evaluate the potential effectiveness of this processing sequence, an investigation of the bridging of secondary cracks in fractured fatigue bars was undertaken. Fractured fatigue Specimen No. 5B-1, containing numerous secondary cracks, was given the coating sequence on one half of its circumference but left uncoated on the other side. After HIP, the specimen was sectioned longitudinally and the relative appearance of cracks on the coated and uncoated sides was compared. Some cracks did remain on the coated side. Most of these were wide cracks and obvious defects in the coating were observed, accounting for the failure to heal during HIP (Figure 19a).

The cracks connected to the uncoated side of the bar all showed a surface zone approximately 30 μm deep consisting primarily of oxidized particles in the surface-connected grain boundaries. These oxidized particles are presumably grain boundary carbide phases (Figure 19b). The cracks bridged by the coating showed no sign of this reaction zone because, although there were defects through the coating causing the cracks not to heal, these passages would be very narrow and therefore getter the gas passing through into the crack.

To minimize the probability of leakage through defects in the PVD coatings during HIP of the fatigue rejuvenation specimens, it was decided that the rejuvenation processing sequence would be supplemented by a ceramic overcoating. This appeared to constitute the surest surface sealing technique on the basis of earlier experiments. It was reasoned

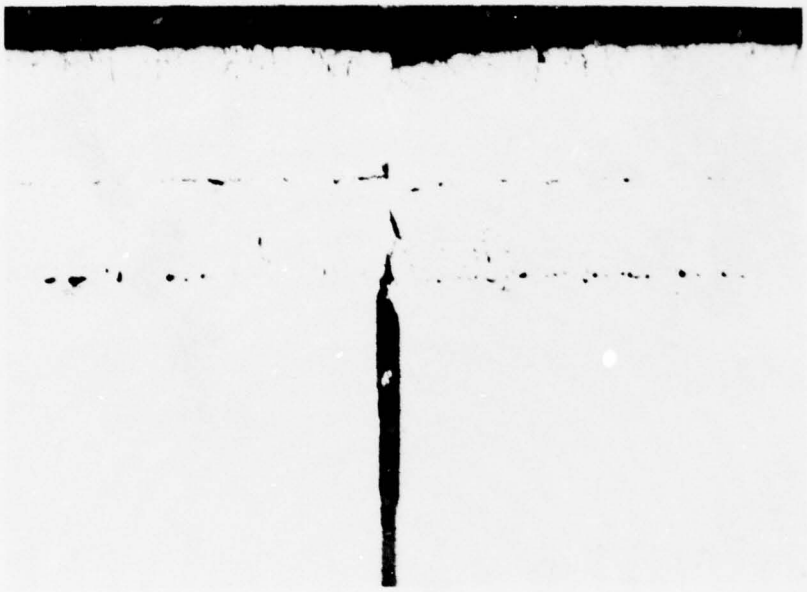

3J573 250X

Figure 18. As Polished Surface of Specimen 2-4 Showing Shift of Opposite Sides of the Crack, Rupturing the Coating.

250X

(a) Crack under coating with defect. Crack opening is about 45 μm

500X

(b) Crack intersecting glass bead shot peened but uncoated surface of specimen

Figure 19. Appearance of Secondary Cracks on Coated and Uncoated Surfaces of Fracture Fatigue Bar 5B-1 after HIP.
The Surface Reaction Zone Which Developed During HIP Extends about 30 μm Deep Below the Surface. Longitudinal Section.

that the use of both coating techniques in tandem might be necessary in practice. The PVD metallic coating would serve to (i) restore dimensional integrity where service-oxidized material had to be removed during pre-rejuvenation cleaning, (ii) act as a barrier to the chemical interaction observed between ceramic coatings and substrate material, and (iii) inhibit intrusion of the ceramic coating into the cracks during HIP. The ceramic overcoat, on the other hand, would serve as the backup surface defect sealing agent, and limit the interaction of the alloy surface with the HIP atmosphere. The final surface and coating treatment used for the fatigue bars was described earlier in the Experimental Procedures section.

APPLICATION OF REJUVENATION PROCESS TO FATIGUE DAMAGE

Baseline Fatigue Properties

Results of the tests useful in establishing the baseline fatigue resistance of IN-718 extruded and STA material are presented in Tables 8, 9, and 10. Recall that all tests were carried out at 538 C. The majority of testing was carried out in argon, there being no discernible difference in the results of tests performed in argon or in air. The quantities Δe^t, Δe^e and Δe^p are defined in the usual way[10]. Results from Tables 9 and 10 are plotted in Figure 20, as the open symbols. Data plotted are for total life. Figure 20a presents these data on the basis of total strain, whereas, Figure 20b presents them on coordinates of plastic strain. It might be noted that, as compared to Figure 20a, data plotted on coordinates of plastic strain range and life in Figure 20b are "spread out". In Figure 20b the plastic strain-life to separation trend line has been established, giving consideration to three major factors:

(1) The distribution of the fatigue failure data
(2) The value of the true fracture strain range (measured from a tensile test) through which the curve should pass
(3) The characteristic slope of such Coffin-Manson plots.

The failure trend curve drawn has a slope of about -0.5, passes through the true fracture strain, and provides a reasonable fit through the failure data. Figure 20a also shows as broken lines two fatigue resistance trend curves established for this material in the corresponding condition, as reported in the literature[14,15]. Note that the data developed as a part of this program tend to fall below these total strain-life trends*. However, when these data are compared on the basis of the plastic strain-life relationship as shown in Figure 20b, they correspond closely, except at lives less than about 100 cycles. This behavior can be attributed to the previously noted differences in the monotonic stress response which showed this material on the low side

---

* The material in this program, although extruded, retains much of the character of an as-cast material except it has fine grain size. The broken line data is for wrought material.

TABLE 8

RESULTS OF INCREMENTAL PREDAMAGE STUDY OF STA IN-718[a]

Specimen Number	Damage Level,[b] percent	Strain Range, percent: Control Δe^t	Strain Range, percent: Stable Components Δe^e	Strain Range, percent: Stable Components Δe^p	Stable Stress Range: MPa	Stable Stress Range: ksi	Number of Cycles: Of Prior Damage	Number of Cycles: To Initiation[c]	N_i/N_f,[d] percent	Remarks
5C-1	73	0.80	0.705	0.093	1250	181.4	4800	(4400)	(66)	Valid
5D-2	~100	0.805	0.667	0.128	1280	185.7	6400	(-)[e]	--	Valid
8D-1	24	0.795	0.705	0.090	1264	183.3	1600	(-)[f]	--	Valid
8D-2	48	0.805	0.695	0.105	1273	184.6	3200	(3000)	(45)	Valid
11B-1	40	1.32	0.75	0.57	1406	203.9	400	(320)	(32)	Valid
11C-1	20	1.30	0.75	0.55	1440	208.9	200	(-)[f]	--	Valid
11C-2	60	1.32	0.76	0.56	1388	201.3	600	(268)	(27)	Valid
12C-1	80	1.32	0.76	0.56	1408	204.3	800	(180)	(18)	Valid

(a) Fully reversed strain controlled testing.
(b) Based on lives to fracture of 6620 cycles at 0.80 percent and 1000 cycles at 1.32 percent, where these lives to fracture are estimated based on the results of Table 9.
(c) Reported are the life to visible cracking and that found by back extrapolation of the asymmetic load drop; visible cracking is tabulated in parentheses.
(d) Ratio of cycles to initiation to cycles to fracture based on the least of the entries in Note (c) and assuming a life to fracture based on mean response.
(e) Back extrapolation is inaccurate because the number of post-initiation cycles is zero or too small.
(f) No visible cracks.

TABLE 9

RESULTS OF EXPERIMENTS TO ESTABLISH THE BASELINE FATIGUE RESISTANCE OF STA IN-718[a]

Specimen Number	Strain Range, percent			Stable Stress Range		Number of Cycles			N_i/N_f,[d] percent	Comments on Failure
	Control	Stable Components				To Initiation[b]	To Initiation[c]	To Fracture		
	$\Delta\varepsilon^t$	$\Delta\varepsilon^e$	$\Delta\varepsilon^p$	MPa	ksi					
3B-1	2.12	--	--	1923	279.0	(e)	--	--	--	(e)
3C-1	2.00	0.83	1.17	1581	229.5	(70)	240	248	(29)	Valid
3E-2	1.46	0.73	0.73	1458	211.5	(220)	459	471	(47)	Valid
4D-1	1.01	0.74	0.27	1317	191.0	2,359(-)	3,057	3,524	67	Valid
4D-2	0.525	0.502	0.023	917	133.4	44,590(e)	--	--	--	(e)
5B-1	2.03	0.79	1.24	1599	231.9	(80)	--	84[e]	(e)	(f)

(a) Fully reversed strain controlled testing.
(b) Back extrapolated from asymmetric load response; visual record in parentheses when observed early in the life.
(c) Cycles to 5 percent asymmetric load drop.
(d) Ratio of cycles to initiation to cycles to fracture; initiation values as indicated in Note (b).
(e) Test terminated prematurely due to test system instabilities.
(f) Valid to initiation; extensometer slipped subsequently.

TABLE 10

RESULTS OF EXPERIMENTS TO ESTABLISH THE INFLUENCE OF REJUVENATION PROCESSING ON THE BASELINE FATIGUE RESISTANCE OF IN-718[a] (All tests at nominally 0.8 percent strain range.)

Specimen Number	Condition[b]	Strain Range, percent: Control $\Delta\varepsilon_t$	Stable Components: $\Delta\varepsilon_e$	Stable Components: $\Delta\varepsilon_p$	Stable Stress Range: MPa	Stable Stress Range: ksi	Number of Cycles: To Initiation[c]	Number of Cycles: To Initiation[d]	Number of Cycles: To Fracture	N_i/N_f,[e] percent	Remarks
2B-1	STA	0.80	0.65	0.15	1278	185.4	3,985 (3,275)	4,235	5,237	76 (63)	Valid
2C-1		0.80	0.691	0.109	1239	179.7	42,700 (--)	45,800	45,960	91	Valid
3C-2		0.793	0.688	0.105	1211	175.7	5,160 (--)	6,971	6,985	74	Valid
4C-1		0.79[f]									Valid
4C-2		0.80	0.60	0.20	1242	180.2	5,550 (--)	6,775	9,625	58	Valid
7C-1		0.798	0.69	0.108	1308	189.7	3,660 (--)	4,450	6,398	57	Valid
11B-2		0.808	0.683	0.125	1253	181.7	4,080 (--)	4,530	4,855	84	Valid
3D-1	STA+H	0.798	0.698	0.10	1275	185.0	-- (--)	--	6,467	--	Valid
3D-2		0.80	0.718	0.082	1313	190.4	4,617 (3,000)	5,835	6,110	76 (49)	Valid
4B-2		0.80	0.69	0.11	1279	185.5	6,207 (--)	7,345	9,016	69	Valid
2B-2	STA+C+H	0.80	0.69	0.11	1275	184.9	9,700 (--)	10,070	10,400	93	Valid
3B-2		0.80	0.672	0.128	1288	186.9	10,465 (--)	12,845	14,312	73	Valid
12C-2		0.80	0.67	0.13	1270	184.3	9,765 (--)	10,700	12,390	79	Valid

(a) Fully reversed strain controlled testing.
(b) STA: solution treated and aged, H: hot isostatically processed. C: physical vapor deposition plus ceramic coated.
(c) Back extrapolated from asymmetric load response; visual record in parentheses when observed early in the life.
(d) Cycles to 5 percent asymmetric load drop.
(e) Ratio of cycles to initiation to cycles to fracture; initiation values as indicated in Note (c).
(f) Test terminated prematurely due to test system instabilities.

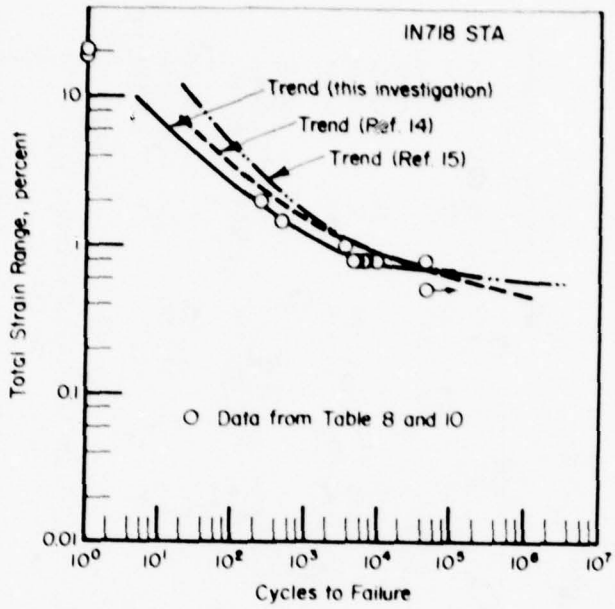

a. Total strain range

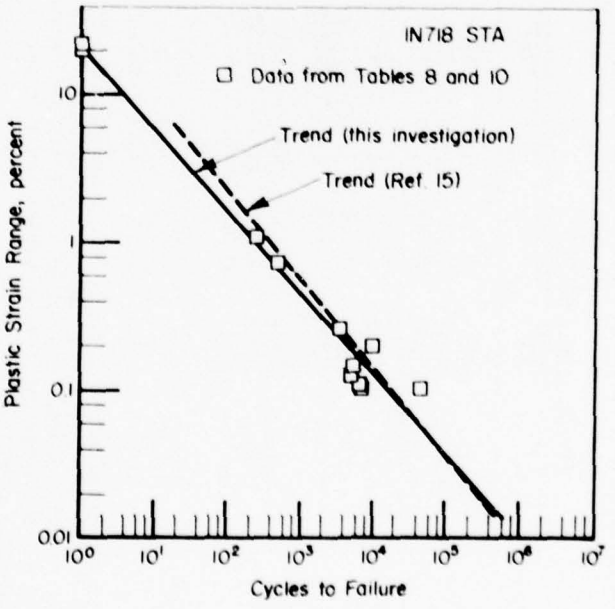

b. Plastic strain range

Figure 20. Life Response for Fully Reversed Strain Control of IN-718 in the STA Condition

of the trend curves at 538 C (Figure 5). Plastic strain, therefore, provides a common basis to compare fatigue resistances, at least on the basis of total life.

Total Life

With respect to the results of six valid baseline tests at the selected strain range for HIP rejuvenation in this program (0.8 percent)*, of 16,149 (Figure 20, Table 10). Based on these six results, the mean and dispersion are strongly biased by an apparent outlier (Specimen 2C-1) for which the life was 45,960 cycles. Because of this inordinately long life, a second test was performed using a specimen from Bar 2, the life being 5237 cycles. It was, therefore, concluded that the result for 2C-1 was an outlier and not representative of Bar 2 material. Excluding this result, the mean life to fracture for the baseline 0.8 percent case is 6620 cycles with a standard deviation of 1887 cycles. The corresponding coefficient of variation is 29 percent.

Crack Initiation Life

As noted in the tables, the number of cycles to crack initiation, N_i, is herein defined as that life at which the tensile component of the cyclic stress response first began decreasing asymmetrically as compared to the stable compression response. Also included in some cases is the life at a 5 percent load drop. Such a definition obviously includes a portion of the life spent propagating the fatigue crack and is therefore an upper bound on the actual N_i. For the baseline 0.8 percent case, the results in Table 10 (excluding Specimen 2C-1) give a mean cycles to initiation, N_i, of 4487 cycles with a standard deviation of 819 cycles, giving a coefficient of variation of 18 percent.

Alternatively, results reported in Tables 9 and 10 are also useful in establishing the relative fractions of life spent initiating and propagating fatigue cracks in these tests. Such a demarcation is essential to establish predamage levels for pre- and post- crack initiation damage rejuvenation studies.

A value for N_i can also be obtained by examining its variation with strain amplitude. Data from the tabulations of N_i/N_f where N_f is the cycles to fracture have been plotted as a function of strain range in Figure 21.

---

* For rationale in selecting 0.8 percent for $\Delta\varepsilon^t$ see Test Program Section.

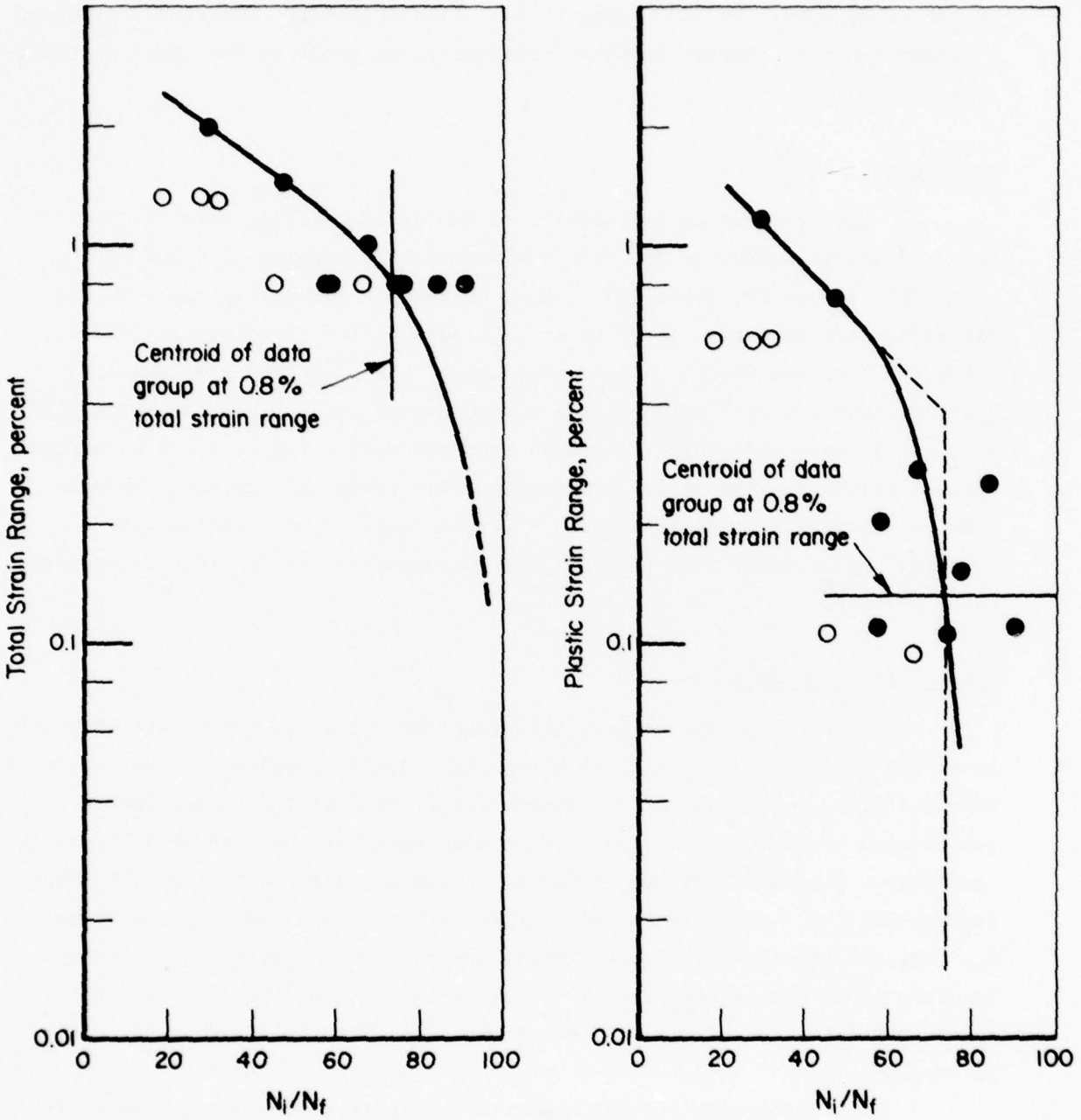

a. Total strain range

b. Plastic strain range

Figure 21. Fractions of Life Spent in Crack Initiation and Crack Propagation

The solid points represent actual observations, whereas the open symbols represent results from the incremental damage study (Table 8) and are, therefore, based on an assumed (mean) fracture life established in other tests. Based on the upper bound trend shown in Figure 21a and the characteristic dominance of stress (elastic-strain) on fatigue resistance at longer lives (total strain ranges less than 0.70 percent) shown in Figure 20, the upper bound trend for the plastic strain range is constructed as the solid line in Figure 21b. For purposes of convenience later on, this trend is assumed to be represented by the bilinear trend shown as the broken line. Based on this bilinear representation, the value of the ratio N_i/N_f is 0.73 at plastic strain ranges less than 0.375 percent (total range of about 1.10 percent). Since the total life (life to separation), shown as the solid line in Figure 20, represents the sum of the life fractions spent in crack initiation and propagation, an initiation trend curve can be obtained by subtracting the number of cycles spent in crack propagation, computed using the trend curve in Figure 21, from the number of cycles to failure computed from the solid curve in Figure 20. This line corresponds closely with the initiation data which are shown by the open symbols in Figure 22.

Crack Propagation Life

Given the scatter in the results of Figure 21, it is difficult to establish whether the ratio of N_i/N_f remains constant at plastic strain ranges less than 0.375 percent. Analytical techniques used in the previous study of Ti-6Al-4V[4] could be used to aid in such an assessment. However, the material constants necessary to compute the crack propagation period are lacking. Therefore, the number of propagation cycles included in the previously adopted definition for crack initiation cannot be directly ascertained. Indirect estimates of N_i based on early visual sightings of the specimens during the fatigue test indicated that, in extreme cases, this definition actually includes propagation periods as great as 10 percent of the total life. With respect to the question of whether N_p or N_i/N_p is constant, the only remaining alternative to provide an answer is to examine the statistical variation in crack propagation period as compared to that for total life and cycles to

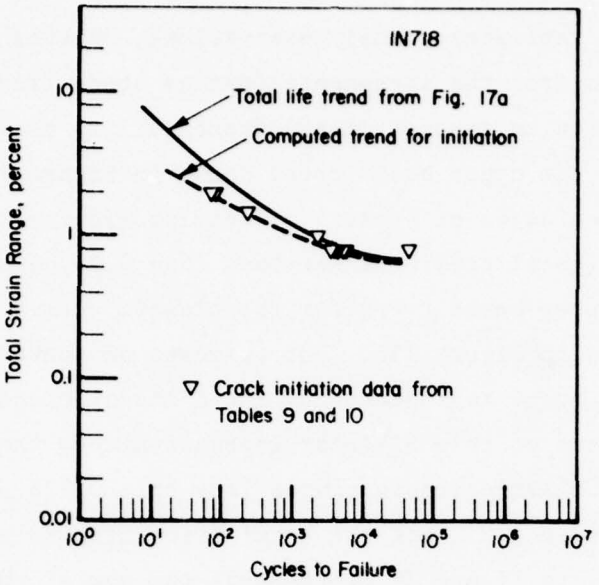

a. Total strain range

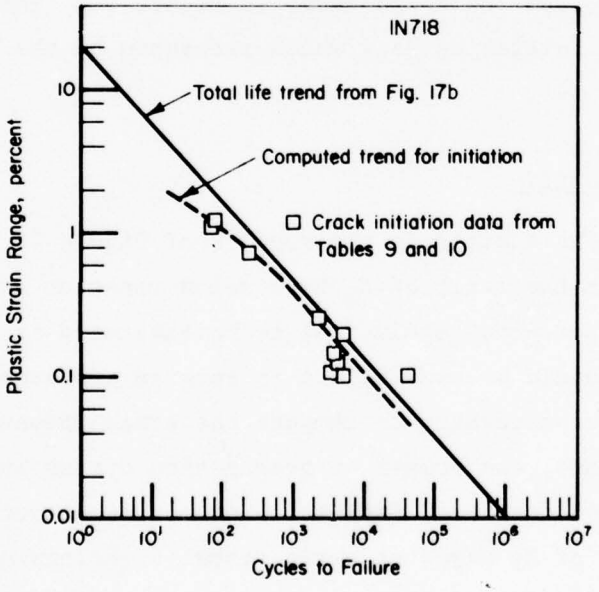

b. Plastic strain range

Figure 22. Crack Initiation Fatigue Life Resistance of IN-718 in the STA Condition

crack initiation. The five baseline test results in Table 10 bear directly on this computation; the specimens being 2B-1, 2C-1, 3C-2, 4C-1, 7C-1, and 11B-2 (with the outlier 2C-1 being excluded). As noted in the previous section, the initiation statistics are a mean of 4487 cycles with a standard deviation of 819 cycles, giving a coefficient of variation of 18 percent. The corresponding propagation statistics are 2133 cycles and 1308 cycles, giving a coefficient of variation of 61 percent. Clearly, there is less relative scatter in the initiation data, at least in the context of total strain. The corresponding statistics for the ratio of N_i/N_f reflect this, yielding a coefficient of variation of 19 percent. Based on these results, it may be concluded that the character of the initiation data dominates the character of the total life, the crack propagation period being quite variable and perhaps not constant for a given total strain. Unfortunately, no direct inference can be drawn.

Other Baseline Data Analysis

It is worthwhile to examine the remainder of the pertinent baseline data to establish to what extent they correspond with the results considered thus far. These five results, from Table 8, for Specimens 5C-1, 8D-2, 11B-1, 11C-2 and 12C-1 are plotted as open triangles on coordinates of each of total and plastic strain versus life in Figure 23. Because these tests were not taken to failure, only crack initiation results are available. Note that for these data, the crack initiation trend replotted on these figures from Figure 22 serves as an upper bound on life. This is a result of using the upper bound on the ratio N_i/N_f (Figure 21) to establish these initiation trend curves. Also plotted in this figure are the initiation data developed as a part of the predamage processing of the fatigue bars to be rejuvenated (as reported in Table 11). Both results for Specimens 7B-1, 7B-2, 7C-2, 8B-1, 11D-1, 12B-1 and 12B-2, for which initiation life was measured, and specimens 5C-2, 5D-1, 7D-1, 7D-2, 8B-2, 8C-1, 8C-2 and 9B, which define a lower bound on initiation because initiation was not observed, are included. Data which define initiation are shown as open squares, whereas data which bound initiation below are indicated by crosses. Clearly, these additional data

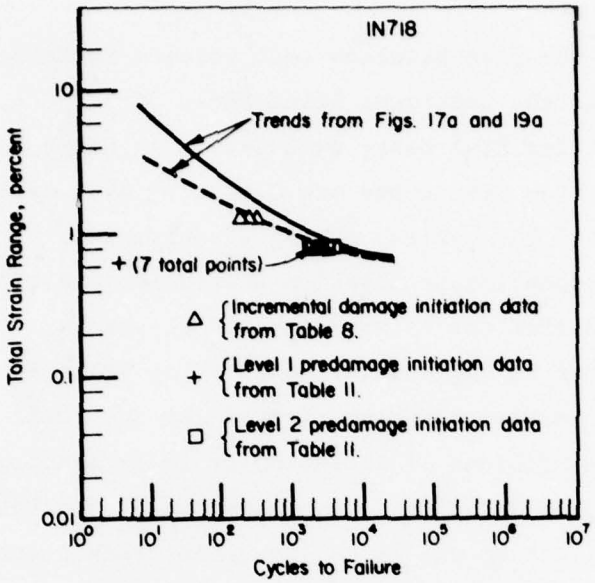

a. Total strain range

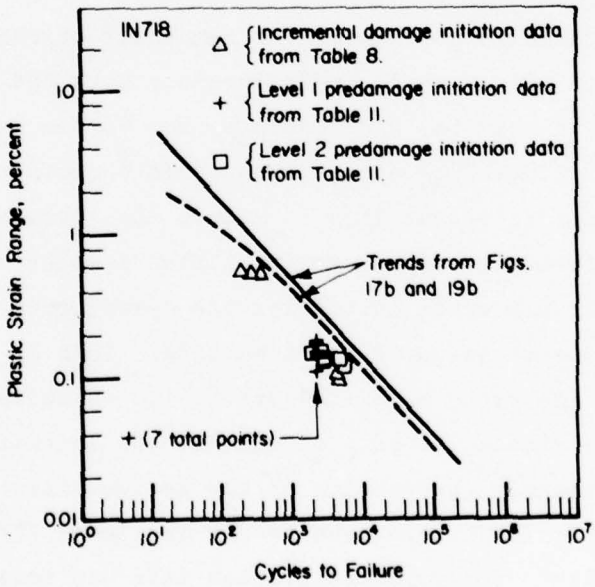

b. Plastic strain range

Figure 23. Comparison of Initiation Data from Incremental Damage and Predamage Studies with Baseline Trends

suggest that the ratio of N_i/N_f may be less than that indicated by the upper bound curves shown in Figure 21, or may not be constant at all. Based on the total initiation data set (14 specimens), the mean life to initiation at the program total strain range of 0.8 percent is 3487 cycles, with a standard deviation of 1119 cycles. This is in strong contrast to the results of Figure 21 and the mean fracture life for this condition which show that the average life to crack initiation is 4833 cycles*. This difference is apparently due to the fact that Figure 21 provides an upper bound on initiation. Given the same average fracture life for the complete data set, the value of N_i/N_f is 0.53**.

The above value of 0.53 is less than that reported in the literature for similar material (wrought bar in the STA condition) and testing environment, when initiation is defined as the crack length observed for decohesion of a heavy shear band (defined as a thin deformation twin) extending over a distance of one or two grains[15]. In that study, developing such decohesion cracks about 70 μm long took about 70 percent of the life. If this result can be considered to mean that N_i/N_f as shown in Figure 21 (73 percent) is correct, then the average number of cycles to fracture for this total data set (including all 14 specimens) would be less than the mean of 6620 cycles for the reduced data set (including only the five specimens from Table 10, Figure 20). In this case, the mean fracture life would be 4777 cycles***, about 72 percent of, or 1843 cycles less that, 6620 cycles. This mean of 4777 cycles lies just within one standard deviation of the 6620 cycle mean. Finally, note that both the 4777 cycle mean and the 6620 cycle mean lie above the assumed lower bound for initiation of 2100 cycles. Initiation occurred after 2100 cycles in all but one case (Specimen 7C-2). As such, the propagation period, N_p, ranges from 6620-1925 = 4695 cycles to 4777-2100 = 2677 cycles at the extremes of the observed results.

Consider now the influence of the rejuvenation process on the baseline extruded plus STA IN-718 fatigue resistance.

---

* Assuming $N_i/N_f = 0.73$ and $N_f = 6620$.

** Given $N_i = 3487$ and $N_f = 6620$; $N_i/N_f = 0.53$.

*** Given $N_i = 3487$ cycles and $N_i/N_f = 0.73$; $N_f = 4777$ cycles.

Influence of Rejuvenation Processing on Baseline Properties

Figures 20 to 23 document graphically the baseline fatigue resistance of the STA IN-718 at 538 C, these plots being derived from data in Tables 8, 9, 10 and 11. As noted in the approach and detailed in the actual test matrix, Table 1, one of the purposes of this program is to asses the relative influence of the processing parameters on the fatigue properties so that the effect of the rejuvenation on fatigue damage can be determined. The purpose of this section, then, is to address data developed to isolate the influence of the processing parameters on the baseline fatigue resistance. Data useful in this assessment, in addition to that discussed thus far, are reported in Table 10.

Data reported in Table 10 are plotted in Figure 24. Figure 24a plots these data as open symbols on coordinates of total strain and life, along with the initiation and fracture trends taken from Figures 22 and 20 respectively. Note that for the sake of clarity, only the fracture data (open symbols) are reported in Figure 24a, whereas Figure 24b includes initiation data (slashed symbols). It is evident that the rejuvenation processing gives rise to a marginally increased total fatigue resistance on a total strain basis (Figure 24a). The coat plus HIP treatment (C + H, data shown as triangles) has a somewhat larger beneficial effect than HIP alone (H, data shown as squares). Now, with reference to Figure 24b, note that while the same trends present in Figure 24a exist here, the choice of a plastic strain basis for data comparison tends to (i) spread out the data, and (ii) suggest, because of a reduction in apparent scatter, that the improvement in fatigue resistance for both initiation (slashed symbols) and total life is not as great as for total strain. Nevertheless, there is an improvement for each of the H and C + H treatments.

A direct comparison of the mean values of fatigue life for the three baseline conditions is as follows. The STA condition had a mean life of 6620 cycles, with a standard deviation of 1887 cycles; the H condition had a mean life of 7197 cycles with a standard deviation of 1585 cycles; and C + H condition had a mean life of 12,367 cycles with a standard deviation of 1956 cycles.

TABLE 11

RESULTS OF THE FATIGUE EXPERIMENTS AFTER HIP TO ASSESS FEASIBILITY OF HIP REJUVENATION OF FATIGUE DAMAGE (All Tests at Nominally 0.8 Percent Strain Range)

Specimen Number	Damage Level[a]	Rejuvenation Treatment After Damage[b]	Strain Range, percent Control	Stable Components		Stable Stress Range		Number of Cycles Before Rejuvenation		After Rejuvenation		Total Life	Remarks	Crack Initiation Site[e]
			$\Delta\varepsilon^t$	$\Delta\varepsilon^e$	$\Delta\varepsilon^p$	MPa	ksi	Prior Damage	To Initiation[c]	To Initiation[c]	To Fracture			
5C-2	1	STA+C+H	0.80	0.715	0.085	1350	195.8	2,100	--	7,000	15,215	17,315	Valid	Normal
5D-1	1		0.795	0.725	0.07	1296	188.0	2,100	--	8,750	9,650	11,750	Valid	Normal
7C-2	1[d]		0.80	0.735	0.065	1291	187.3	2,100	1,925	2,800	11,628	13,550	--	Flaw
7D-1	1		0.79	0.74	0.05	1341	194.5	2,100	--	3,920	5,768	7,868	Valid	Flaw
7D-2	1		0.80	0.737	0.063	1375	199.5	2,100	--	4,894	6,702	8,802	--	Flaw
8B-2	1		0.795	0.707	0.088	1306	189.5	2,100	--	6,915	8,073	10,173	Valid	Normal
8C-1	1		0.80	0.695	0.105	1263	186.1	2,100	--	960	8,742	10,842	Valid	Flaw
8C-2	1		0.793	0.710	0.083	1268	184.0	2,100	--	4,505	4,935	7,035	Valid	Normal
9B	1		0.795	0.687	0.108	1264	183.4	2,100	--	2,710	3,466	5,566	Valid	Flaw
7B-1	2	STA+C+H	0.805	0.69	0.115	1304	189.2	3,515	2,160	8,150	9,709	13,224	Valid	Normal
7B-2	2		0.805	0.672	0.133	1257	182.4	3,625	2,370	1,180	2,147	5,772	Valid	Flaw
8B-1	2		0.795	0.677	0.118	1287	186.7	3,962	2,600	1,663	2,159	6,121	Valid	Flaw
11D-1	2		0.793	0.702	0.098	1294	187.7	3,915	2,550	4,062	12,516	17,431	Valid	Flaw
12B-1	2		0.795	0.725	0.070	1357	196.9	4,640	3,290	4,980	5,674	10,314	Valid	Flaw
12B-2	2		0.80	0.73	0.070	1316	190.9	5,440	4,090	4,050	5,689	11,129	Valid	Flaw

(a) Damage levels as defined in text: 1, preinitiation; 2, post initiation.

(b) See note (b) on Table 10.

(c) See note (c) on Table 10.

(d) Because a crack formed, this result is really a part of the Level 2 data set.

(e) Describes the appearance of the crack initiation site on the fracture surface. 'Normal' indicates the crack initiation site had the same appearance as the initiation sites of the specimens in Table 10, C+H condition, which had not been predamaged. 'Flaw' indicates the initiation site to be semi-circular, relatively smooth, region about 0.5 to 2 mm long and 0.25 to 1 mm deep, immediately adjacent to the original specimen surface.

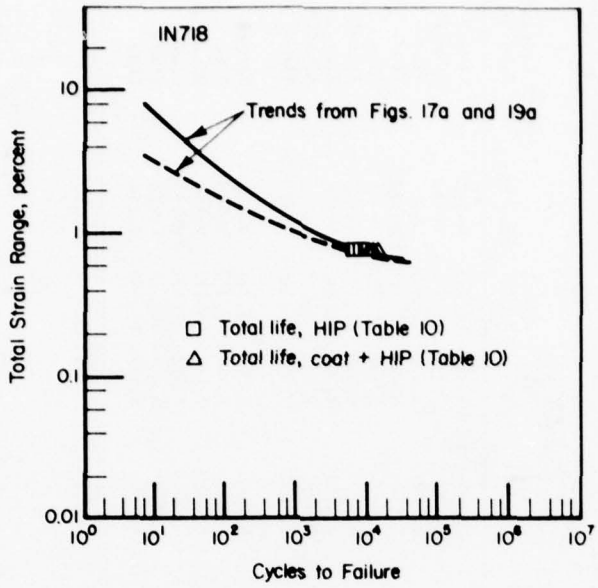

a. Total strain range

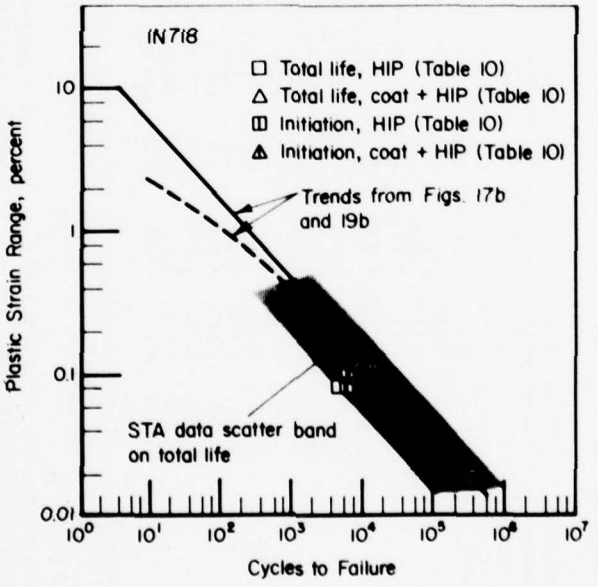

b. Plastic strain range

Figure 24. Influence of HIP on the Baseline Fatigue Resistance of IN-718

Based on the results reported for the influence of HIP on the microstructure, one might surmise that the increased fatigue resistance is due in part to the homogenization of the microstructure described earlier (Figure 9). If homogenization removed potential crack initiation sites associated with coarse, brittle phases and weak interphase interfaces, it would be expected to impact most substantially on the crack initiation stage of life, as detailed below.

Simple statistical calculations are useful in assessing to what extent the improvements in total life may be traced directly to the initiation stage. First, with respect to the baseline data set (5 specimens, Table 10), the mean life to crack initiation (excluding as before, the outlier, Specimen 2C-1) is 4487 cycles with a standard deviation of 819 cycles. In contrast, the mean initiation life for the HIP processed bars (Table 10) is 5412 cycles with a standard deviation of 1124 cycles, while that for the coated plus HIP processed bars (Table 10) is 9976 cycles, with a standard deviation of 424 cycles. As such, on the average, HIP gives rise to an increase in life to initiation of 925 cycles, whereas the surface treatment and coating aspect contributes 5489 cycles of increased life when used in conjunction with HIP. With respect to the corresponding results for improvements in total life, note that for the HIP condition the increase in initiation and fracture lives correspond closely - 943 cycles in total life and 925 cycles in initiation life. Likewise, for the coated plus HIP condition; the further life increase is 4804 cycles, whereas the increase in initiation life is 4564 cycles. It can, therefore, be concluded that more than 95 percent of the increase in total life is due to changes in the crack initiation fatigue resistance.

For the same baseline block of data, the average crack propagation period is 2321 cycles with a standard deviation of 1258 cycles. The mean propagation period for the H case is 2151 cycles and that for the C+H case is 2391 cycles, whereas that for the complete set, including data for both conditions (11 specimens), is 2309 cycles, with a standard deviation of 1178 cycles. Thus, one can conclude that the propagation period is apparently insensitive to the rejuvenation processing steps. On the other hand, the initiation stage is not.

The reasons for the modest increase in the baseline life for HIP alone and the substantial increase after coating and HIP together cannot be simply isolated. The most obvious effect of HIP that could

be expected to increase fatigue resistance is the homogenization of the microstructure. Numerous near-surface and internal cracks associated with inhomogeneities were observed after fatigue testing the STA specimens. This internal cracking was absent in specimens fatigue tested after HIP.

There are two other effects to consider the effect of the grain growth occurring during HIP and the effect of surface treatment and coating. The effect of grain growth is usually to decrease fatigue life with increasing grain size. The grain size of a number of H and C+H fatigue specimens was measured after fracture, including predamaged specimens from Table 11. Although there was a trend towards increasing N_i with increasing grain size, the range of grain size was too limited and the scatter in the N_i was too great to give a definitive indication of the grain size dependence of the initiation life. Excluding the H condition, the grain sizes for the specimens in Tables 10 and 11 were in the range 170 to 260 μm (mean planar intercept), with the baseline C+H specimens having a grain size range of 186 to 201 μm (2 of 3 specimens measured). The baseline specimens in the H condition showed a size range of 370 to 420 μm (2 of 3 specimens measured). If the ratios of the mean initiation lives are compared to the ratios of possible grain size dependences of the initiation lives, the possibility of accounting for the differences in life by grain size differences emerges. The ratio of the initiation lives for the H and C+H baseline conditions (Table 10) is 5412/9977 = 0.54. The ratio predicted by an inverse grain size dependence of life is 0.49 and that predicted by an inverse square root grain size dependence is 0.70.

The effect of surface treatment can either increase or decrease fatigue life. The specimens in the H condition were machined in the STA condition, then HIP. Thus, machining could have caused small surface cracks associated with brittle phases or weak interfaces intersecting the surface to develop. These small surface cracks would not be removed by HIP and could conceivably shorten life after HIP. By surface treatment, shot peening and coating the machined surface before HIP, these small defects would be healed. In addition the coated specimens appeared to have a shallow, variable-depth, layer of nominally finer grains about 15 μm deep at the original surface of the specimen. These presumably resulted

from recrystallization of the shot-peened layer. In addition, the coating itself was fine grained and approximately 15 μm of the original 75 μm thick coating remained on the specimen after polishing the surface for post-HIP fatigue testing. The effects of these fine-grained layers would tend to inhibit crack initiation and thereby prolong the fatigue life.

The large increase in life shown by the coated and HIP control specimens was unexpected, since the HIP-only specimens included in a preliminary HIP run to check the effect of the HIP conditions on the baseline fatigue properties had shown only a modest increase over the STA baseline life. The coated, undamaged specimens were included in the final HIP run along with the predamaged fatigue specimens after the coating parameters had been defined. Therefore, instead of having a situation where the processing variables had little effect on the baseline life as originally intended, the processing had a large effect on the reference lifetime, compared to the number of predamage cycles.

Rejuvenation of Predamaged Specimens

Rejuvenation data for damage Levels 1 and 2 are tabulated in Table 11, whereas the corresponding baseline data are reported in Table 10. It is important to note that while each of the tests performed to develop these data was done at nominally the same total strain range (0.80 percent), the corresponding stable plastic strain range varied from 0.82 to 0.20 percent. The majority of the data, however, were grouped between 0.10 and 0.15 percent plastic strain range. In that it has often been argued that plastic strain controls the rate of fatigue damage accumulation in the life regime of interest in this program, a broad dispersion in plastic strain would be expected to mask otherwise real trends in these data if compared only on the basis of total strain range. However, the dispersion on plastic strain is very small in this study, and the plots of N_i and N_f versus plastic strain range had little effect on reducing the scatter in Figures 20 and 22. The results will, therefore, be considered only in the context of total strain. However, because the rejuvenation steps and the possible presence of unhealed damage apparently do influence the initiation stage of life,

it is essential to assess the feasibility of HIP rejuvenation for both pre- and post-crack initiation predamage levels, as well as for the total life. Consequently, all the data will first be considered by direct comparison of total life with the reference C+H baseline life, then effects of a typical crack initiation will be assessed, and finally rejuvenation in terms of the effect of coating and HIP on the initiation life of predamaged specimens will be addressed.

Total Life Analysis

Data for the baseline cases of: as extruded and STA IN-718, H and C+H, are shown in Figure 25a. A total of 12 data points are presented in this bar graph (6 for STA, 3 for STA+H and 3 for STA+C+H). As just discussed, the H and C+H conditions give rise to increased fatigue resistance as compared to the STA baseline condition.

Of these three baseline conditions, that for the C+H state is selected as the reference condition for rejuvenation of both Levels 1 and 2, respectively, for the total life analyses. This approach assumes that (i) the fatigue predamage induced in the STA condition reacts to rejuvenation identically to predamage which would have been induced in the STA+C+H material, and (ii) the damage accumulates at the same cyclic rate in both conditions. Alternatively the same baseline could be selected, assuming that the pre-crack initiation damage in the STA condition has no effect on the subsequent fatigue resistance of the STA+C+H condition. With reference to Figure 25b, it is apparent that the rejuvenation processing failed to increase the mean total life of the rejuvenated specimens beyond that of the reference STA+C+H data base.

For specimens having Level 1 predamage, the life to initiation was 4957 cycles with a standard deviation of 2527 cycles and the life to fracture was 7819 cycles with a standard deviation of 3619 cycles, giving a total life, including predamage cycles, of 9906 cycles with a standard deivation of 3624 cycles. For the Level 2 damage specimens, the mean predamage life was 3885 cycles with a standard deviation of 1032 cycles. After HIP, the mean life to initiation was 3841 cycles with a standard deviation of 2340 cycles, the fracture life was 7074 cycles with a standard deviation of 4274 cycles, and the total life, including predamage, was 11,077 cycles with a standard deviation of 4171 cycles. For both predamage

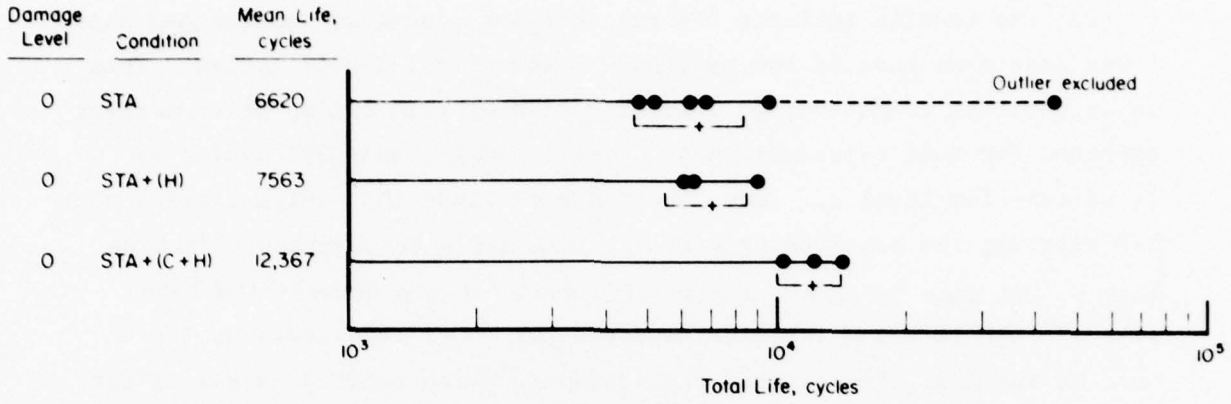

(a) Comparison of STA baseline and rejuvenation processing baseline conditions

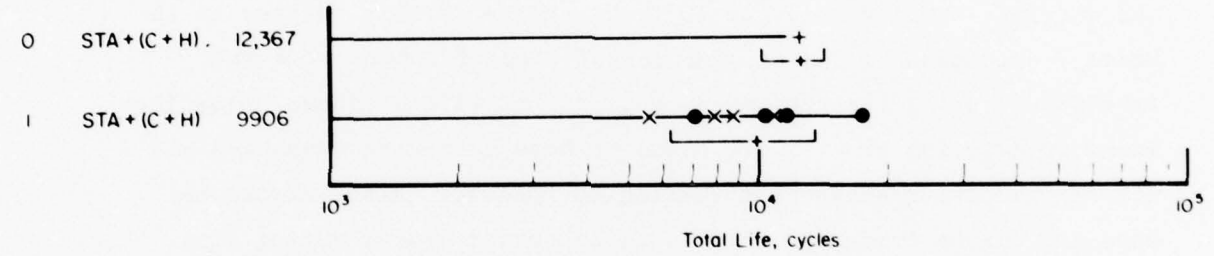

(b) Comparison of rejuvenation processing baseline and Level 1 conditions

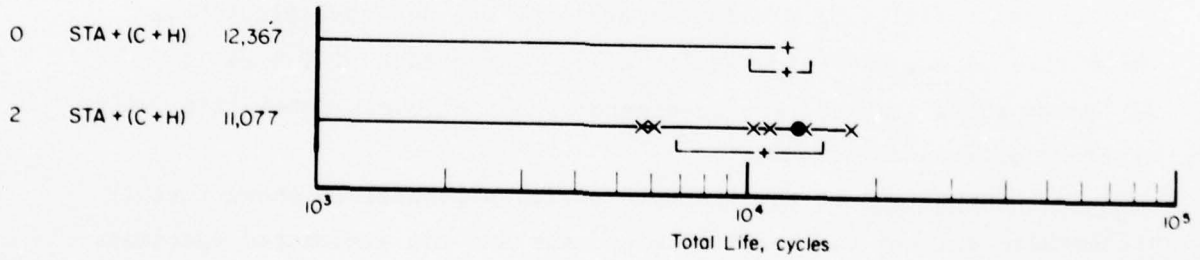

(c) Comparison of rejuvenation processing baseline and Level 2 conditions

Figure 25. Analysis of Rejuvenation of Fatigue Damage in IN-718 Based on Total Life.

The Dots Represent Specimens Showing "Normal" Crack Initiation and the X's Represent Specimens Having a "Flaw-Type" Initiation. The + is the Mean of the Fatigue Lives and the Bracket Spans the Standard Deviation.

levels, the results indicate the rejuvenation processed samples had mean lives less than that of the reference state, i.e., 12,367 cycles. This is in contrast to an average life extension of 2100 cycles or 17 percent expected for full rejuvenation of Level 1 damage, and 3885 cycles or 31 percent for Level 2. Thus, one might conclude that while coating plus HIP improves the baseline properties, this fails to rejuvenate fatigue damage, and that because the mean life does not lie between the baseline STA+C+H life and the life expected for total rejuvenation, there must be residual effects from the predamage which exert a larger effect on the final fatigue life than assumed above.

It should be noted that the scatter in the fatigue results after predamage and rejuvenation (Table 11) is much larger than that for the baseline specimens (Table 10). One cause of this scatter in the Level 2 specimens is the origination of final fracture at a site introduced during the predamage cycling. It will be shown later that known preexisting cracks were found to bond during rejuvenation and not reopen during subsequent testing to failure. Also, cracks not detected during predamage were found as bonded cracks during final sectioning after fracture. However, correlation of the final fracture locations in Level 2 specimens after rejuvenation with the mapped locations of cracks detected during the predamage cycles showed that two specimens failed at previous cracks and one specimen might have. These results are presented in Table 12. Comparison of Tables 11 and 12 indeed shows that the two specimens with the lowest total life failed at known preexisting cracks.

Inspection of the fracture surfaces themselves shows further differences between the baseline specimens and the predamaged specimens. For both the Level 1 and Level 2 specimens, the crack initiation sites apparent on the fracture surface have two different appearances. One of these is the same as the initiation sites on the C+H baseline specimen fracture surfaces, wherein the initiation site is located right at the specimen surface. This is defined as a "normal" initiation site. The other type shows a relatively smooth, well-defined semicircular area extending in from the original specimen surface to a depth of 0.25 to 0.5 mm, and is defined

TABLE 12

COMPARISON OF LOCATION OF VISIBLE CRACKS NOTED BEFORE REJUVENATION

TO FAILURE INITIATION SITE IN LEVEL 2 SPECIMENS

Specimen Number	Crack Location Before Rejuvenation		Failure Site(s) Location		Failure at Previously Observed Crack
	Distance, cm[a]	Angle, deg.[b]	Distance, cm[a]	Angle, deg.[b]	
7B-1	1.86	80			
	2.26	100			
	2.38	190			
	--	--	2.62	45	No
7B-2	1.20	10			
	2.39	10			
	2.11	80			
	2.02	110			
	3.20	140	3.30	135	Yes
	1.48	150			
	2.95	220	3.02	225	
	2.95	260			
	2.86	270	2.90	300	
	3.19	340			
8B-1	2.02	90			
	2.34	315	2.46	300	Yes
	2.45	320			
11D-1	2.51	90	1.93	80	Possible
	1.44	120			
	3.26	180			
	2.87	220			
	2.50	290			
	3.14	290			
12B-1	--	--	1.68	0	No
	2.35	80			
	2.75	315			
12B-2	--	--	2.24	0	No
	1.69	180			

(a) Distance from a reference mark on the specimen shoulder.
(b) Azimuth from a reference mark on the specimen shoulder.

as a "flaw". Since these flaw types were observed only in predamaged specimens, it is believed that they originated from fatigue damage, for example, incompletely bonded, undetected fatigue cracks. The description of the initiation sites on the fracture surfaces are presented in the right column in Table 11. Note that with the exception of Specimen 7B-1 all the Level 2 specimens had flaw-type initiation sites. Also, half the Level 1 specimens had flaw-type initiation sites.

The test bars showing a flaw-type initiation site on the fracture surfaces are indicated by an x in Figures 25b and 25c. For the Level 1 damage, the flaw-initiated fractures lie within the lower life end of the scatter (Figure 25b). The statistics on the Level 1 specimens showing normal initiation sites are a mean life to initiation of 6792 cycles with a standard deviation of 1744 cycles, a mean life to fracture of 9468 cycles with a standard deviation of 4303 cycles, and a total life, including predamage cycles, of 11,568 cycles with a standard deviation of 4303 cycles. Thus, allowance for a possible preexisting crack initiation site has increased the mean life to initiation and fracture and decreased the standard deviation in both. However, the mean life is still not up to the mean baseline C+H life. The single Level 2 specimen having a normal initiation site does not provide a sufficient basis for comparison. It did have a life comparable to the baseline life, but the crack initiation life was still well below the C+H baseline initiation life.

It is interesting to compare the Level 2 and Level 1 specimens that failed at flaws (but not at previously mapped cracks). Note that several of these specimens lie well above the Level 1 specimens (Figures 25b and 25c, the x points). The Level 1 flaw-initiated specimens had a total life of 8270 cycles with a standard deviation of 2189 cycles while the Level 2 flaw-initiated specimens had a total life of 13,106 cycles with a standard deviation of 3194 cycles. A comparison of the mean life after rejuvenation shows a life for Level 1 of 6170 cycles with a standard deviation of 2189 cycles, and a life for Level 2 of 8876 cycles with a standard deviation of 3707 cycles. Therefore, not all of the difference

in total life is due to a difference in predamage cycles. However, the Level 2 mean contains two specimens with a very long propagation life (specimens 7C-2 and 11D-1). To minimize this effect, a comparison of crack initiation life can be made; for Level 1 the mean initiation life for flaw-initiated specimens is 3121 cycles with a standard deviation of 1695 cycles, while that for Level 2 is 3973 cycles with a standard deviation of 895 cycles. Thus, the Level 2 initiation life is also longer than the Level 1 initiation life. Since there is no reason to believe that increasing predamage should prolong post-rejuvenation life but there is reason to believe just the opposite, these two sets of data could possibly be considered as equivalent, and represent the fatigue life in the presence of a flaw, possibly an undetected, incompletely bonded crack induced by the predamage cycles.

To reach some understanding of why rejuvenation of fatigue damage was not observed even when the initiation sites for fracture after rejuvenation appeared to be similar to the baseline initiation sites, it is instructive to examine the possible fatigue damage mechanisms and speculate on what effect the rejuvenation processing might have on this damage. As mentioned earlier, pre-crack initiation damage consists of the formation of heavy shear bands within the grains.[15,16] The magnitude of the accumulated shear in these bands evidently increases in intensity with increasing cycles until decohesion occurs within a band near or at the specimen surface, thereby forming a crack. The γ'' and γ' precipitates are possibly resolutioned within these bands.[16] The crack then propagates in a predominantly transgranular mode. In addition there may be internal cracking at Level 1 damage in the STA condition, associated with the Laves phases and concentrations of carbide particles, inclusions, and coarse Ni_3Nb. Post-crack-initiation damage consists of all of the above plus visible surface-connected cracks 0.5 to 1 mm in length. What is rejuvenation processing expected to do to this damage?

The observation of extensive grain growth during HIP and resolution of the coarse Ni_3Nb, Laves phase, and some of the carbides suggests that the Level 1 damage should be virtually eliminated. The grain size increases by almost 10 times, from 22 to 30 μm in the STA condition to 200 μm or more in the C+H condition. Thus, the bulk of the specimen has been swept by grain boundaries. This effect, along with resolutioning of the γ'' and γ'

precipitates, would be expected to homogenize the microstructure and eliminate any significant effect of the predamage shear bands on post-rejuvenation fatigue life. In addition, HIP closes all internal cracks and supposedly bonds them together. This line of reasoning indicates that rejuvenation should have been observed after Level 1 damage, i.e., the mean total life should have been 14,467 cycles after rejuvenation.

For the Level 2 damage, the same discussion applies to the non-crack damage. As for the predamage cracks, it is shown later that bonding of many predamage cracks had occurred, and the bonded cracks did not reopen during subsequent fatigue testing. Also only two specimens definitely fractured at previously mapped cracks (Table 12). The specimens not failing at previously mapped cracks (Table 12) are the five longest life points in Figure 25c.

Taking now the case where the rejuvenation process has presumably removed or bonded all preexisting flaws (cracks) in both Level 1 (if there were undetected cracks present) and in the specimen 7B-1 from Level 2, why was there no apparent rejuvenation of fatigue life? It is expected that the bulk of the specimen is swept clear of previous damage and a new precipitate distribution is developed during post-HIP aging. Thus, if the predamaged specimens do not fail at preexisting cracks or flaws, there must be some type of residual fatigue damage which is resistant to grain boundary migration and to resolution and reprecipitation of the secondary phases. These types of damage are difficult to visualize or evaluate in the absence of a detailed examination of the microstructure. However, one possible form of damage of this type is the surface offsets associated with heavy shear bands intersecting the surface during predamage. These may not be wholly eliminated or neutralized by the surface rejuvenation treatment. The peening either did not completely remove them or it transformed them into a condition to aid subsequent crack initiation. These offsets would be preserved beneath the coating after the first coating application, and they would not have been removed by the bulk microstructural changes occuring during HIP. There might be other types as well, such as cracked carbides or inclusions that did not rebond during HIP.

If it is assumed that some type of fatigue damage similar to this is present and has not responded fully to the type of rejuvenation

process used in this program, then a baseline other than total life must be used to measure the degree of rejuvenation. The new baseline must take into account the nonresponsive fatigue damage introduced into the STA material and what its affect might be on the STA+C+H condition. This is considered in the next section.

Partitioned Life Analysis

Consider the split of the C+H improvement on baseline properties between the initiation and propagation stages of life. Recall that over 95 percent of the increased total life of the baseline properties due to the C+H treatment resided in an increased crack initiation resistance. Because of this, damage analysis to assess the extent of rejuvenation is not as straightforward as that used above (Figure 25). Obviously, since the baseline fatigue resistances of the STA and the STA+C+H conditions differ significantly, the damage accrued in one material condition should not be considered directly in the context of the other. In this case, the difference in fatigue resistance resides in an increased resistance to crack formation in the C+H condition, whereas the propagation rates are comparable (Table 13). The assessment presented in Figure 25 ignores this aspect. It assumed that damaged STA material after rejuvenation had the same fatigue resistance as the undamaged STA+C+H material. Although this is the most conservative assumption, it is unrealistic, and therefore a different approach is presented. The approach adopted here applies a linear damage rule based on both the material and the stages of life. It is assumed that the fatigue damage mechanisms could be the same in both the STA and STA+C+H conditions but that the damage accumulates at different rates in the two conditions, the rate being proportional to the ratio of their crack initiation lives. This causes the baseline lives to be different for Level 1 and Level 2 damage.

Assuming damage accumulates linearly, and using an average baseline life to crack initiation of 4487 cycles for the STA IN-718*, 2100 cycles of Level 1 predamage exhausts 47 percent of the total initiation lifetime. Assuming the applicability of such a linear damage theory, only 53 percent of the initiation period of 9976 cycles for the STA+C+H condition** should

---

* Result from section on Baseline Fatigue Resistance using the data in Table 10.

** Result from section on Influence of Rejuvenation Processing on Baseline Properties using data in Table 10.

AD-A068 333 BATTELLE COLUMBUS LABS OHIO F/G 11/6
INVESTIGATION OF REJUVENATION OF FATIGUE DAMAGE IN IN-718.(U)
AUG 78 A H CLAUER, B N LEIS, G HOOVER F33615-76-C-5100
UNCLASSIFIED AFML-TR-78-90 NL

2 OF 2
AD A068333

END
DATE FILMED
6-79
DDC

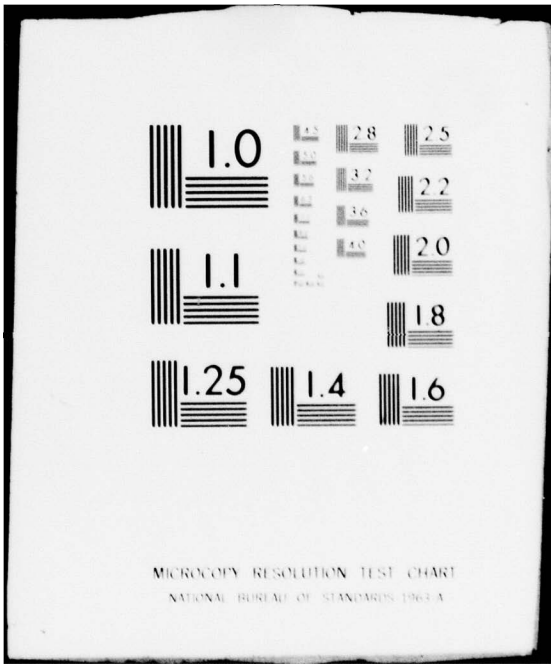
1.0
1.1
1.25
1.4
1.6
2.8
3.2
3.6
4.0
2.5
2.2
2.0
1.8
MICROCOPY RESOLUTION TEST CHART
NATIONAL BUREAU OF STANDARDS 1963-A

TABLE 13

CRACK PROPAGATION PERIOD AS A FUNCTION OF MATERIAL CONDITION

Baseline Data			Predamage/Rejuvenation Data		
Condition	Mean Propagation Period, cycles	Standard Deviation, cycles	Level	Mean Propagation Period, cycles	Standard Deviation, cycles
STA	2321	1258	1	2863	3212
STA+H	2150	--(a)	2	2301	3048
STA+C+H	2391	--(a)	Grouped Data (15 Results)	2623	3035
Grouped Data (11 Results)	2309	1178			

(a) Standard deviation not computed because of limited sample size.

be included in establishing the reference for rejuvenation assessments. The average increase in remaining life in the STA+C+H condition is 12,367 - 0.47 (9976) = 7678 cycles in addition to the 2100 predamage cycles. This reference life of 9778 cycles represents the total fatigue life of a material which exists initially in the STA condition, is damaged to 2100 cycles, and is then processed into the STA+C+H condition.

Similar calculations can be made for the Level 2 state, in which case there is no initiation period to increase as a result of the C+H process. Consequently, the life of the initial STA condition provides the approximate reference by which to assess the extent of rejuvenation, including the predamage cycles, represented by the initial crack initiation life, plus the crack propagation period.

Making use of the above reference lives as a basis to measure the extent of rejuvenation gives the results shown in Figure 26. For Level 1, the predamage of 2100 cycles in the STA condition converts to 4689 cycles in the STA+C+H condition, so full rejuvenation requires a total life of 14,467 cycles. With reference to Figure 26a, the observed total life of 9906 cycles indicates rejuvenation of Level 1 damage did not occur but neither did a decrease in fatigue life relative to the baseline life. For Level 2 damage, the total life related to full rejuvenation is 12,367 + 4487 = 16,854 cycles*. Reference to Figure 26b shows that the observed total life of 11,077 cycles after rejuvenation is intermediate between the baseline and full rejuvenation lives. This indication of rejuvenation was not observed in the total life approach.

Clearly, the results when examined in a context which accounts for the impact of fatigue damage on crack initiation in the C+H condition indicate the possibility of rejuvenation in terms of a total strain analysis (Figure 26). For the Level 1 specimens, those which showed normal initiation tend to lie in the rejuvenation range of total life. For the Level 2 specimens, only those 2 specimens which failed at previously mapped

---

* This includes the predamage cycles to crack initiation in the STA condition plus complete rejuvenation of the initiation period in the STA+C+H condition and the crack propagation period.

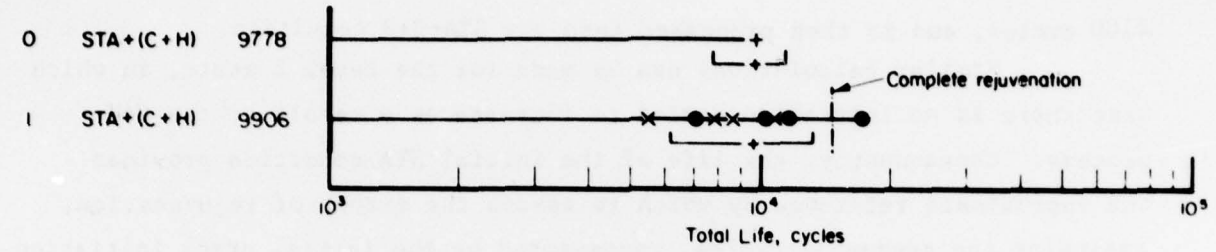

(a) Comparison of weighted baseline and Level 1 lives

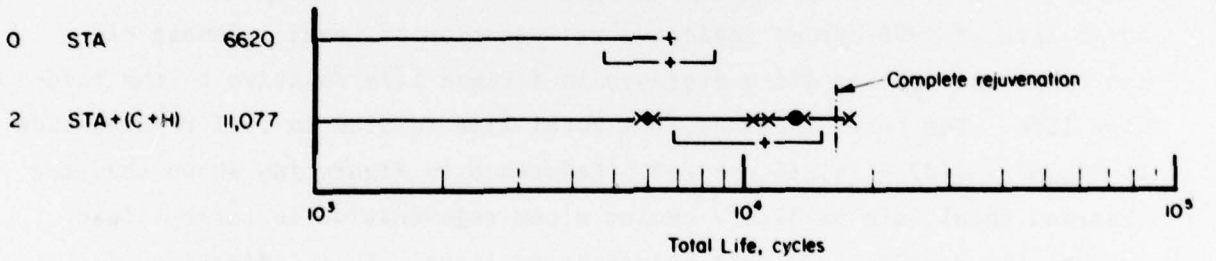

(b) Comparison of baseline and Level 2 lives

Figure 26. Analyses of Fatigue Damage Rejuvenation in IN-718, Based on Representative Baseline Fatigue Resistance.

The Dots Represent Specimens Showing "Normal" Crack Initiation and the X's Represent Specimens Having a "Flaw-Type" Initiation.
The + is the Mean of the Fatigue Lives and the Bracket With It Spans the Standard Deviation.

cracks have lives lower than the baseline life. All the others are grouped toward the full rejuvenation life.

Much of the scatter in life after rejuvenation appears to be due to scatter in the propagation period. Although the propagation period remains comparable on the average to its assumed constant value, it shows an extremely high coefficient of variation, as evident in Table 13. Specifically, the mean propagation period for Level 1 is 2863 cycles as compared to the assumed constant value of 2309 cycles, with a standard deviation of 3212 cycles for a coefficient of variation of 112 percent. Similar trends exist in the Level 2 predamage rejuvenation results. In this case, the mean propagation period is 2301 cycles as compared to the assumed constant value of 2309 cycles. The standard deviation is 3048 cycles so that the coefficient of variation is 132 percent.

The conclusion from this analysis is that the Level 1 predamage responded very little, if at all, to rejuvenation processing. This could be attributed to damage such as surface offsets whose effect was not reversed by the surface treatment, or to internal damage such as the flaws noted on the fracture surfaces of many of the predamaged specimens. If these flaws are not incompletely bonded cracks, they might represent some other type of Level 1 damage which did not respond to rejuvenation. The rejuvenation present in the Level 2 case can be attributed to the closure and bonding of the cracks. This required some additional time to be spent in a crack initiation period before reentering the crack propagation period after rejuvenation.

Metallographic Studies of Fatigue Damage

Fatigue Cracks in Baseline Material

A series of fatigue bars were sectioned after fatigue to examine the character of the fatigue-induced cracks. The sections were all

longitudinal sections along the gauge length so that the cracks could be observed in profile.

The first intention was to examine briefly the character of the cracks developed at different total strain amplitudes. Specimens 3C-1, $\Delta\varepsilon^t$ = 2.00%; 5B-1, $\Delta\varepsilon^t$ = 2.03%; 11C-2, $\Delta\varepsilon^t$ = 1.32%; and 5C-1, $\Delta\varepsilon^t$ = 0.80% were selected for sectioning. Of the two high strain amplitude specimens, the fatigue lives were quite different even though they were tested under essentially the same conditions of temperature and total strain amplitude. The cracks in Specimen 3C-1 shown in Figure 27 are typical of most of the cracks observed. The cracks follow a mostly transgranular path, but do have some intergranular segments and also deflect along twin boundaries. There are both relatively straight cracks with little branching (Figures 27a and 27b), and wandering cracks (Figures 27c and 27d). Less often a seemingly subsurface initiated crack is seen, Figure 27c.

In contrast to the long, narrow crack opening configuration usually found, the other specimen tested at a strain amplitude of 2 percent, No. 5C-1, had numerous short, wide cracks (Figure 19b). This same specimen had a short life, 84 cycles, compared to Specimen 3C1 (Figure 27) which lasted 248 cycles. This could indicate some difference in composition or microstructure in this bar compared to the others. If so, it is localized because another specimen from the same bar, Specimen 5D-2, showed the typical crack configuration.

Fatigue cracks representative of the Level 2 predamage developed at the strain amplitude $\Delta\varepsilon^t$ = 0.80%, selected for the test matrix of this study, are shown in Figure 28. These cracks are typical of both $\Delta\varepsilon^t$ = 1.32%, Specimen 11C-2, and $\Delta\varepsilon^t$ = 0.80%, Specimen 5D-2. These configurations are shown in Figure 28: the wide opening, straight type (Figure 28a); the narrow opening, straight type (Figure 28b); and the narrow opening, branchy type (Figure 28c). The tighter and branchy cracks appear to be most common. What appears to be an internal, subsurface initiation crack is seen to the left of the wide crack in Figure 28a. The specimen surface

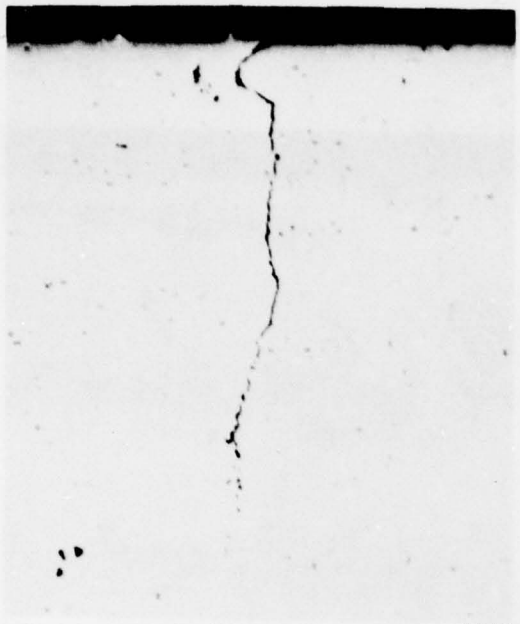

100X

(a) As-polished

100X

(b) Same as (a) plus etched

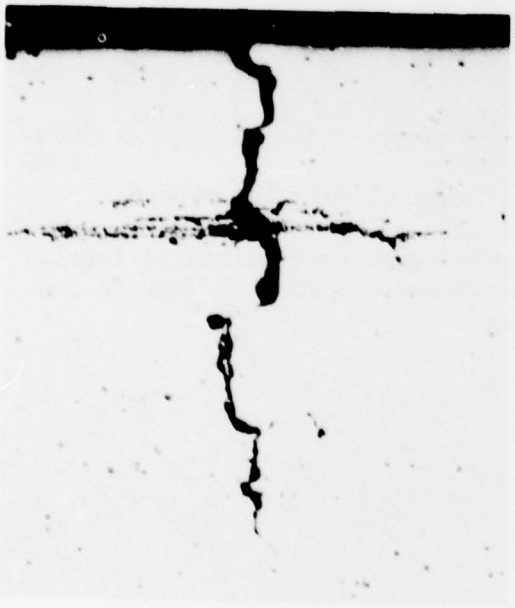

100X

(c) As-polished

100X

(d) Same as (c) plus etched

Figure 27. Fatigue Cracks in Baseline, Extruded and STA Condition Tested at a High Strain Amplitude to Failure. Specimen 3C-1, $\Delta\varepsilon^t$ = 2.00 Percent, 248 Cycles to Failure. Longitudinal Section. (a), (b) Typical Narrow, Straight Crack, (c), (d) Typical Wide, Wandering Crack.

500X

(e) As-polished

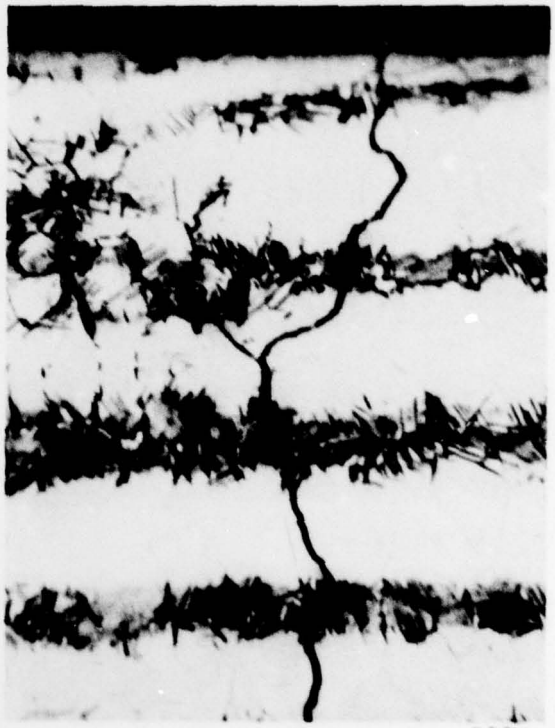

500X

(f) Same as (e) plus etched

Figure 27. Continued. (e), (f) Possible Subsurface Initiated Crack. It is Much Wider Below the Surface Than at the Surface.

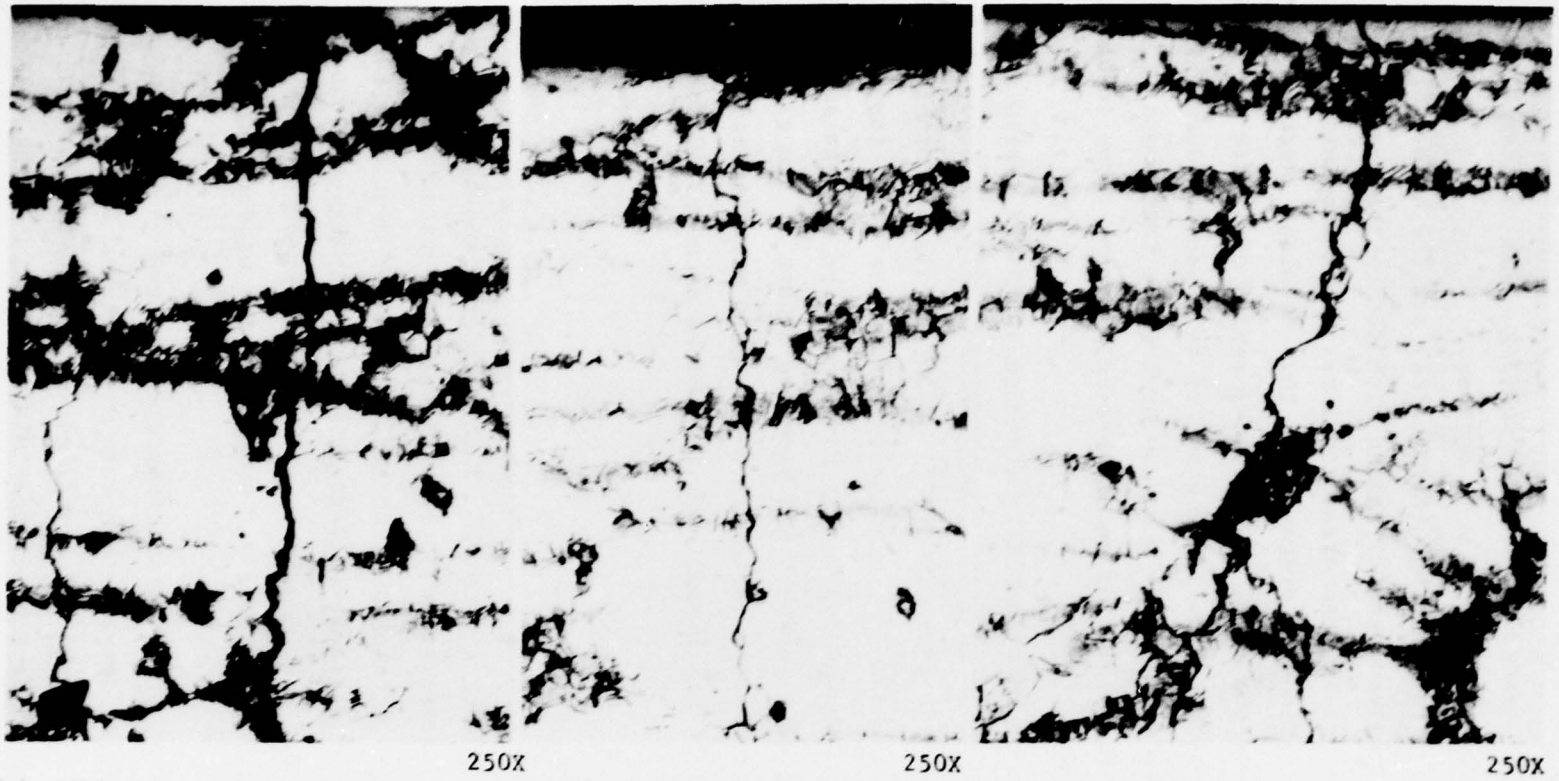

250X 250X 250X

(a) Wide, straight crack (b) Narrow, straight crack (c) Branchy crack

Figure 28. Appearance of Cracks in Unfailed Fatigue Bar Taken to Almost 100 percent of Average Life. Specimen 5D-2, at $\Delta\varepsilon^t$ = 0.80 percent, longitudinal section.

crack opening width of the wide crack is about 3 μm, well below the 15 to 25 μm range which can be bridged by the PVD coating. The tighter cracks have surface crack opening widths of 1 μm or less.

Both the wide, straight crack (Figure 28a) and the branchy crack (Figure 28c) occur in regions heavily banded with the coarse, acicular Ni_3Nb. Although these are favored areas for local crack branching, the cracks do not always continue to propagate in this fashion. Regions such as the void appearing on the crack in the lower center of Figure 28c were possibly due to a clump of grains falling out of the specimen during preparation. Possibly they fractured along weak or brittle interphase boundaries during fatigue. Similar voids were only rarely found in undamaged material.

It has been shown that the fatigue damage in IN-718 tested under the conditions of this study consist of well-defined bands of heavy shear strain extending across the grains.[15, 16] Decohesion areas within intense slip bands (also called twins[15]) ultimately act as the sites for crack initiation. Evidence of these heavy slip bands could be seen in some areas of metallographically polished and etched sections of the extruded and STA baseline material after fatigue. However, no more-intense regions of slip were specifically associated with the cracks as compared to regions away from the cracks.

Response of Fatigue Cracks to Rejuvenation Processing

One of the principal objectives of this program was to demonstrate closure and bonding of preexisting fatigue cracks after cleaning, coating, and HIP. This was first attempted in an early HIP experiment by cleaning, coating, and HIP half of a fractured fatigue bar containing numerous surface cracks. This was Specimen 5B-1, already described previously as having atypical wide cracks (Figure 19) which were too wide for the PVD bridging process.

Later, two halves of different fractured fatigue bars were processed identically to the fatigue damaged test bars and included in the last HIP experiment. However, after the HIP experiment it was decided instead to section actual pre-cracked test bars after HIP and final fatigue testing to failure. This had the advantage of (i) knowing the exact location of the visible cracks induced during the pre-HIP fatigue to the crack

propagation stage, (ii) the rejuvenation processing being that for the fatigue test bars, and (iii) determining whether fatigue cycling subsequent to HIP was sufficient to reopen any closed and bonded cracks.

This was done with two specimens, 7B-1 and 12B-1, both of which failed at a site well away from the mapped pre-rejuvenation cracks (Table 12). The halves of the fractured specimens containing the locations of the pre-rejuvenation cracks were serial sectioned in a longitudinal section in 250 μm increments so as to intercept the mapped crack locations with the expectations of (i) finding no cracks at all, indicating the cracks had bonded completely; (ii) finding the location of the now-bonded cracks marked by "dirt", precipitates, or voids as in the case of the Ti-6Al-4V[4]; or (iii) finding an open, nonbonded crack.

The result was the finding of bonded cracks whose former location was delineated by small particles or voids. Two of the three mapped cracks in 7B-1 were located and found to be identical in appearance. These are shown in Figures 29 to 32. The other crack in Specimen 7B-1 was not pursued. In addition, the previously mapped crack and two other healed, but not previously observed, cracks were also found in Specimen 12B-1 which were identical to those shown in Figures 29 to 32. Thus, there were certainly preexisting cracks in some of the other specimens which also were not observed before rejuvenation.

The appearance of the cracks on the as-polished section shows a "track" of particles of about 5 μm wide (Figures 30a and 32a). Therefore, there must be precipitates associated with the crack, lying just beneath the original crack surface, as well as possible residual voids, oxide, or dirt along the bond line itself. It is believed there was not sufficient time at temperature during the predamage cracking phase of testing to develop a significant alloy depleted zone, but the severe etching attack of the cracks over much of their length indicates there must be significant composition differences along the bond line. Since subsequent fatigue did not open up a new crack at or near any of the observed bonded cracks, neither the residual particles, voids, or any alloy depleted zone represented most-favored sites for subsequent fatigue crack initiation. The particles would not be expected to act as initiation sites because of their small size, less than 1 μm.

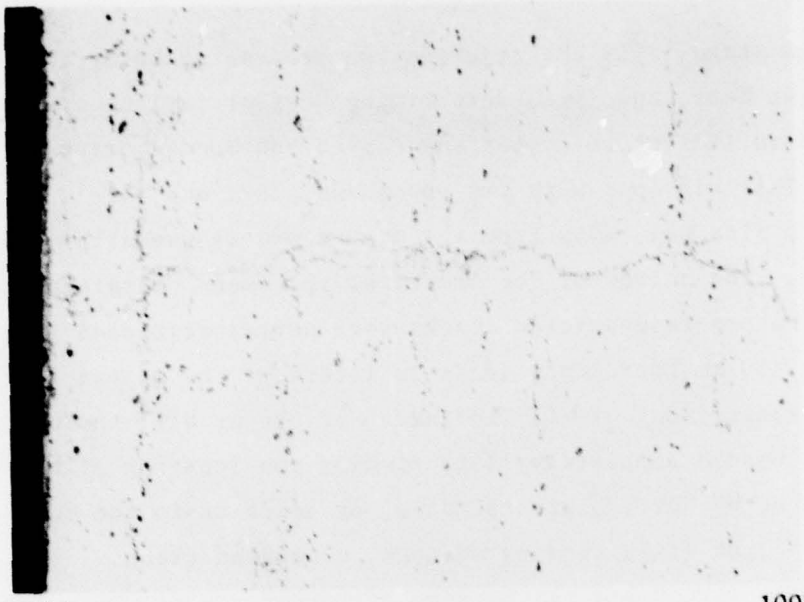

4J836 100X
(a) As-polished

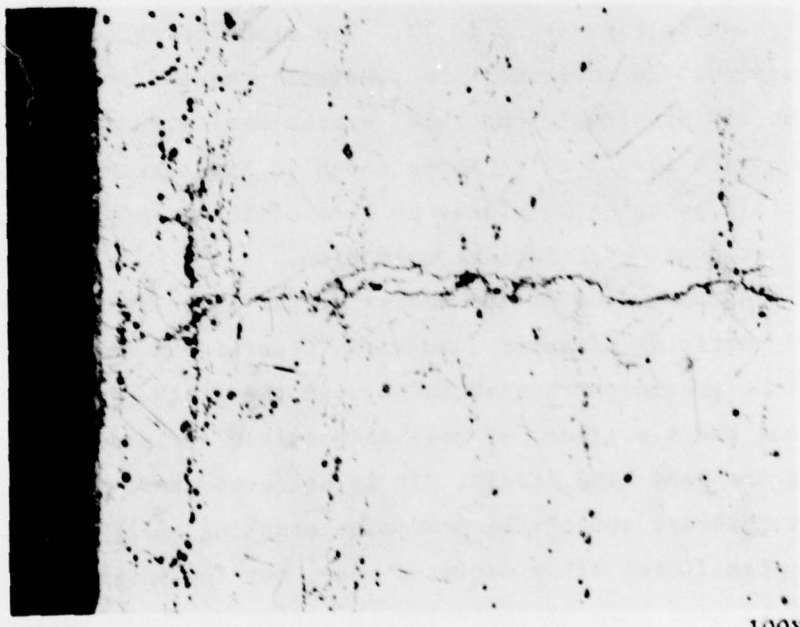

4J840 100X
(b) Polished and etched

Figure 29. Micrographs of a Bonded Fatigue Crack after Rejuvenation Processing and Fatigue Testing to Failure. Specimen 7B-1, longitudinal section.

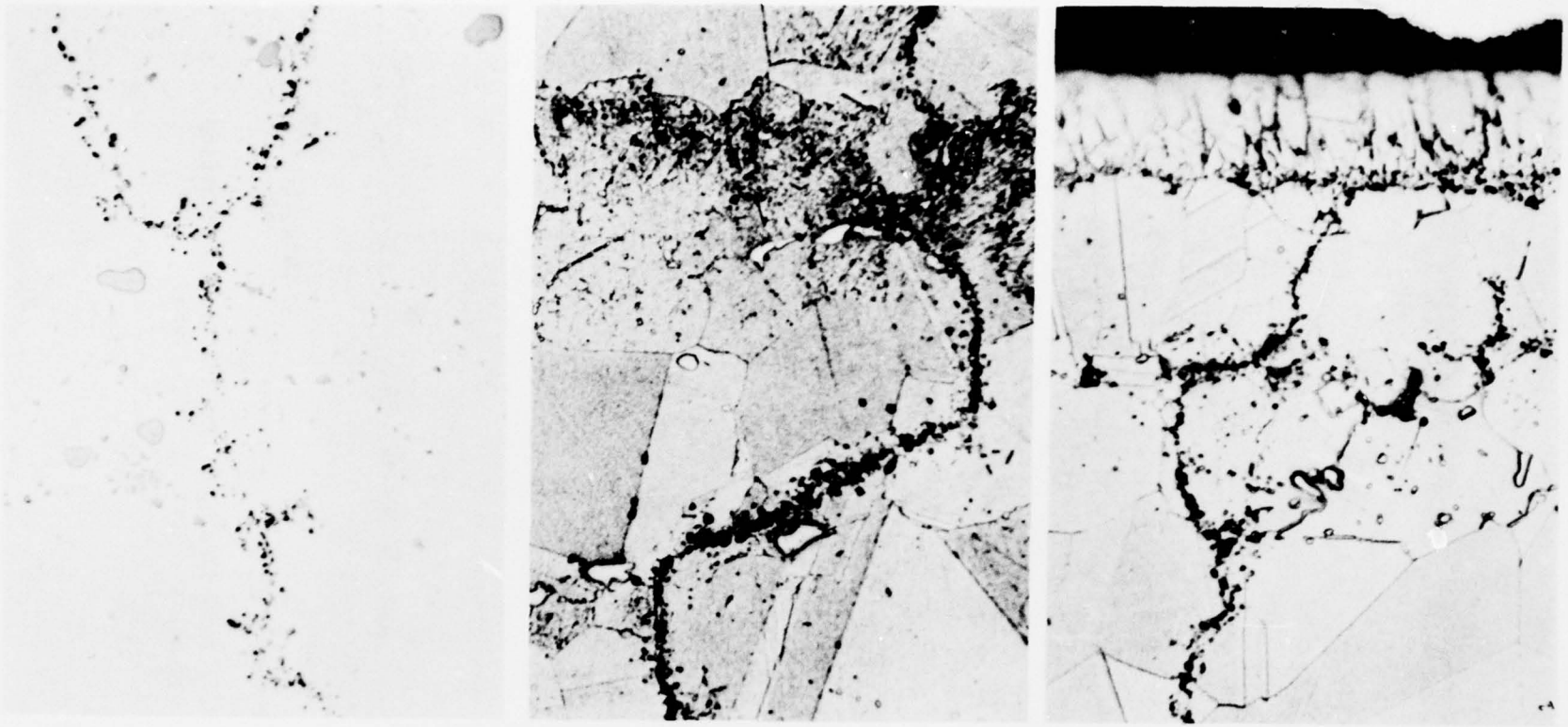

4J839 1000X
(a) As-polished

4J845 1000X
(b) Polished and etched

4J844 1000X
(c) Polished and etched, at surface

Figure 30. High Magnification Micrographs of Same Crack Shown in Figure 29.

4J837 100X

(a) As-polished

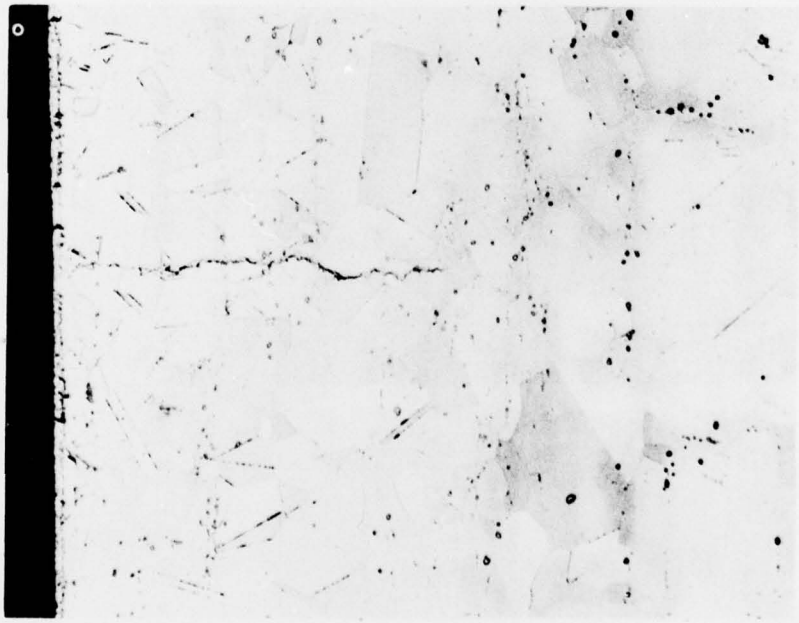

4J841 100X

(b) Polished and etched

Figure 31. Micrographs of a Bonded Fatigue Crack After Rejuvenation Processing and Fatigue Testing to Failure.

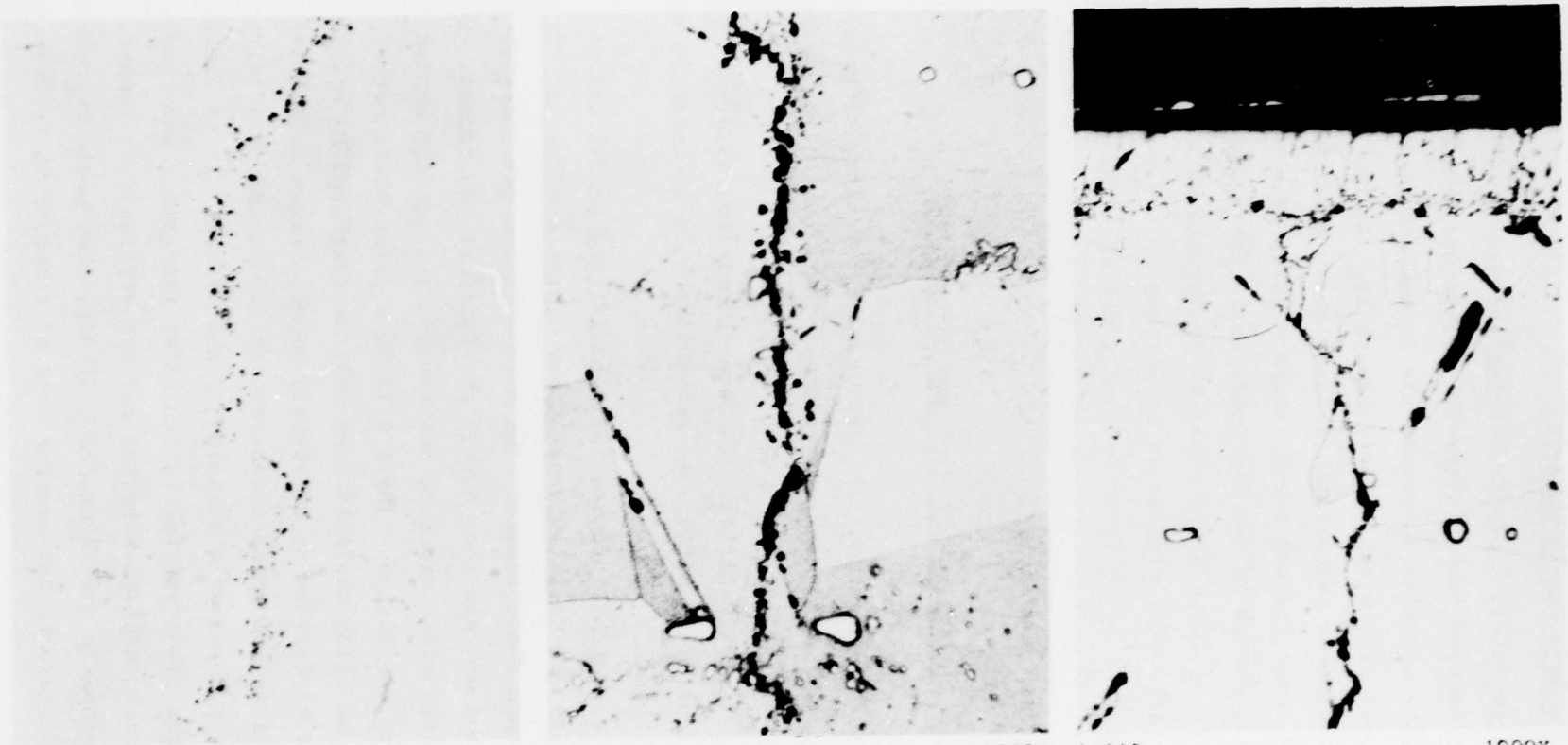

4J838 1000X
(a) As-polished

4J843 1000X
(b) Polished and etched

4J842 1000X
(c) Polished and etched, at surface

Figure 32. High Magnification Micrographs of Same Crack as Shown in Figure 31.

Fatigue Damage in Rejuvenated Material

The heavy shear bands traversing the grains were much more visible in the specimen fatigue tested after HIP. This was because the larger grain size in this material increased the length and therefore the displacement or shear within the individual cracks. If the primary crack initiation mechanism is decohesion of these heavy shear bands, then this is the probable cause for the trend toward a grain size dependence of the crack initiation life observed in the C+H condition. There did not appear to be any concentration of these heavy shear bands associated with the cracks.

The cracks were similar in appearance to those shown earlier, except there appeared to be fewer secondary cracks. The cracks propagated in a transgranular mode for the most part but did show some deflection along twin and grain boundaries.

SUMMARY DISCUSSION AND CONCLUSIONS

It should be noted at the outset that the material used in this program was not given much work before use. Therefore, although it has some of the characteristics of wrought material, it also retained some characteristics of cast material. To some extent the results of the program will reflect this difference and this should be borne in mind when evaluating them.

It is clear that properly bridged fatigue cracks can be closed and bonded. There are definitely secondary phases, oxides, or "dirt" from shot peening within these cracks. The size of these particles is quite small, less than 1 μm, and they should not initiate new cracks. However, the different localized microstructure and chemistry along the bonded crack might favor crack initiation. There will be a point where better cleaning is required and an alloy depleted zone must be addressed to ensure a sound bond. The observed failure at previously mapped cracks in some of the pre-damaged, rejuvenated specimens indicates the importance of a reliable crack bridging process and reliable cleaning of the cracks. It is not known what type of damage the flaw-type initiation sites represent, but they clearly appear in the crack initiation period and are difficult to remove. They are probably improperly bonded cracks. If not, they could represent an important type of fatigue damage in its seeming lack of response to rejuvenation.

It is believed that the PVD coating is desirable to provide primary bridging of the crack and to replace material lost to erosion and corrosion of used disks or blades. It is believed that the coating technique can be improved beyond that demonstrated in this program to provide better surface adherence and bridging of cracks. The ceramic coating must require further development as a reliable backup coating to the PVD coating.

An important result of this program was the lack of response of Level 1 damage to rejuvenation. Since it was surmised that internal damage should be removed during HIP and aging, this is an unexpected result. It is possible that other types of damage such as surface offsets or the flaw-type defects might retain some of their potency through rejuvenation and decrease the total life.

The large increase in fatigue life developed by coating and HIP of the extruded and STA material is striking. It is not clear to what extent the rejuvenation surface treatment, peening and coating, caused this increase compared to the homogenization of the microstructure and the grain size differences. It may be that a HIP homogenized microstructure with a smaller grain size could give the same life as the coated and HIP material. The HIP cycle should be modified to homogenize the microstructure and minimize grain growth in both cast and wrought IN-718 to assess potential benefits in mechanical properties.

The substantial change in the baseline properties of the material after coating and HIP caused great difficulty in interpreting the results. Assumptions had to be made regarding the similarities of fatigue damage mechanisms in the two baseline conditions (STA and STA+C+H), their response to rejuvenation, and the influence of residual fatigue damage carried over from the initial condition on the fatigue resistance of the final, rejuvenated condition. The most conservative analysis showed no rejuvenation effect but instead indicated that residual fatigue predamage was influencing the life after rejuvenation of the predamaged specimens. A second approach to account for this effect indicated little or no rejuvenation of Level 1 damage, but some rejuvenation of Level 2 damage. This is consistent with the observation of bonded fatigue cracks in Level 2 specimens.

A more useful approach would be to homogenize the specimens by HIP before predamage to give approximately the same baseline life before and after rejuvenation. In this way the damage mechanisms would be the same for both conditions and the properties after rejuvenation would be a more direct measure of the relative removal of predamage. In addition, the predamage lives could be a large fraction of the baseline life (N_i is a large fraction of N_f after rejuvenation) and the assessment of rejuvenation by relative increase in total life could be clearly seen.

REFERENCES

(1) Clauer, A. H., and Leis, B. N., "Rejuvenation of Creep Properties in Copper", presented at AIME Annual Meeting, Atlanta, Georgia, March 1977, J. of Metals, 28, A64 (1977).

(2) Leis, B. N., and Clauer, A. H., unpublished results.

(3) Anthony, K. C., and Rodavitch, J. F., "The Effects of HIP Rejuvenation of Turbine Blades", presented at AIME Annual Meeting, Atlanta, Georgia, March 1977, J. of Metals, 28, A25 (1977).

(4) Clauer, A. H., Leis, B. N., and Seifert, D., "Investigation of Rejuvenation of Fatigue Damage in Ti-6Al-4V", AFML-TR-77-107, 1978.

(5) "Inconel Alloy 718", Data Bulletin, Huntington Alloys, Inc.

(6) Eiselstein, H. L., "Metallurgy of a Columbium Hardened Nickel-Chromium-Iron Alloy", ASTM STP 369, 62-79 (1965).

(7) Paulonis, D. F., Oblak, J. M., and Duvall, D. S., "Precipitation in Nickel Base Alloy 718", Trans. ASM, 62, 611-622 (1969).

(8) Cozar, R., and Pineau, A., "Morphology of γ' and γ'' Precipitates and Thermal Stability of Inconel 718 Type Alloys", Met. Trans., 4, 47-59 (1973).

(9) Muller, J. F., and Donachie, M. J., Jr., "The Effects of Solution and Intermediate Heat Treatments on the Notch-Rupture Behavior of Inconel 718", Met. Trans. A., 6A, 2221-2227 (1975).

(10) Morrow, J., "Cyclic Plastic Strain Energy and Fatigue of Metals", in Internal Friction, Damping, and Cyclic Plasticity, ASTM STP 378, 45-84 (1965).

(11) Wagner, H. J., Burns, R. S., Canal, T. E., and Simon, R. C., "Nickel Base Alloys: Alloy 718", DMIC Data Sheet, Battelle's Columbus Laboratories.

(12) Schweikert, W. H., "Manufacturing Methods for Low Cost Turbine Engine Components of Cast Super Alloys", U. S. Air Force Report No. IR 260-5(2), April, 1976, General Electric Co., Evendale.

(13) Feltner, C. E., and Mitchell, M. R., "Basic Research on the Cyclic Deformation and Fracture Behavior of Materials", in Manual on Low-Cycle Fatigue Testing, ASTM STP 465, 100-128 (1969).

(14) Brinkman, C. R., and Korth, G. E., "Strain Fatigue and Tensile Behavior of IN-718 From Room Temperature to 650 C", J. Testing and Evaluation, 2, 249-259 (1974).

(15) Fournier, D., and Pineau, A., "Low Cycle Fatigue Behavior of IN-718 at 298 K and 823 K, Met. Trans. A, 8A, 1095-1105 (1977).

(16) Merrick, H. F., "The Low Cycle Fatigue of Three Wrought Nickel-Base Alloys", Met. Trans., 5, 891-897 (1974).

*U.S.Government Printing Office: 1979 — 657-002/509